THESIS FOR THE DEGREE OF DOCTOR OF PHILOSOPHY

Quantum Optics and Waveguide Quantum Electrodynamics in Superconducting Circuits

EMELY WIEGAND

Department of Microtechnology and Nanoscience (MC2)

Applied Quantum Physics Laboratory

CHALMERS UNIVERSITY OF TECHNOLOGY

Göteborg, Sweden 2021

Applied Quantum Physics Laboratory
Department of Microtechnology and Nanoscience (MC2)
Chalmers University of Technology
SE-412 96 Göteborg
Sweden
Telephone: +46 (0)31-772 1000

Cover
Illustration of an excited atom in front of a mirror

Quantum Optics and Waveguide Quantum Electrodynamics in Superconducting Circuits
EMELY WIEGAND
Department of Microtechnology and Nanoscience (MC2)
Applied Quantum Physics Laboratory
Chalmers University of Technology

Abstract

Waveguide circuit quantum electrodynamics (waveguide circuit QED) studies light-matter interaction with superconducting circuits in one dimension. In circuit QED, natural atoms are replaced by superconducting qubits consisting of a non-linear Josephson junction, resulting in an anharmonic energy spectrum just like real atoms. With superconducting qubits, it is possible to study quantum optical phenomena and reach new regimes hard to achieve with real atoms due to weak coupling to the electromagnetic field. The reduction to one dimension in waveguide QED increases the electromagnetic field's directionality, which results in reduced losses.

In this thesis, we first introduce circuit quantisation, giving the basis for the next part, where we investigate a transmon, a charge-insensitive artificial atom, coupled to a semi-infinite transmission line. An atom coupled to a semi-infinite waveguide is referred to as an *atom in front of a mirror* and is the subject of all appended papers. We proceed by summarising Paper I and III's main results: in Paper I, we investigate the spontaneous emission of a transmon coupled to a semi-infinite transmission line, where we take time-delay effects into account. We find that the system dynamics strongly depend on the coupling strength to the transmission line and the atom's position with respect to the electromagnetic field, leading to the Purcell effect or the convergence to a dark state with finite excitation probability. In the high-impedance regime, which we investigate in Paper III, the properties of the transmon coupled to the high-impedance transmission line change drastically. It becomes highly reflective and creates its own cavity with the mirror, resulting in the emergence of cavity modes and vacuum Rabi oscillations in the spontaneous emission dynamics.

In the next chapter of the thesis, we demonstrate how to quantise an electromagnetic field and derive a light-matter interaction Hamiltonian within dipole approximation. We then give an introduction to open quantum systems and derive the quantum-optical master equation in Lindblad form. Furthermore, we introduce the dressed state picture, where the interaction of light and matter is so strong that the individual energy levels of light and matter are no longer separable. Both the quantum optical master equation and the dressed state picture are relevant in Paper II and IV. In Paper II, an experimental collaboration, we perform several experiments to characterise and discriminate different decay rates of a superconducting qubit coupled to the end of a transmission line. One experiment measured the atomic fluorescence spectral density, which shows an asymmetry for off-resonant driving, resulting from pure dephasing: an effect that we explain in more detail in this thesis and Paper II. In Paper IV, we theoretically investigate amplification mechanisms realised by different set-ups of an atom coupled to a semi-infinite waveguide. In the considered systems, the amplification of a probe field happens either due to population inversion between the pure states or dressed states or multiphoton processes. We find that compared to an open waveguide, we can achieve a higher gain in the amplification with a semi-infinite waveguide.

Keywords: Quantum Optics, Circuit Quantum Electrodynamics, Waveguide Quantum Electrodynamics, Superconducting Qubits, Artificial Atoms

Acknowledgements

Taiwan was one of the highlights of my time as a PhD student, and I am grateful for our collaboration.

Last but not least, I want to thank my family and friends for their support.

LIST OF PUBLICATIONS

This thesis presents a summary and an extension to the following appended papers:

[I] E. Wiegand, B. Rousseaux, and G. Johansson, "Semiclassical analysis of dark-state transient dynamics in waveguide circuit QED", Phys. Rev. A **101**, 033801 (2020).

[II] Y. Lu, A. Bengtsson, J. J. Burnett, E. Wiegand, B. Suri, P. Krantz, A. F. Roudsari, A. F. Kockum, S. Gasparinetti, G. Johansson, and P. Delsing, "Characterizing decoherence rates of a superconducting qubit by direct microwave scattering", npj Quantum Information **7**, 35 (2021).

[III] E. Wiegand, B. Rousseaux, and G. Johansson, "Transmon in a semi-infinite high-impedance transmission line: Appearance of cavity modes and Rabi oscillations", Phys. Rev. Research **3**, 023003 (2021).

[IV] E. Wiegand, P. Y. Wen, P. Delsing, I. Hoi, and A. F. Kockum, "Ultimate quantum limit for amplification: a single atom in front of a mirror", New Journal of Physics (2021).

We always refer to these publications as paper I, II, . . . , according to the labeling in the list above.

CONTENTS

1 Introduction

In the early 20th century, scientists observed many effects, such as the black-body radiation and the photoelectric effect, that could not be explained by the established theories at the time [1]. These and other discoveries have led to the emergence of *quantum mechanics*, a theory that could explain these newly discovered phenomena and revolutionised our understanding of the world on a fundamental level. One quantum mechanical concept is the wave-particle duality, stating that particles have wave properties and vice versa. Other exciting quantum effects are *superposition* and *entanglement* of quantum states. These two effects require a description based on quantum mechanics and cannot be explained classically. There has been tremendous progress over the past decades to use these new quantum mechanical theories to our advantage and develop new technologies. One fundamental problem in achieving practical applications based on quantum theories is the accessibility and *controllability* of quantum systems, which was a challenging task in the early times of quantum mechanics.

However, in the past decades, it has become possible to address single quantum systems individually. In 2012, David Wineland and Serge Haroche received the Nobel prize for their pioneering work in accessing single quantum systems. In Wineland's experiment, single ions were trapped in a vacuum and probed by a laser, leading to entanglement between different states of the ion [2]. In Haroche's work, a microwave field was trapped inside a cavity, and single excited Rydberg atoms were sent through the cavity, creating entanglement between the atoms and the cavity field [3]. Both experiments laid a foundation for new technologies based on the measurement and control of single quantum systems [4].

With these new findings, the proposal that Richard Feynman made in the early '80s might become realisable in the near future: He suggested that a *quantum computer* might be able to solve certain problems more efficiently than a classical computer [5]. His reasoning was that a computer based on quantum mechanics itself would be better at simulating nature, as nature behaves quantum mechanically. A quantum computer uses en-

tanglement and superposition to perform computation and is believed to solve certain problems exponentially faster than a classical computer [6]. The controllability of individual qubits is crucial to the pursuit of building a quantum computer. The goal is to develop quantum algorithms specifically made for the quantum computer that either solve problems faster than classical algorithms or do not have a classical counterpart at all [7]. Areas in which a quantum computer might be useful are optimization problems [8–10], quantum chemistry [11–13], machine learning [14–16] and the simulation of many-body physics [17, 18].

It is currently of high interest to build a quantum computer and find useful and applicable quantum algorithms. It is still challenging to build a fault-tolerant high-fidelity quantum processors consisting of many qubits with long coherence times that can run quantum algorithms with low losses and noise. Another difficulty is to find useful algorithms to solve problems that cannot be simulated on a classical computer in polynomial time. Only after solving these problems, we can say that we have achieved a so-called *quantum advantage*, which would prove that a quantum computer can indeed solve certain problems exponentially faster than a supercomputer [19–24]. However, much work is done in quantum error correction to increase the fidelity of quantum processors [23, 25, 26] and Noisy Intermediate-Scale Quantum (NISQ) computers without error-corrected qubits already exist [27–30]. Quantum advantage was recently claimed by Arute *et al.* [28]. They built a quantum computer consisting of 53 superconducting qubits and performed an exclusively quantum mechanical algorithm in 200 seconds, whereas they claim that the classical equivalent would take approximately 10 000 years. However, IBM claims that with optimised techniques, a supercomputer would, in fact, be able to compute the problem in only 2,5 days [31].

The qubits used by Arute *et al.* [28] are programmable superconducting charge qubits [25, 32–38], of the same kind as the ones considered in this thesis and all the appended articles. Superconducting qubits are *artificial atoms* built from an electrical circuit and work in the microwave regime. The crucial part is to incorporate a Josephson junction into the circuit, consisting of two superconducting leads separated by a thin insulator. The phase-dependence of the Cooper pairs tunnelling through the insulator leads to a non-linearity in the potential energy [39–41]. Therefore, the artificial atom's energy spectrum becomes anharmonic, resembling the energy spectrum of real atoms. One of the simplest possible superconducting qubits is the single Cooper-pair box (SCPB), which has a supercon-

ducting island to which the Cooper pairs can tunnel on and off [42–44]. However, the SCPB is very sensitive to small fluctuations in the charge, making the energy levels unpredictable and therefore a bad candidate for a controllable qubit. A better version of the SCPB is the transmon qubit that consists of an additional capacitance to shunt the superconductors, which decreases the sensitivity to charge noise [45]. Moreover, some types of transmon consist of a superconducting quantum interference device (SQUID) instead of only one Josephson junction, which makes it possible to tune the transition frequencies of the energy levels by using an external magnetic field. Another essential property of not only artificial atoms but all atoms used in experiments is the coherence time. Quantum systems, like atoms, that interact with their environments, such as a coherent laser field, lose their quantum coherence over time, a process called *decoherence.* Superconducting qubits have typical coherence times of $\approx 100\,\mu$s [46]. In order to understand and be able to engineer superconducting qubits, it is crucial to characterise and distinguish the different decay and decoherence rates [47], which is the subject of Paper II.

Superconducting qubits are not only suitable for the construction of quantum processors but also to perform quantum optical experiments and reaching new regimes. The field that studies quantum optical phenomena in superconducting circuits is called circuit quantum electrodynamics (circuit QED) [35, 48–51]. In quantum optical systems, where the interaction between light and matter, such as atoms or molecules, is studied, the coupling between the electromagnetic field and matter is limited by the size of the fine structure constant and is, therefore, rather weak [52]. In many experiments, unwanted losses to the environment exceed the coupling strength between atoms and photons, making information transfer difficult. To reduce the information loss, it is advantageous to engineer both the atom and the environment, making it possible in circuit QED to reach the strong and ultrastrong coupling regime [52–60]. The possibility of reaching the strong coupling regime in circuit QED made it possible to achieve superradiance [61–64] which is a well-studied quantum optical phenomenon [65–67]. There are a plethora of other quantum optical phenomena demonstrated in circuit QED [50, 51, 68], e.g., lasing [69–72].

Another way to reduce losses is the restriction of the environment to one dimension [68, 73–75], which is done in waveguide QED [73, 74, 76]. This increases the directionality of the electromagnetic field inside the waveguide resulting in reduced losses [77, 78]. In circuit QED, a typical one-dimensional waveguide is a coplanar waveguide or transmission line (TL).

The considered waveguides can either be open, made into resonators, or be shorted at one end (semi-infinite waveguides) [25, 48–50, 79–82]. We consider the latter in all appended papers. When the semi-infinite waveguide is coupled to an atom, the system is referred to as an *atom in front of a mirror*. The atom in front of a mirror has been studied both experimentally and theoretically [83–90]. In some cases, a semi-infinite TL can be more advantageous than an open one. For instance, in Paper IV, we show that with an atom in front of a mirror, it is possible to achieve a higher gain in the reflection of a probed field [84, 91], leading to a higher amplification compared to an open TL [92, 93]. Furthermore, interesting effects can be studied with an atom in front of a mirror, e.g., time-delay effects, resulting in a non-Markovian system [74, 94–100]. Similar effects occur with giant atoms, artificial atoms that couple to an electromagnetic field at several points [101–104]. In Paper I and III, we consider a transmon coupled to a semi-infinite TL and take time-delay effects into account to investigate the resulting system dynamics.

Transmission lines can be modelled by lumped elements consisting of several coupled LC-oscillators and typically have a characteristic impedance of $Z_0 \approx 50\,\Omega$, which is much smaller than the quantum resistance. However, recent studies show that it is possible to reach impedances comparable to the quantum resistance or higher [105–111], which can be realized by building circuits made of arrays of Josephson junctions [107, 108, 110–114] or high-kinetic-inductances materials, called superinductors [106, 109, 115–118]. High impedance Josephson junction arrays and superinductors are, for example, used in the Fluxonium qubit [119–122], another type of superconducting qubit besides the transmon, which has reduced charge noise sensitivity and can have relaxation times up to milliseconds [121, 123]. One application of a charge insensitive qubit with high characteristic impedance is in metrology since the current can be measured very accurately [124]. Furthermore, high-impedance resonators are suitable for light-matter interaction to reach strong coupling regimes due to strong coupling to vacuum fluctuations [125]. In Paper III, we theoretically investigate the dynamics of a transmon coupled to a high-impedance TL. We find that the system properties in the high-impedance regime change drastically. For instance, even when probed off-resonantly, the transmon becomes highly reflective in the high-impedance regime, acting as a mirror. If coupled to a semi-infinite TL, the atom creates its own cavity together with the mirror, resulting in the emergence of cavity modes and vacuum Rabi oscillations in the spontaneous emission dynamics. Other

systems that show cavity-free Rabi splitting and contain atoms that act like mirrors have been studied both theoretically and experimentally [101, 126–128].

1.1 Organization of the thesis

This thesis is organised as follows. In chapter 2, we give an introduction to circuit quantisation. More specifically, we introduce superconducting circuits and their elements, starting from essential components and continuing to TLs and superconducting qubits. In chapter 3, we give a follow up to chapter 2, by discussing a transmon coupled to a TL. We investigate different regimes and effects of an atom coupled to an open and semi-infinite TL, considered in Paper I and III. In chapter 4, we derive a light-matter interaction Hamiltonian by field quantisation. Despite being circuit QED systems, the systems investigated in all articles discuss light-matter interaction with artificial atoms in the microwave regime, using quantum optics methods. The same holds for chapter 5, where we introduce open quantum systems and derive the quantum optical master equation in Lindblad form. These methods have been used in Paper II and IV. Furthermore, we introduce the dressed state picture of an atom coupled to a laser field in chapter 6, which is relevant in Paper II and IV. In the last chapter, chapter 7, we give an overview of all appended articles.

2 Circuit quantization

All appended articles deal with artificial atoms coupled to waveguides, or more specifically, one-dimensional (1D) transmission lines. Whereas we start with quantum optical models in Paper II and IV, we derive the Hamiltonian of the system through circuit quantization in Paper I and III. That is why we start the first chapter of this thesis by introducing the circuit quantization procedure and its most essential elements [129, 130]. We introduce the circuit's basic components and their quantization and demonstrate how to derive the Hamiltonian for a transmission line with different boundary conditions. Further, we introduce artificial atoms or superconducting qubits, a fundamental building block in modern quantum technology. We start with the simplest superconducting qubit, the single Cooper-pair box (SCPB) and later introduce the transmon, a charge insensitive superconducting qubit considered in most of our articles.

2.1 Lagrangian and generalised coordinates

The first step in the circuit quantization process is to define generalized coordinates ϕ_n of the system and write down the Lagrangian $\mathcal{L}$ of the circuit that contains the kinetic and potential energies, $\mathcal{T}$ and $\mathcal{V}$, respectively,

$$\mathcal{L}(\phi_n, \dot{\phi}_n, t) = \mathcal{T} - \mathcal{V}. \tag{2.1}$$

The kinetic energies depend on the time derivative of the generalized coordinates $\dot{\phi}_n$, and the potential energies, in non-dissipative systems, depend on the generalized coordinates ϕ_n themselves. For an electrical circuit, it is convenient to use the node fluxes ϕ_n as generalized coordinates. The node fluxes are defined as the time integral of the voltage V_n at a node n,

$$\phi_n = \int_{-\infty}^{t} V_n(t)\, \mathrm{d}t. \tag{2.2}$$

In the table below, we summarised some of the most essential non-dissipative elements with their circuit symbols and their contribution to the energies.

7

Circuit Element	Symbol	Energy
Capacitor		$\mathcal{T} = \frac{1}{2}C\dot{\phi}^2$
Inductor		$\mathcal{V} = \frac{1}{2L}\phi^2$
Josephson Junction		$\mathcal{V} = E_J\left(1 - \cos\left(2\pi\frac{\phi}{\phi_0}\right)\right)$

2.2 Quantization of an LC-oscillator

We demonstrate the quantization process of an electrical circuit by means of an LC-oscillator, depicted in Fig 2.1. The Lagrangian of this system is given by

$$\mathcal{L}(\phi, \dot{\phi}) = \frac{1}{2}C\dot{\phi}^2 - \frac{1}{2L}\phi^2, \tag{2.3}$$

with a kinetic energy term, $\mathcal{T} = \frac{1}{2}C\dot{\phi}^2$, coming from the capacitive part and the potential energy term, $\mathcal{V} = \frac{1}{2L}\phi^2$, coming from the inductive part of the circuit. The next step is to calculate the Hamiltoian $\mathcal{H}$ of the system. The Hamiltonian is a function of the node flux and its conjugate momentum, which is generally defined by

$$p_n = \frac{\partial\mathcal{L}}{\partial\dot{\phi}_n}, \tag{2.4}$$

and here corresponds to the node charge

$$p_n = \int_{-\infty}^{t} I_n(t)\,\mathrm{d}t, \tag{2.5}$$

where I_n is the node current. For the LC-oscillator, the conjugate momentum is given by the charge on the capacitor,

$$p = \frac{\partial\mathcal{L}}{\partial\dot{\phi}} = C\dot{\phi}. \tag{2.6}$$
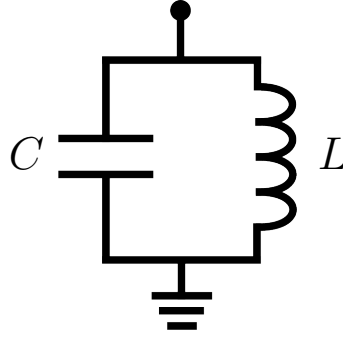
Figure 2.1: *Sketch of an LC-circuit consisting of a capacitor with capacitance C and an inductor with inductance L.*

In general, the Hamiltonian can be calculated by performing a change of variables using the Legendre transformation of the Lagrangian,

$$\mathcal{H}(\phi_n, p_n, t) = \sum_n p_n \dot{\phi}_n - \mathcal{L}(\phi_n, \dot{\phi}_n, t). \tag{2.7}$$

However, in the case of the LC-oscillator, it is even simpler since the system is non-dissipative and holonomous-scleronomous. This means that the potential energies do not depend on the time derivative of the conjugate variable, $\partial \mathcal{V}/\partial \dot{\phi} = 0$, and the kinetic energies are quadratic in the generalised velocities $\mathcal{T}(a\dot{\phi}) = a^2 \mathcal{T}(\dot{\phi})$, where a is an arbitrary real number [131]. So the Hamiltonian is simply given by the total energy of the system

$$\mathcal{H}(\phi, q) = \mathcal{T}(p) + \mathcal{V}(\phi) = \frac{p^2}{2C} + \frac{\phi^2}{2L}. \tag{2.8}$$

This resembles the Hamiltonian of a harmonic oscillator $\mathcal{H} = \frac{p^2}{2m} + \frac{m}{2}\omega^2 x^2$ with frequency $\omega = 1/\sqrt{LC}$ which is the resonance frequency of the LC-oscillator and "mass" $m = C$. Now we quantize the system by promoting ϕ and p to operators

$$\phi \rightarrow \hat{\phi}, \tag{2.9}$$
$$p \rightarrow \hat{p}, \tag{2.10}$$

which fulfil the canonical commutation relation

$$\left[\hat{\phi}, \hat{p}\right] = i\hbar. \tag{2.11}$$

Now, we can rewrite the Hamiltonian in terms of ladder operators a and $a^\dagger$ by defining

$$\hat{\phi} = \sqrt{\frac{\hbar}{2}\frac{1}{C\omega}}\left(a^\dagger + a\right) = \sqrt{\frac{\hbar}{2}Z}\left(a^\dagger + a\right) \tag{2.12}$$

$$\hat{p} = i\sqrt{\frac{\hbar}{2}C\omega}\left(a^\dagger - a\right) = i\sqrt{\frac{\hbar}{2Z}}\left(a^\dagger - a\right), \tag{2.13}$$

where we have introduced the characteristic impedance of the oscillator $Z = \sqrt{L/C}$. The ladder operators a and $a^\dagger$ obey the bosonic commutation relation $\left[a, a^\dagger\right] = 1$ and operate on the energy eigenstates $|n\rangle$ in the following way

$$a|n\rangle = \sqrt{n}|n - 1\rangle \tag{2.14}$$

$$a^\dagger|n\rangle = \sqrt{n + 1}|n + 1\rangle. \tag{2.15}$$

The rewritten Hamiltonian is given by

$$\mathcal{H} = \hbar\omega\left(a^\dagger a + \frac{1}{2}\right), \tag{2.16}$$

where $a^\dagger a = N$ is the number operator which fulfils the eigenequation $N|n\rangle = n|n\rangle$ and $\frac{\hbar\omega}{2}$ is the zero-point energy of the LC-oscillator.

2.3 Transmission line

Transmission lines are one-dimensional waveguides and form an important part of circuit QED, since they provide channels for transmitting signals. They can also be used as quantum optical *reservoirs*, dissipatively removing energy from the system. They can be open systems, resonators, or semi-infinite systems with one shorted end. The differences are given by the boundary condition of the circuit configuration. We will first discuss the open transmission line and then describe possible boundary conditions.

In our system, a transmission line can be modelled with many coupled LC-oscillators, depicted in Fig 2.2 [132, 133]. The Lagrangian is given by the sum over the energies of all nodes,

$$\mathcal{L}_{TL} = \sum_n \left[\frac{1}{2}\Delta x C_0 \dot{\phi}_n^2 - \frac{1}{2}\frac{\left(\phi_n - \phi_{n-1}\right)^2}{\Delta x L_0}\right]. \tag{2.17}$$
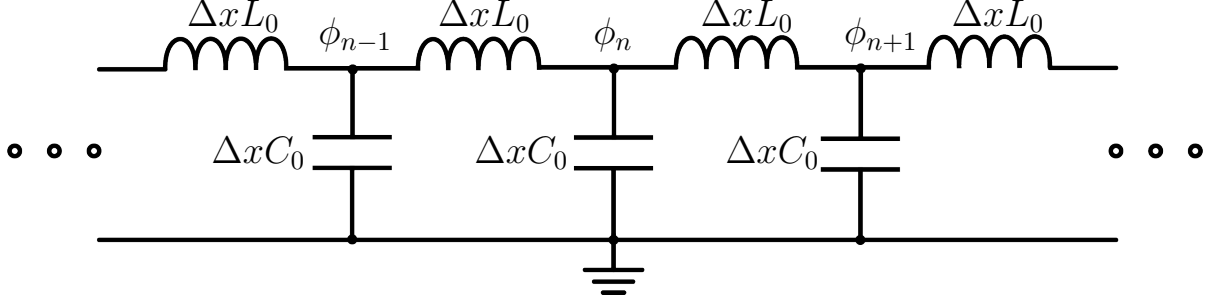
Figure 2.2: *Circuit configuration of an open transmission line. It consists of parallel grounded capacitors with capacitance C_0 per unit length Δx and inductors in series with inductance L_0 per unit length. The characteristic impedance of the transmission line is $Z_0 = \sqrt{L_0/C_0}$.*

Here, the capacitances C_0 and inductances L_0 are the capacitance and inductance per unit length since we start with a discrete circuit model. The transmission line has a characteristic impedance of $Z_0 = \sqrt{L_0/C_0}$, which gives the ratio of the amplitudes of current and voltage of a wave propagating along the TL and is given in the units of resistance. In the continuum limit $\Delta x \to 0$, the Lagrangian becomes

$$\mathcal{L}_{TL} = \int_{-\infty}^{\infty} \left[\frac{C_0}{2} \left(\frac{\partial \phi(x,t)}{\partial t} \right)^2 + \frac{1}{2L_0} \left(\frac{\partial \phi(x,t)}{\partial x} \right)^2 \right] \mathrm{d}x. \tag{2.18}$$

Now we can calculate the Euler-Lagrange equations of motion

$$\frac{\partial}{\partial t} \frac{\partial \mathcal{L}}{\partial \frac{\partial \phi}{\partial (t,x)}} - \frac{\partial \mathcal{L}}{\partial \phi} = 0. \tag{2.19}$$

For the Lagrangian (2.18) we arrive at two equations which can be combined to

$$\frac{\partial \phi^2(x,t)}{\partial t^2} - c^2 \frac{\partial \phi^2(x,t)}{\partial x^2} = 0. \tag{2.20}$$

This resembles the massless Klein-Gordon equation with velocity $c = 1/\sqrt{C_0 L_0}$. Alternatively, we obtain the same equation of motion by deriving the Hamiltonian and calculating the Heisenberg equations of motion. The conjugate momenta are charges given by

$$p_n = \frac{\partial \mathcal{L}}{\partial \dot{\phi}_n} = \Delta x C_0 \dot{\phi}_n \tag{2.21}$$

so the Hamiltonian becomes

$$\mathcal{H}_{TL} = \sum_n \left[\frac{1}{2} \frac{p_n^2}{\Delta x C_0} + \frac{1}{2} \frac{(\phi_n - \phi_{n-1})^2}{\Delta x L_0} \right] \tag{2.22}$$

and in the continuum limit

$$\mathcal{H}_{TL} = \int_{-\infty}^{\infty} \left[\frac{1}{2C_0} p^2(x,t) + \frac{1}{2L_0} \left(\frac{\partial \phi(x,t)}{\partial x} \right)^2 \right] \mathrm{d}x, \qquad (2.23)$$

where we introduced the flux field $\phi(x,t)$ and the charge density field $p(x,t)$. Now we quantise the system by promoting the generalised coordinates to operators which fulfil the commutation relations

$$[\phi(x,t), \phi(x',t)] = [p(x,t), p(x',t)] = 0 \qquad (2.24)$$

$$[\phi(x,t), p(x',t)] = i\hbar \delta(x-x'). \qquad (2.25)$$

We can solve the Klein-Gordon equation (2.20) by introducing the Fourier transform of the flux field and charge density field

$$\phi(x,t) = \frac{1}{\sqrt{2\pi}} \int_{-\infty}^{\infty} \phi(k,t) e^{ikx} \, \mathrm{d}k, \qquad (2.26)$$

$$p(x,t) = \frac{1}{\sqrt{2\pi}} \int_{-\infty}^{\infty} p(k,t) e^{ikx} \, \mathrm{d}k. \qquad (2.27)$$

The Klein-Gordon equation then becomes

$$\frac{\partial \phi^2(k,t)}{\partial t^2} + \omega_k^2 \phi(k,t) = 0, \qquad (2.28)$$

where we used the dispersion relation $\omega_k = ck$. We introduce creation and annihilation operators $a_k^\dagger, a_k$, which create and annihilate a mode with wave vector k, respectively. They obey the bosonic commutation relations

$$\left[a_k, a_{k'}^\dagger \right] = \delta \left(k - k' \right), \qquad (2.29)$$

$$[a_k, a_{k'}] = \left[a_k^\dagger, a_{k'}^\dagger \right] = 0, \qquad (2.30)$$

and have the dimension $1/\sqrt{k}$. We rewrite the flux and charge density in terms of these operators for every mode

$$\phi(k,t) = \sqrt{\frac{\hbar}{2C_0 \omega_k}} \left(a_{-k}^\dagger(t) + a_k(t) \right), \qquad (2.31)$$

$$p(k,t) = i\sqrt{\frac{\hbar C_0 \omega_k}{2}} \left(a_{-k}^\dagger(t) - a_k(t) \right). \qquad (2.32)$$

The flux field and charge density field in real space are given by

$$\phi(x,t) = \sqrt{\frac{\hbar}{4\pi C_0}} \int_{-\infty}^{\infty} \frac{1}{\sqrt{\omega_k}} \left(a_{-k}^{\dagger}(t) + a_k(t) \right) e^{ikx}\, \mathrm{d}k, \tag{2.33}$$

$$p(x,t) = i\sqrt{\frac{\hbar C_0}{4\pi}} \int_{-\infty}^{\infty} \sqrt{\omega_k} \left(a_{-k}^{\dagger}(t) - a_k(t) \right) e^{ikx}\, \mathrm{d}k. \tag{2.34}$$

Inserting this into the Hamiltonian (2.23) we obtain

$$\mathcal{H}_{TL} = \hbar \int_{-\infty}^{\infty} \omega_k \left(a_k^{\dagger} a_k + \frac{1}{2} \left[a_k, a_k^{\dagger} \right] \right) \mathrm{d}k \tag{2.35}$$

where the commutator $\frac{1}{2}\left[a_k, a_k^{\dagger}\right] = \frac{1}{2}\delta(0)$ gives the (infinite) sum over the zero point energies $\hbar\omega_k/2$ of all modes [134, 135].

2.3.1 Resonator

So far, we considered an open transmission line with free propagating electromagnetic waves. Now we want to restrict the propagation by considering a resonator. This can be achieved by shorting the transmission line ends to ground, which we demonstrate here. The circuit model and a sketch of the field of this configuration are depicted in Fig. 2.3. In this case, the field at both ends of the transmission line is zero. Hence, the field contains only modes that fulfil $\omega_n = n\pi c/L$, with $n \in \mathbb{Z}$, the length of the resonator L and the velocity of the electromagnetic waves inside the transmission line $c = 1/\sqrt{L_0 C_0}$. With this restriction, the Hamiltonian $\mathcal{H}_R$ of the resonator becomes

$$\mathcal{H}_R = \sum_n \hbar\omega_n \left(a^{\dagger}(\omega_n)a(\omega_n) + \frac{1}{2} \right), \tag{2.36}$$

where the operators now are dimensionless. If we only consider one mode in the field, we obtain the Hamiltonian of a single-mode quantum harmonic oscillator,

$$\mathcal{H} = \hbar\omega \left(a^{\dagger}a + \frac{1}{2} \right). \tag{2.37}$$
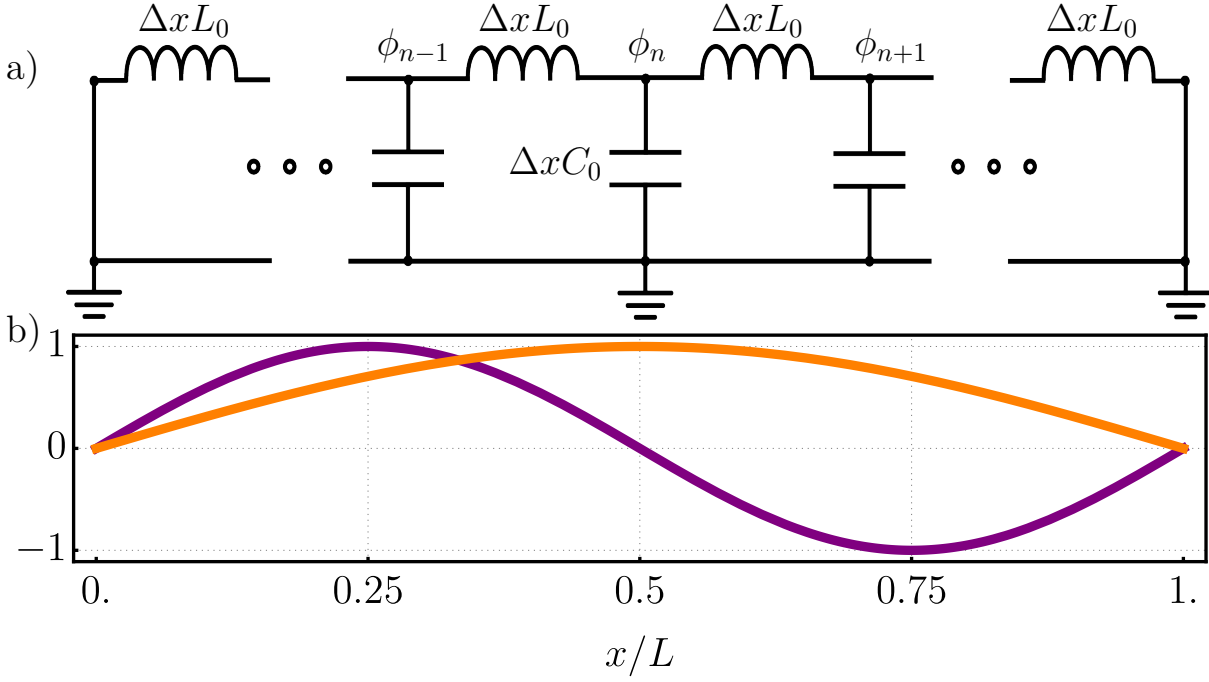
Figure 2.3: *a) Circuit model of a transmission line that is shorted to ground at both ends. By doing so the boundary conditions are restricted and the electromagnetic field has a node at the ends. b) Two modes of the field that fulfil the boundary condition.*

2.3.2 Semi-infinite transmission line

Now we consider the case where the transmission line is open on one side and shorted to ground on the other. The shorted end of the semi-infinite transmission line has the role of a mirror where the electromagnetic waves are reflected, and the value of the field is zero. The circuit model of a semi-infinite transmission line is depicted in Fig. 2.4. The field modes are still continuous but the massless Klein-Gordon equation (2.20) has to be solved with the boundary condition $\phi(x = x_0) = 0$, where the mirror is located at $x = x_0$. The solution, therefore, contains a sine function and is given by

$$\phi(x,t) = \sqrt{\frac{2}{\pi}} \int_0^\infty \phi(k,t) \sin k(x - x_0) \mathrm{d}k \qquad (2.38)$$

$$p(x,t) = \sqrt{\frac{2}{\pi}} \int_0^\infty p(k,t) \sin k(x - x_0) \mathrm{d}k, \qquad (2.39)$$

where $\phi(k,t)$ and $p(k,t)$ can again be written in terms of bosonic creation and annihilation operators, see Eq. (2.31)-(2.32). Using this, the field
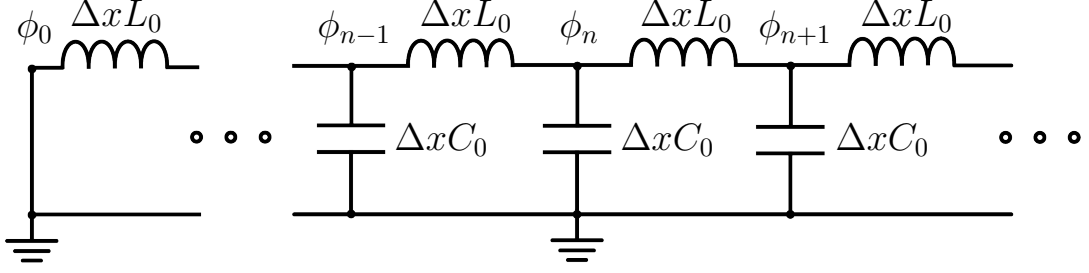
Figure 2.4: *A transmission line that is shorted to ground at one end. This end has the role of a mirror that reflects the electromagnetic waves in the transmission line.*

becomes

$$\phi(x,t) = \sqrt{\frac{\hbar}{\pi C_0}} \int_0^\infty \frac{1}{\sqrt{\omega_k}} \left(a_k^\dagger(t) + a_k(t) \right) \sin k(x - x_0) \mathrm{d}k, \qquad (2.40)$$

$$p(x,t) = i\sqrt{\frac{\hbar C_0}{\pi}} \int_0^\infty \sqrt{\omega_k} \left(a_k^\dagger(t) - a_k(t) \right) \sin k(x - x_0) \mathrm{d}k. \qquad (2.41)$$

In contrast to the open transmission line, the integral only goes from 0 to infinity because the right- and left-moving modes are connected by the mirror. We rewrite these expressions in terms of $\omega = ck$ and put it into the Hamiltonian

$$\mathcal{H}_{\mathrm{Mirror}} = \int_{-\infty}^{x_0} \left[\frac{1}{2C_0} p^2(x,t) + \frac{1}{2L_0} \left(\frac{\partial \phi(x,t)}{\partial x} \right)^2 \right] \mathrm{d}x$$

$$= \int_0^\infty \hbar\omega \left\{ a^\dagger(\omega) a(\omega) + \frac{1}{2} \right\} \mathrm{d}\omega. \qquad (2.42)$$

2.4 Artificial atoms

So far, we have investigated different set-ups of a one-dimensional transmission line that can act as different types of baths or cavities. Now we introduce emitters that can interact with the bath built of circuit elements. More specifically, we are interested in so-called artificial atoms or superconducting qubits with anharmonic energy spectra so they can mimic real atoms and be used as qubits. There are many types of superconducting qubits with different circuit configurations and properties [32, 35]. Some examples are the flux qubit, phase qubit or the one we will introduce, the transmon. The transmon is a charge qubit that consists of a Cooper pair box that is insensitive to charge noise [45]. In the following,
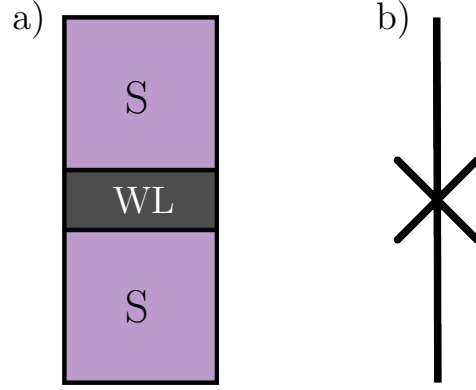
Figure 2.5: *a) A sketch of a Josephson junction. Two superconductors are separated by a weak link, where Cooper pairs can tunnel through. b) The electrical circuit symbol of a Josephson junction.*

we will explain the essential elements of a superconducting qubit, such as the Josephson junction and the simplest version of a superconducting charge qubit, a single Cooper-pair box (SCPB).

2.4.1 Josephson junction

The Josephson junction consists of two superconductors isolated by a weak link. The weak link can consist of a thin insulator, normal metal, or another superconductor [130, 136]. A sketch of a Josephson junction and the electrical circuit symbol are depicted in Fig. 2.5. The Cooper pairs can tunnel coherently through the insulator, leading to a current that varies with the phase difference $\varphi(t)$ across the junction,

$$I(t) = I_c \sin \varphi(t), \tag{2.43}$$

where I_c is the critical current.
The voltage across the junction is also given by the phase difference between the two superconducting leads

$$V(t) = \frac{2e}{\hbar} \frac{\partial \varphi(t)}{\partial t}. \tag{2.44}$$

Using this, we see that the phase difference between the two superconductors $\varphi(t)$ is given by the time integral of the voltage across the Josephson junction, which is also a magnetic flux,

$$\varphi(t) = \frac{2e}{\hbar} \int_0^t V(t')dt' = \frac{2e}{\hbar} \Phi = 2\pi \frac{\Phi}{\Phi_0}, \tag{2.45}$$

where $\Phi_0 = \frac{h}{2e}$ is the magnetic flux quantum. By comparing Eq. (2.43)-(3.41) to the general relation between the current and voltage of an inductor $\dot{I} = \frac{1}{L}V$,

$$\dot{I} = I_c \cos\varphi \frac{\partial\varphi}{\partial t} \tag{2.46}$$

$$= \frac{2\pi}{\Phi_0} I_c V \cos\varphi, \tag{2.47}$$

we find that a Josephson junction acts as a non-linear inductor with inductance

$$L_J = \frac{2\pi}{\Phi_0 I_c \cos\varphi}. \tag{2.48}$$

Now we calculate the energy that is accumulated in the Josephson junction

$$\begin{aligned} U &= \int_0^t I(t)V(t)\,\mathrm{d}t \\ &= \frac{\Phi_0}{2\pi}\int_0^t I(t)\frac{\partial\varphi}{\partial t}\,\mathrm{d}t \\ &= \frac{\Phi_0}{2\pi}\int_0^\varphi I_c \sin\varphi\,\mathrm{d}\varphi \\ &= E_J\left(1 - \cos\varphi\right) \end{aligned} \tag{2.49}$$

where we introduced the Josephson energy $E_J = \Phi_0 I_c / 2\pi$. We see that the Josephson junction has an anharmonic potential energy which opens the possibility to build an anharmonic circuit element to create an artificial atom.

The Lagrangian of a Josephson junction is given by

$$\mathcal{L}_{\mathrm{JJ}} = \frac{1}{2}C_J\dot{\Phi}^2 + E_J \cos\left(2\pi\frac{\Phi}{\Phi_0}\right), \tag{2.50}$$

where we omitted the constant term in the potential energy.

2.4.2 Single Cooper-pair box

The single Cooper-pair box (SCPB) is a simple and fundamental design for a superconducting qubit [44, 136]. It consists of a superconducting island with a number of n Cooper-pair charges connected through a Josephson junction to a superconducting electrode. The number of Cooper pairs on
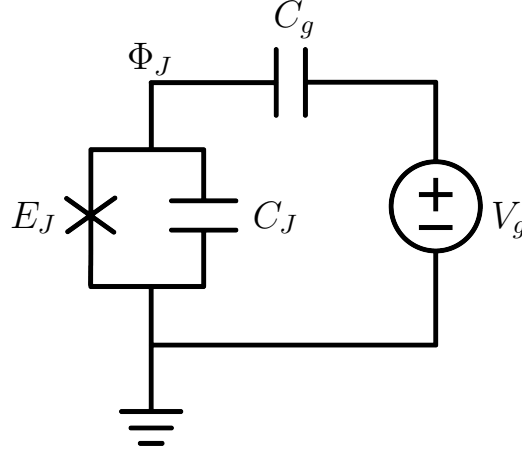
Figure 2.6: *Circuit model of a single Cooper-pair box. A Josephson junction with tunnel junction capacitance C_J and Josephson coupling energy E_J is coupled to a control gate voltage V_g through a gate capacitance C_g. A number n of Cooper pair charges sit on a superconducting island ("box") between the gate capacitor and the junction capacitance.*

the island can be controlled by a gate voltage connected to the island through a gate capacitance. A circuit model for a SCPB is depicted in Fig 2.6. The Lagrangian of the SCPB is given by

$$\mathcal{L}_{SCB} = \frac{1}{2} C_J \dot{\Phi}_J^2 + \frac{1}{2} C_g \left(\dot{\Phi}_J + V_g \right)^2 + E_J \cos \left(2\pi \frac{\Phi_J}{\Phi_0} \right). \qquad (2.51)$$

The conjugate momentum to the node flux is given by

$$q_J = \frac{\partial \mathcal{L}}{\partial \dot{\Phi}_J} = C_J \dot{\Phi}_J + C_g \left(\dot{\Phi}_J + V_g \right) = 2en, \qquad (2.52)$$

where $n = q_J/2e$ is the number of Cooper pairs on the island. The Hamiltonian becomes

$$\mathcal{H}_{\mathrm{SCB}} = 4E_C \left(n - n_g \right)^2 - E_J \cos \left(2\pi \frac{\Phi_J}{\Phi_0} \right), \qquad (2.53)$$

where $E_C = \frac{e^2}{2(C_g + C_J)}$ is the electron charging energy and $n_g = C_g V_g / 2e$ is the (possibly fractional) number of electron pairs that is induced on the island by the control gate. Now we quantize the Hamiltonian by promoting the number of Cooper pairs n and the node flux Φ_J to operators with commutation relation

$$\left[e^{i2\pi \frac{\hat{\Phi}_J}{\Phi_0}}, \hat{n} \right] = -e^{i2\pi \frac{\Phi_J}{\Phi_0}}. \qquad (2.54)$$
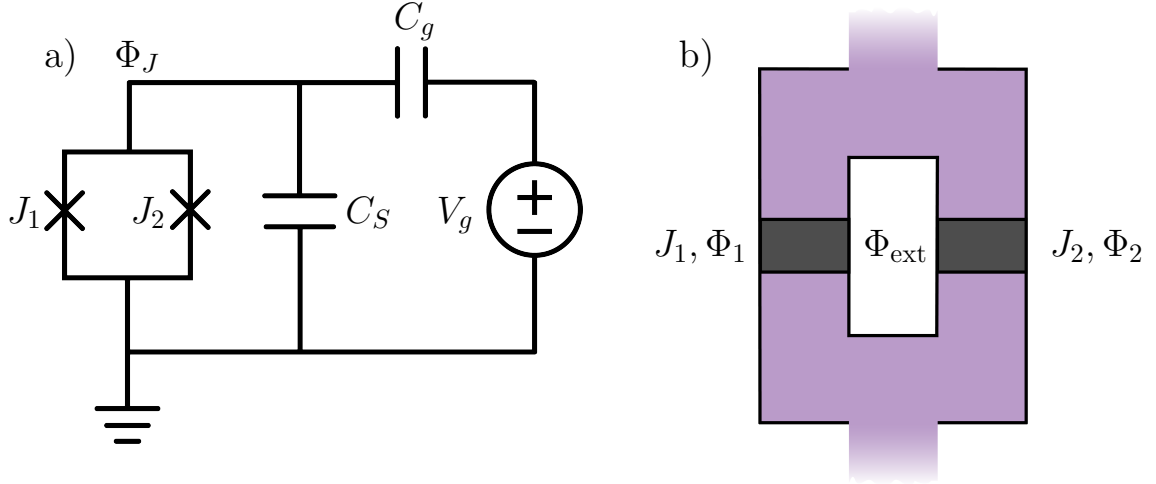
Figure 2.7: *a) Circuit model of a Transmon. A SQUID, consisting of two Josephson junctions J_1 and J_2, with an additional shunting capacitor C_S is coupled to a voltage source V_g through a gate capacitance C_g. b) Sketch of a SQUID. Two (here identical) Josephson junctions are connected in a loop. An external magnetic field induces a current in the SQUID and makes its energy controllable.*

In the charge basis $|n\rangle$ which are eigenstates of the number operator $\hat{n}$, $\hat{n}|n\rangle = n|n\rangle$, the Hamiltonian can be rewritten as follows [44, 135–137]

$$\mathcal{H}_{\text{SCB}} = \sum_n \left[4E_C \left(n - n_g\right)^2 |n\rangle\langle n| - \frac{1}{2}E_J \left(|n+1\rangle\langle n| + |n-1\rangle\langle n|\right) \right]. \tag{2.55}$$

With this Hamiltonian, we can calculate the energy spectrum of the SCPB. For the set-up we presented in this chapter, the charging energy E_C is usually much bigger than the Josephson energy E_J, leading to a charge-sensitive energy spectrum. We discuss this in more detail in the next section and present a charge-insensitive qubit, the *transmon*.

2.4.3 The transmon and the SQUID

The transmon is a charge-insensitive superconducting qubit which was first introduced by Koch *et al.* [45] in 2007. The transmon is a modified version of the SCPB described in the previous section. The main difference is an additional capacitance shunting the two superconductors, see Fig. 2.7 a). It is also important to mention that instead of only using one Josephson junction to create a superconducting island, the transmon often consists of a superconducting quantum interference device (SQUID), making the transition frequency tunable. A sketch of a SQUID is depicted

in Fig 2.7 b). By using a SQUID, the Josephson energy E_J can be manipulated through an external magnetic field, with flux Φ_{ext}, since the phases of the two Josephson junctions $\Phi_{1,2}$ depend on each other [42],

$$\Phi_1 - \Phi_2 + \Phi_{\text{ext}} = n\Phi_0, \tag{2.56}$$

where the integer number n is the number of flux quanta in the loop. The total potential energy of a SQUID (with two identical Josephson junctions) becomes

$$U = -E_{J_1} \cos\left(2\pi\frac{\Phi}{\Phi_0} + \pi\frac{\Phi_{\text{ext}}}{\Phi_0}\right) - E_{J_2} \cos\left(2\pi\frac{\Phi}{\Phi_0} - \pi\frac{\Phi_{\text{ext}}}{\Phi_0}\right) \tag{2.57}$$

$$= -E_J(\Phi_{\text{ext}}) \cos\left(2\pi\frac{\Phi}{\Phi_0}\right), \tag{2.58}$$

where $E_J(\Phi_{\text{ext}}) = 2E_{J_1} \cos\left(\pi\frac{\Phi_{\text{ext}}}{\Phi_0}\right)$ is the tunable Josephson energy. Using a SQUID instead of a single Josephson junction leads to the same Hamiltonian (2.53) but with a tunable Josephson energy. However, the important element in the transmon that leads to reducing the sensitivity to charge noise is the additional shunting capacitance, as mentioned before. With this capacitance, the charging energy $E_C = e^2/2C_\Sigma, C_\Sigma = C_J + C_g + C_S$ can be made small compared to the Josephson energy E_J. Both energies are now engineerable, and the ratio E_J/E_C can be manipulated. Both the anharmonicity of the qubit and the sensitivity to charge noise depend on this ratio. In Fig 2.8 we show the energy spectrum of the transmon as a function of the gate charge n_g. One can clearly see the reduction of sensitivity to fluctuations in gate charge by increasing the ratio E_J/E_C, since the energy levels become flat. The anharmonicity of the energy levels decreases too, but it is still sufficient that the transmon can be used as a qubit.

In the limit of small excitation amplitude $|\Phi_J/\Phi_0| \ll 1$ and $E_J \gg E_C$, where the zero point fluctuations are small, the transmon can be approximated as a harmonic oscillator [130], where we expand the cosine term of the potential for small Φ_J,

$$\mathcal{H} = \frac{1}{2C_\Sigma}q_j^2 - E_J \cos\left(2\pi\frac{\Phi_J}{\Phi_0}\right)$$

$$\approx \frac{1}{2C_\Sigma}q_j^2 + \frac{1}{2L_J}\Phi_J^2, \tag{2.59}$$
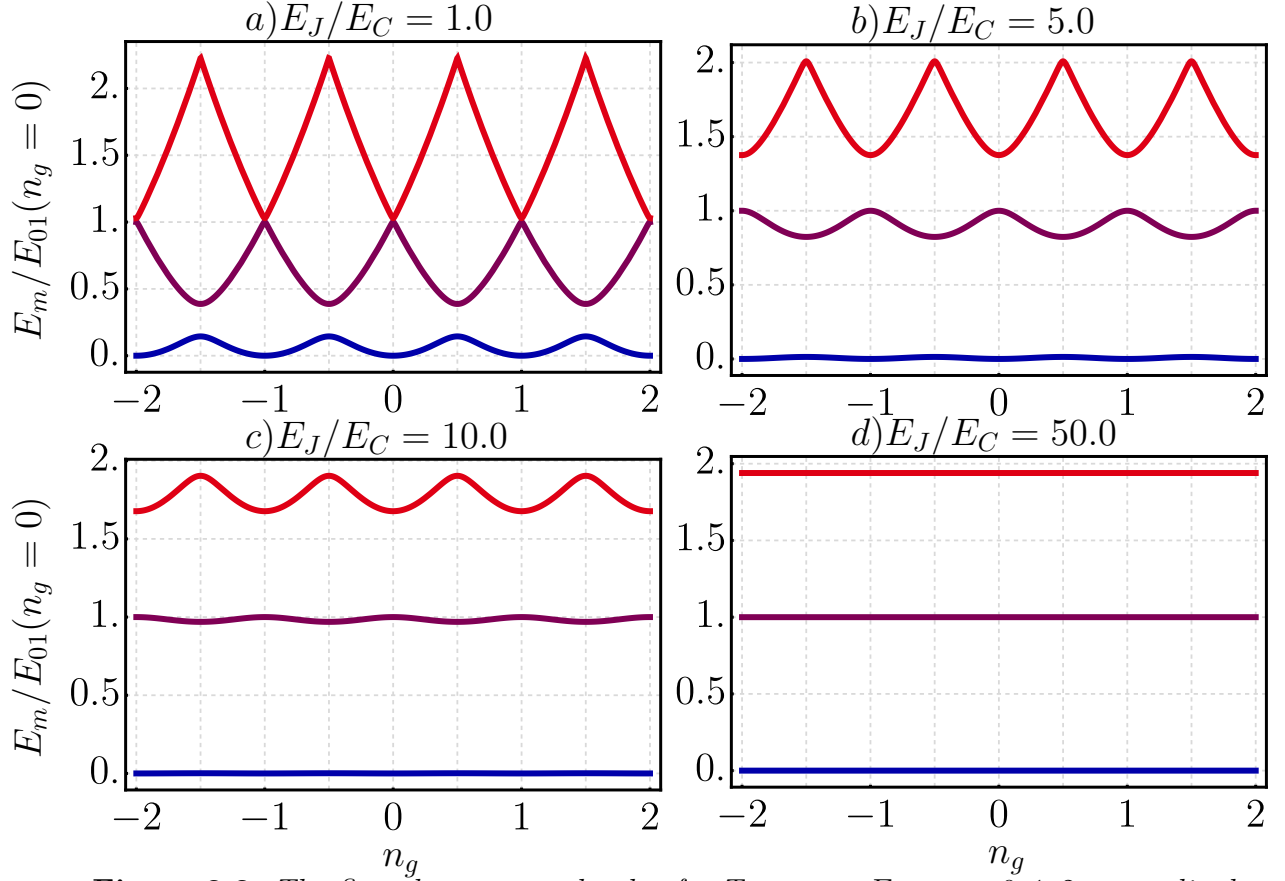
Figure 2.8: *The first three energy levels of a Transmon E_m, $m = 0, 1, 2$ normalised by the energy of the first transition E_{01} at $n_g = 0$ as a function of the charge noise n_g. The sensitivity to charge noise clearly decreases by increasing E_J/E_C.*

where $L_J = \left(\frac{\hbar}{2e}\right)^2 \frac{1}{E_J}$ is the effective inductance of the oscillator. The frequency

$$\Omega_J = \frac{1}{\sqrt{C_\Sigma L_J}} = \frac{1}{\hbar}\sqrt{8E_J E_C} \tag{2.60}$$

is the resonance frequency of the harmonic oscillator and the transition frequency from the ground state to the first excited state of the transmon.

3 Transmon coupled to a microwave transmission Line

In chapter 2 we introduced the quantization of electrical circuits. We discussed elements of a circuit, such as transmission lines with different boundary conditions, which can be viewed as reservoirs. We also introduced the circuit equivalent of an atom, superconducting qubits. In the following, we investigate the combination of these two elements: A superconducting transmon qubit coupled to both open and semi-infinite TL's, which has been the subject of all our articles. Especially in Paper I and III, we investigate the dynamics of a transmon qubit coupled to a 1D TL derived from the circuit model. We investigate transient and steady-state dynamics of an initially excited transmon qubit and scattering at a transmon both in the low and high impedance regime. To investigate the dynamics of a transmon in a semi-infinite TL (atom in front of a mirror), we take time-delay effects, given by the distance to the mirror, into account. In the following, we derive the equations of motion for the circuit model used in Paper I and III and discuss some of the main results.

3.1 Circuit QED model

The system we investigate in Paper I and III consists of a transmon coupled to a 1D semi-infinite transmission line. A sketch of the system is depicted in Fig 3.1. The Hamiltonian of the system is given by the sum of all capacitive and inductive energies,

$$H(\phi_i, p_i) = \frac{1}{2C_0 \Delta x} \sum_{n \neq 0} p_{n \neq 0}^2(t) + \frac{1}{2C_c} p_0^2(t) + \frac{1}{2C_J} \left[p_J(t) + p_0(t) \right]^2 +$$

$$+ \frac{1}{2L_0 \Delta x} \sum_{-\infty}^{N} \left[\phi_{n+1}(t) - \phi_n(t) \right]^2 - E_J \cos \left[\frac{2e}{\hbar} \phi_J(t) \right]. \qquad (3.1)$$

The Hamiltonian is a function of the generalized coordinates: ϕ_i, the node fluxes and p_i, the node charges. For details on how to derive the

23
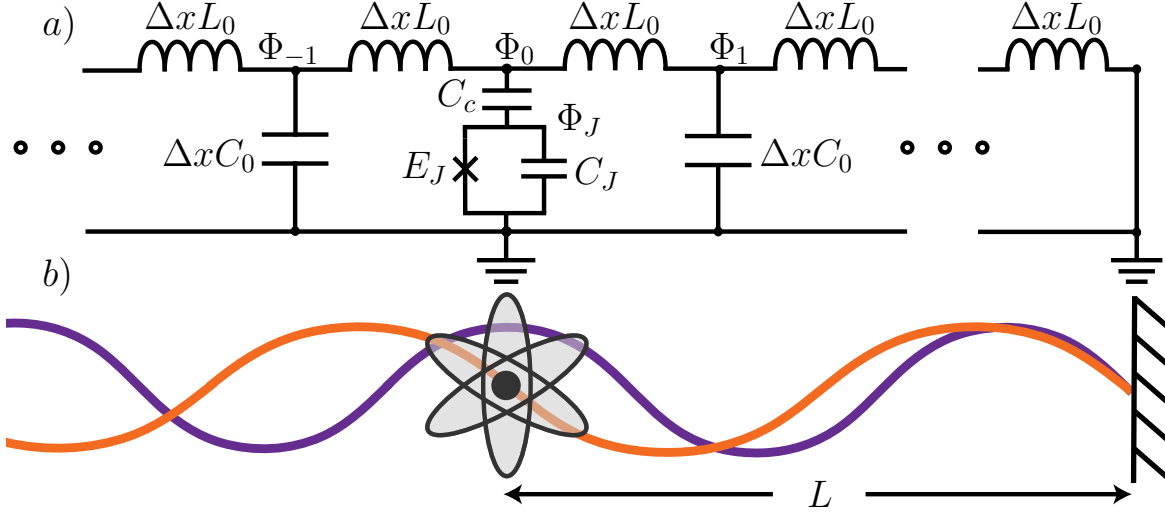
Figure 3.1: *a)Circuit model of a transmon coupled to a 1D-TL by a coupling capacitance C_c. The TL is grounded at one end. The inductive energy, flux and capacitance of the transmon are denoted by E_J, Φ_J and C_J, respectively. The TL is modelled by LC oscillators with capacitance $\Delta x C_0$ and inductance $\Delta x L_0$. The flux of the nodes between the LC-oscillators are denoted by Φ_n. b) Sketch of the system. It depicts an atom in front of a mirror. The distance $L = Tv/2$ to the mirror with respect to the electromagnetic field can be changed, which makes it possible to either enhance or suppress the coupling to the semi-infinite TL.*

Hamiltonian, see chapter 2. We now promote the generalized coordinates to operators that fulfil the canonical commutation relations

$$[\phi_i, p_j] = i\hbar\delta_{i,j}, \tag{3.2}$$

$$[\phi_i, \phi_j] = [p_i, p_j] = 0, \tag{3.3}$$

and calculate the Heisenberg equations of motion

$$\frac{\mathrm{d}}{\mathrm{d}t}A(t) = \frac{i}{\hbar}[H, A(t)] + \frac{\partial A(t)}{\partial t}, \tag{3.4}$$

where $A(t)$ is an arbitrary time-dependent operator. However, our considered variables do not explicitly depend on time, and the last term of Eq (3.4) vanishes. The equations of motion at the coupling point x_0, where the Transmon is coupled to the TL, become

$$\partial_t\phi_0(t) = \frac{C_c + C_J}{C_c C_J}p_0(t) + \frac{1}{C_J}p_J(t), \tag{3.5}$$

$$\partial_t\phi_J(t) = \frac{1}{C_J}\left(p_J(t) + p_0(t)\right), \tag{3.6}$$

$$\partial_t p_J(t) = -E_J \frac{2e}{\hbar} \sin\left(\frac{2e}{\hbar}\phi_J(t)\right),$$ (3.7)

$$\partial_t p_0(t) = \frac{1}{L_0 \Delta x}\left(-2\phi_i(t) + \phi_{i+1}(t) + \phi_{i-1}(t)\right).$$ (3.8)

These are discrete equations of motion since they are derived from a discrete circuit model. We want to make these equations continuous by taking the limit $\Delta x \to 0$. Eq. (3.5)-(3.7) remain unchanged, but Eq. (3.8) can be rewritten as

$$\begin{aligned}
\partial_t p_0(t) &= \lim_{\Delta x \to 0} \frac{1}{L_0 \Delta x}\left(-2\phi(x_0,t) + \phi(x_0 + \Delta x, t) + \phi(x_0 - \Delta x, t)\right)\\
&= \lim_{\Delta x \to 0} \frac{1}{L_0}\left(\frac{\phi(x_0 + \Delta x, t) - \phi(x_0, t)}{\Delta x} - \frac{\phi(x_0, t) - \phi(x_0 - \Delta x, t)}{\Delta x}\right)\\
&= \frac{1}{L_0}\left(\partial_x \phi(x_0^+, t) - \partial_x \phi(x_0^-, t)\right),
\end{aligned}$$ (3.9)

where we identified the two terms of the second row as first-order spatial derivatives. $\phi(x_0^+, t)$ denotes the flux field on the right side of the qubit, and $\phi(x_0^-, t)$ denotes the field on the left side of the qubit.

3.1.1 Linearisation of the Qubit

One important step we take to simplify our system is the linearisation of the qubit. As we showed in section 2.4, the Transmon has an anharmonic energy spectrum. In the limit $E_J \gg E_C$, the energy spectrum is only slightly anharmonic and can be approximated by a harmonic oscillator. However, we want to treat the Transmon as a qubit, where only the first two energy levels are considered. In general, one has to be careful not to drive the qubit too strongly so that the higher energy levels are not affected. In our case, we work in the single excitation regime without driving, where the qubit can indeed be treated as a harmonic oscillator. To linearise the qubit, we expand the potential energy up to second order:

$$\begin{aligned}
\mathcal{V}(\phi_J) &= -E_J \cos\left(\frac{2e}{\hbar}\phi_J\right)\\
&\approx \frac{\phi_J^2}{2L_J},
\end{aligned}$$ (3.10)

similar as in Eq. (2.59) with the inductance $L_J = \frac{\hbar^2}{4e^2 E_J}$. In the last line, we neglected the constant term of the potential energy. Making this
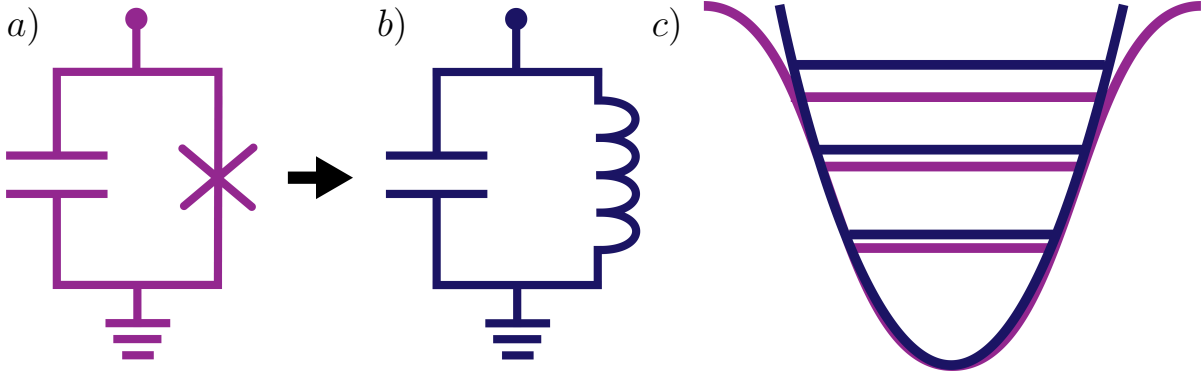
Figure 3.2: *Linearisation of the qubit means that the transmon, a), is replaced by a harmonic LC-oscillator, b). c) Anharmonic potential of the transmon and harmonic potential of the LC-oscillator. The horizontal lines denote the energy levels.*

approximation means we replace the non-linear Josephson junction in the circuit with an inductive element, see Fig 3.2. After the linearization, Eq (3.7) becomes

$$\partial_t p_J(t) = -\frac{1}{L_J}\phi_J(t) \tag{3.11}$$

and we obtain a new set of differential equations for the generalized coordinates at the coupling point

$$\partial_t \phi_0(t) = \frac{C_c + C_J}{C_c C_J}p_0(t) + \frac{1}{C_J}p_J(t), \tag{3.12}$$

$$\partial_t \phi_J(t) = \frac{1}{C_J}(p_J(t) + p_0(t)), \tag{3.13}$$

$$\partial_t p_J(t) = -\frac{1}{L_J}\phi_J(t), \tag{3.14}$$

$$\partial_t p_0(t) = \frac{1}{L_0}\left(\partial_x \phi(x^+, t) - \partial_x \phi(x^-, t)\right). \tag{3.15}$$

3.2 Impedance of the transmission line

In Paper I and Paper III, we investigate a transmon coupled to a (semi-infinite) TL in different impedance regimes. In Paper I, we assumed that the TL's characteristic impedance is small compared to the transmon's characteristic impedance, which is usually the case. However,
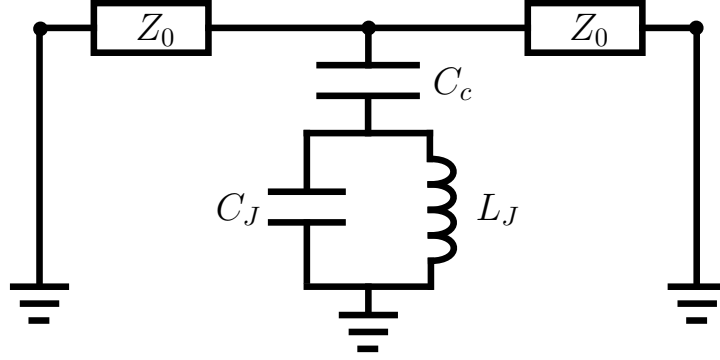
Figure 3.3: *Effective circuit model of a transmon coupled to an open TL. The transmon is replaced by an LC-oscillator with capacitance C_J and inductance L_J and is coupled to the TL via a coupling capacitance C_c. The transmission line is represented by its characteristic impedance Z_0.*

we found that the system behaviour changes drastically in the high-impedance regime, which we investigate further in Paper III. In the following, we want to discuss the regimes of low and high impedance and show how it affects the system dynamics in the following sections.

A convenient way to discuss the impedance of the TL is by introducing an effective circuit model, where a harmonic LC-oscillator (representing the linearised transmon) is coupled to an open TL represented by its characteristic impedance $Z_0 = \sqrt{L_0/C_0}$, see Fig. 3.3. The transmon is replaced by an LC-oscillator with capacitance C_J, inductance L_J and characteristic impedance

$$Z_J = \sqrt{\frac{L_J}{C_J}} = R_Q \sqrt{\frac{2E_C}{E_J}}, \tag{3.16}$$

where $E_C = e^2/(2C_J)$ is the charging energy of the transmon and $R_Q = \hbar/(2e)^2 \approx 1.0\,\mathrm{k\Omega}$. We consider an undriven initially excited oscillator whose emitted photons can escape to both sides of the transmission line, which are represented by parallel-connected resistors. In the following, we want to discuss the behaviour of the system demonstrated in Fig. 3.3 by comparing the impedance of the transmission line Z_0 to the characteristic impedance of the LC-oscillator Z_J. If $Z_0/Z_J \ll 1$, the coupling capacitance C_c is grounded and the system describes an undamped oscillator with resonance frequency $\omega_0 = 1/\sqrt{L_J(C_J + C_c)}$. On the other hand, if we consider the opposite case $Z_0/Z_J \gg 1$, we find an undamped oscillator with resonance frequency $\omega_J = 1/\sqrt{L_J C_J}$. A common transmission line has an impedance of $Z_0 \approx 50\,\Omega$ and the impedance of a transmon is

given by $Z_J \approx \sqrt{2}\,k\Omega/\sqrt{E_J/E_C}$. The ratio E_J/E_C does usually not exceed $E_J/E_C \approx 100$, so usually we can assume that $Z_0/Z_J \leq 1$, but it has a finite value. However, the high-impedance regime has recently become accessible [105] which opens the possibility to investigate new physics. We are interested in the dissipated energy since it gives an insight into the linearised transmon's properties, more specifically, its decay rate. The decay rate is defined by the energy dissipation of the LC-oscillator,

$$E(t) = E(0)e^{-\gamma t}, \tag{3.17}$$

where $E(0)$ is the initial energy of the LC oscillator. In Paper I, we derive a general expression for the decay rate

$$\gamma = \frac{2}{Z_0 C_J}\frac{\eta}{1+\eta}, \quad \eta = \omega^2 \frac{Z_0^2 C_c^2}{4}\frac{C_J}{C_J + C_c}. \tag{3.18}$$

In the low-impedance regime, we find $\eta < 1$ and by using that the resonance frequency of the coupled qubit is given by $\omega_0 = 1/\sqrt{L_J(C_J + C_c)}$, the decay rate becomes

$$\gamma_0 = \frac{Z_0}{2L_J}\frac{C_c^2}{(C_J + C_c)^2}. \tag{3.19}$$

In the high-impedance regime, the decay rate becomes

$$\gamma_J = \frac{2}{Z_0 C_J}, \tag{3.20}$$

which interestingly does not depend on the coupling capacitance C_c any more, and in contrast to γ_0, it decreases by increasing Z_0. The reason for this is that if the TL impedance is high, the amount of current flowing through the TL is small and can not significantly change the voltage on the coupling capacitance C_c. Furthermore, the resonance frequency of the qubit changes to $\omega_J = 1/\sqrt{L_J C_J}$, which is the resonance frequency of the uncoupled LC-oscillator.

In the following sections, we investigate the field inside the TL for an open TL and a semi-infinite TL, calculate the qubit's reflection, and investigate spontaneous emission concerning low- and high-impedance regimes.

3.3 Field inside the transmission line

Now we take a closer look at the field inside the transmission line. The presence of the mirror creates a boundary condition where the microwaves can not propagate freely. We want to get a close insight into how the mirror's presence affects the qubit dynamics. Therefore, we derive the equations of motion for the field and formulate boundary conditions. Additionally, we are interested in the scattering on the transmon in an open TL, which is why we express the field in terms of the charge at the coupling point of the transmon. From the reflection coefficient, we can get a closer insight into the atom's properties for the different impedance regimes.

Similar to the previous chapter, the Heisenberg equations of motion of the transmission line part of the Hamiltonian 3.1 are given by

$$\partial_t \phi_n(t) = \frac{1}{C_0 \Delta x} p_n(t), \tag{3.21}$$

$$\partial_t p_n(t) = \frac{1}{L_0 \Delta x} \left(-2\phi_n(t) + \phi_{n+1}(t) + \phi_{n-1}(t) \right). \tag{3.22}$$

Again we apply the continuous limit by defining the flux field $\phi(x_n) = \phi_n(t)$ and charge density field $p(x_n, t) = p_n(t)/\Delta x$ with the spatial coordinates $x_n = n\Delta x$. In the continuum limit $\Delta x \to 0$, giving $x_n \to x$, Eq. (3.21) and (3.22) become

$$\partial_t \phi(x, t) = \frac{1}{C_0} p(x, t), \tag{3.23}$$

$$\partial_t p(x, t) = \lim_{\Delta x \to 0} \frac{1}{L_0 \Delta x} (-2\phi(x, t) + \phi(x + \Delta x, t) + \phi(x - \Delta x, t))$$

$$= \lim_{\Delta x \to 0} \frac{1}{\Delta x L_0} \left(\frac{\phi(x + \Delta x, t) - \phi(x, t)}{\Delta x} - \frac{\phi(x, t) - \phi(x - \Delta x, t)}{\Delta x} \right)$$

$$= \frac{1}{L_0} \partial_x^2 \phi(x, t), \tag{3.24}$$

where we identified the terms in the second row of Eq. (3.24) as second spatial derivatives. As we already showed in section 2.3, $\phi(x, t)$ and $p(x, t)$ obey the massless Klein-Gordon equation

$$\left(\partial_t^2 - c^2 \partial_x^2 \right) \phi(x, t) = 0, \tag{3.25}$$

with the velocity $c = 1/\sqrt{L_0 C_0}$ inside the transmission line. We write the

solution in terms of right ($\rightarrow$) and left ($\leftarrow$) moving terms

$$\phi^{\rightleftarrows}(x,t) = \sqrt{\frac{\hbar}{4\pi C_0}} \int_0^\infty \frac{\mathrm{d}k}{\sqrt{\omega_k}} \left(a_k^{\rightleftarrows} e^{-i(\omega_k t \mp kx)} + \text{h.c.} \right), \qquad (3.26)$$

and the corresponding expression for the charge density field

$$p^{\rightleftarrows}(x,t) = i\sqrt{\frac{\hbar C_0}{4\pi}} \int_{-\infty}^\infty \mathrm{d}k \sqrt{\omega_k} \left(a_k^{\rightleftarrows} e^{-i(\omega_k t \mp kx)} - \text{h.c.} \right), \qquad (3.27)$$

where $a_k^\dagger$ and a_k are creation and annihilation operators that create or annihilate a photon with wave vector k, respectively. They fulfil the commutation relations

$$\left[a_k, a_{k'}^\dagger \right] = \delta\left(k - k'\right), \qquad (3.28)$$

$$\left[a_k, a_{k'} \right] = \left[a_k^\dagger, a_{k'}^\dagger \right] = 0. \qquad (3.29)$$

We can rewrite the solutions in terms of frequencies ω, and we obtain

$$\phi^{\rightleftarrows}(x,t) = \sqrt{\frac{\hbar Z_0}{4\pi}} \int_0^\infty \frac{\mathrm{d}\omega}{\sqrt{\omega}} \left(a_\omega^{\rightleftarrows} e^{-i(\omega t \mp k_\omega x)} + \text{h.c.} \right), \qquad (3.30)$$

where $k_\omega = \omega/c$. In order to be able to formulate boundary conditions for the field inside the semi-infinite transmission line, we calculate the voltage $V(x,t) = \partial_t \phi(x,t)$,

$$V^{\rightleftarrows}(x,t) = -i\sqrt{\frac{\hbar Z_0}{4\pi}} \int_0^\infty \mathrm{d}\omega \sqrt{\omega} \left(a_\omega^{\rightleftarrows} e^{-i(\omega t \mp k_\omega x)} - \text{h.c.} \right) \qquad (3.31)$$

and similarly, the current $I(x,t) = \partial_x \phi(x)/L_0$,

$$I^{\rightleftarrows}(x,t) = -i\sqrt{\frac{\hbar}{4\pi Z_0}} \int_0^\infty \mathrm{d}\omega \sqrt{\omega} \left(a_\omega^{\rightleftarrows} e^{-i(\omega t \mp k_\omega x)} - \text{h.c.} \right). \qquad (3.32)$$

We find the relation between the voltage and the current

$$I^{\rightleftarrows}(x,t) = \frac{V^{\rightleftarrows}(x,t)}{Z_0}. \qquad (3.33)$$

Now we take a look at the voltage V_0 at the coupling point x_0. Since the voltage is continuous, it can be written as the sum of the ingoing V^{in} and
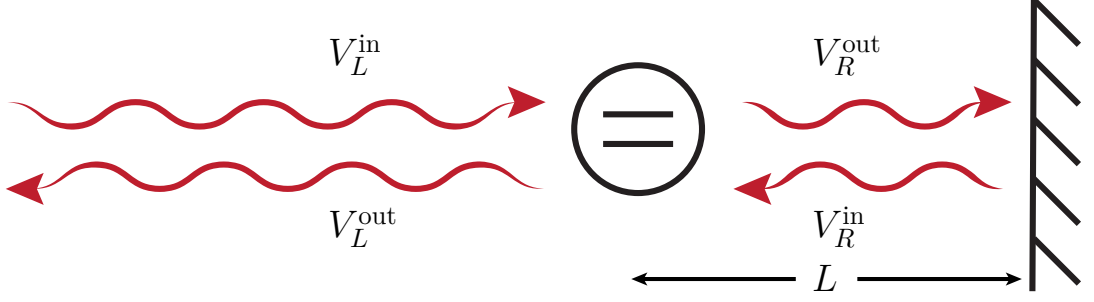
Figure 3.4: *Sketch of an atom in front of a mirror with all different field components represented by the voltage $V_{L/R}^{in/out}$ in the TL. The mirror couples the incoming and outgoing fields on the right side of the qubit to each other according to $V_R^{in}(t) = -V_R^{out}(t-T)$, where $T = 2L/v$ is the propagation time of the electromagnetic waves from the atom to the mirror and back. The fields depicted in the sketch also represent the fields for an open TL but with different boundary conditions that are further explained in the main text.*

outgoing V^{out} voltage field on the left (L) and the right (R) sides of the qubit

$$V_0(t) = V_L^{\text{in}}(t) + V_L^{\text{out}}(t) = V_R^{\text{in}}(t) + V_R^{\text{out}}(t) = \partial_t \phi_0(t), \qquad (3.34)$$

where $V_L^{\text{in}} = V^{\rightarrow}(0^-,t)$, $V_L^{\text{out}} = V^{\leftarrow}(0^-,t)$, $V_R^{\text{in}} = V^{\leftarrow}(0^+,t)$ and $V_R^{\text{out}} = V^{\rightarrow}(0^+,t)$ are the in- and out-going voltage fields at the left (L) and right $R)$ side of the coupling point, respectively and ϕ_0 is the flux field at the coupling point. A sketch of the different components of the field inside the TL is depicted in Fig. 3.4. In the following, we investigate the connection between the field in the TL and the transmon degrees of freedom for two different cases: An open TL and a semi-infinite TL with a mirror.

3.3.1 Open TL

From now on, we treat the fields and charges in our circuit as averages, $\bar{p}_0(t) = \langle p_0(t) \rangle$, $\bar{p}_J(t) = \langle p_J(t) \rangle$, which allows us to solve the equations of motion of the system semi-classical. For simplification, we drop the bar from the average variables in the following. Since we consider an initially excited atom with no external driving, we assume that the average incoming vacuum field to the transmon is zero: i.e., $\langle V_L^{\text{in}} \rangle = \langle V_R^{\text{in}} \rangle = 0$. With these assumptions, we find from Eq. (3.34) that the outgoing fields to the left and the right are equal,

$$V_0(t) = V_L^{\text{out}}(t) = V_R^{\text{out}}(t) = \partial_t \phi_0(t). \qquad (3.35)$$

Using that the current inside the TL is conserved, we find

$$I_0 = \partial_t p_0(t) = \frac{1}{Z_0}(V_{\text{in}} - V_{\text{out}}) \tag{3.36}$$

$$= -\frac{1}{Z_0}\left(V_L^{\text{in}} + V_R^{\text{in}} - V_L^{\text{out}} - V_R^{\text{out}}\right) \tag{3.37}$$

and finally, arrive at a new set of equations of motion for average system variables of the transmon coupled to an open TL in terms of the microwave fields inside the TL

$$\partial_t \phi_J(t) = \frac{1}{C_J}(p_J(t) + p_0(t)), \tag{3.38}$$

$$\partial_t p_J(t) = -E_J \frac{2e}{\hbar} \sin(\frac{2e}{\hbar}\phi_J(t)) \approx -\frac{\phi_J(t)}{L_J}, \tag{3.39}$$

$$\frac{C_c + C_J}{C_c C_J} p_0(t) + \frac{1}{C_J} p_J(t) + \frac{Z_0}{2} \partial_t p_0(t) = V_L^{\text{in}}(t) + V_R^{\text{in}}(t), \tag{3.40}$$

$$V_{L/R}^{\text{out}}(t) = V_{R/L}^{\text{in}}(t) - \frac{Z_0}{2}\partial_t p_0(t). \tag{3.41}$$

3.3.2 Semi-infinite TL

Since the mirror is located on the right side, see Fig. 3.1, the incoming field on the right side of the qubit is given by the reflected field at the mirror. Therefore, we can write it in terms of the outgoing field on the right side with a time delay T,

$$V_R^{\text{in}}(t) = \pm V_R^{\text{out}}(t - T), \tag{3.42}$$

where the delay-time $T = 2L/v$ is the time it takes for the microwaves to travel to the mirror and back. The sign is determined by the type of mirror, where the negative sign belongs to the shorted end that we consider. With the boundary condition above (3.42), the equations of motion of the transmon coupled to an open TL (3.38)-(3.41) can be easily modified for a transmon in front of a mirror

$$\partial_t \phi_J(t) = \frac{1}{C_J}(p_J(t) + p_0(t)), \tag{3.43}$$

$$\partial_t p_J(t) = -E_J \frac{2e}{\hbar} \sin(\frac{2e}{\hbar}\phi_J(t)) \approx -\frac{\phi_J(t)}{L_J}, \tag{3.44}$$

$$\frac{C_c + C_J}{C_c C_J} p_0(t) + \frac{1}{C_J} p_J(t) + \frac{Z_0}{2} \partial_t \left(p_0(t) \mp p_0(t - T) \right) = V_L^{\text{in}}(t) \mp V_L^{\text{in}}(t - T),$$
$$(3.45)$$

$$V_{L/R}^{\text{out}}(t) = V_{R/L}^{\text{in}}(t) - \frac{Z_0}{2} \partial_t p_0(t). \tag{3.46}$$

These are time-delay differential equations that make the solution non-trivial. However, due to the linearization of the qubit, we can find a solution by Fourier and Laplace transforms, as we will demonstrate in the following.

3.4 Scattering at the transmon

3.4.1 Open TL

After having derived the equations of motion for the transmon coupled to an open TL, we can calculate the reflection of an incoming field on the transmon. We assume that the incoming field comes from the left side of the transmon (and no incoming field from the right side $V_R^{\text{in}} = 0$), so the reflection coefficient is given by the ratio of the outgoing and the ingoing field on the left side

$$r = \frac{V_L^{\text{out}}}{V_L^{\text{in}}}. \tag{3.47}$$

To find an explicit expression for the reflection coefficient, we simply Fourier transform the equations of motion (3.38)-(3.41),

$$-i\omega p_0 = \frac{V_L^{\text{in}} - V^{\text{out}}}{Z_0}, \tag{3.48}$$

$$V_L^{\text{in}} + V_L^{\text{out}} = \frac{C_c + C_J}{C_c C_J} p_0 + \frac{1}{C_J} p_J, \tag{3.49}$$

$$i\omega p_J = \frac{1}{L_J} \phi_J, \tag{3.50}$$

$$-i\omega \phi_J = \frac{1}{C_J} \left(p_0 + p_J \right). \tag{3.51}$$

Using that $V_L^{\text{out}} = (V^{\text{out}} - V_L^{\text{in}})/2$, we find

$$r(\omega) \equiv \frac{V_L^{\text{out}}(\omega)}{V_L^{\text{in}}(\omega)} = \frac{C_c Z_0 \omega \left(\frac{\omega^2}{\omega_J^2} - 1 \right)}{2i \left(1 - \frac{\omega^2}{\omega_0^2} \right) + C_c Z_0 \omega \left(\frac{\omega^2}{\omega_J^2} - 1 \right)}. \tag{3.52}$$

a)

b)
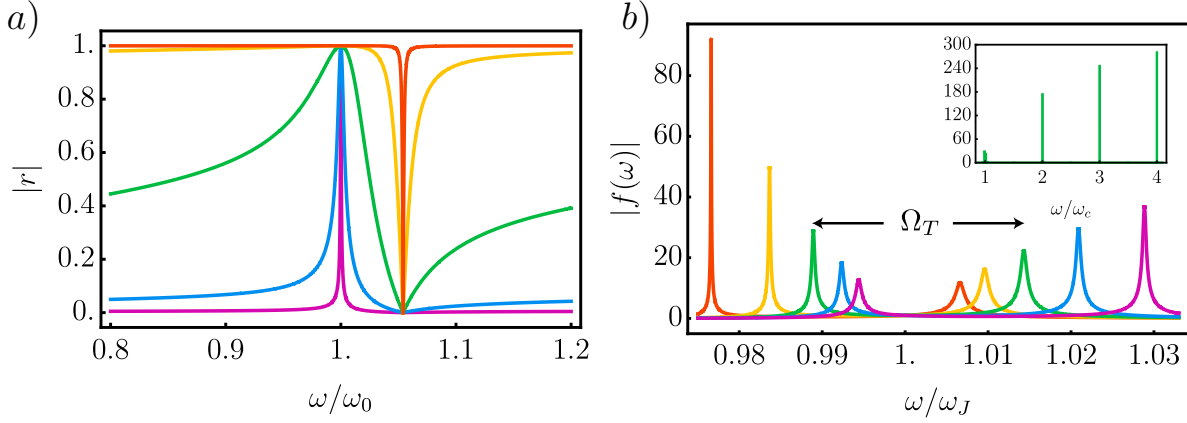
Figure 3.5: *a) Reflection $|r|$ of a transmon in an open TL as a function of the probe frequency ω/ω_0 for different values of the ratio of the TL and qubit impedance Z_0/Z_J. The coupling capacitance is kept constant at $\frac{C_c}{C_c+C_J} = 0.1$ for all curves and the different colours show: $Z_0/Z_J = 0.1$ (purple), $Z_0/Z_J = 1$ (blue), $Z_0/Z_J = 10$ (green), $Z_0/Z_J = 100$ (yellow), and $Z_0/Z_J = 1000$ (red).*
b) Amplitude of the Field between the transmon and the mirror $|f(\omega)| = |V_R^{out}(\omega)/V_L^{in}(\omega)|$ for $\frac{C_c}{C_J} = 0.1$ and $Z_0/Z_J = 1000$ and $T = 2\pi n/\omega_c, n = 1$. The different colours show the field amplitude for different detunings between the cavity frequency and the uncoupled qubit frequency ω_c/ω_J, where $\omega_c/\omega_J = 0.98$ (red), $\omega_c/\omega_J = 0.99$ (yellow), $\omega_c/\omega_J = 1$ (green), $\omega_c/\omega_J = 1.01$ (blue), $\omega_c/\omega_J = 1.02$ (purple). All curves show a vacuum Rabi splitting. The inset shows higher cavity modes of the green curve in the main panel $\omega_c/\omega_J = 1$.

By analysing and plotting this expression, see Fig. 3.5 a), it is easy to discuss the different impedance regimes. For low impedance $Z_0 C_c \omega < 1$, the reflection converges to zero, except for resonance at the coupled qubit frequency $\omega = \omega_0$, which is what we expect [138]. In the high-impedance regime, on the other hand, the reflection behaviour changes completely. The probe field is perfectly reflected at all frequencies except the uncoupled resonance frequency of the qubit $\omega = \omega_J$, where the reflection is zero for all values of Z_0. The reason for the high reflectance in the high impedance regime is the strong capacitive coupling to the ground at the transmon. Due to the high TL impedance, not much current passes through the TL, and the voltage on the coupling capacitance does not significantly change. In the low impedance regime, the large currents that pass through the TL keep the voltage at the coupling point close to zero, and the transmon acts as an open circuit away from its coupled resonance frequency ω_0. In the following, we investigate how this drastic change in the reflectance affects the properties of a transmon in front of a mirror.

3.4.2 Semi-infinite TL

To analyse the effect of an incoming field from the open side of the TL (the left side in our case), we now calculate and plot the ratio of the field that is trapped between the atom and the mirror V_R^{out} and the incoming field from the left V_L^{in}, $f(\omega) = |V_R^{\text{out}}(\omega)|/|V_L^{\text{in}}(\omega)|$. Similar to the case of an open TL, we Fourier transform the equations of motion and find

$$f(\omega) = \frac{\left(\frac{\omega^2}{\omega_0^2} - 1\right)}{\left(1 - \frac{\omega^2}{\omega_0^2}\right) - i\frac{C_c Z_0 \omega}{2}\left(\frac{\omega^2}{\omega_J^2} - 1\right)\left(e^{i\omega T} - 1\right)}, \tag{3.53}$$

the absolute value of this function is shown in Fig. 3.5 b), where we introduce a new relevant system frequency $\omega_c = 2\pi/T$ which can be understood as the resonance frequency of the *cavity created between the highly reflective transmon and the mirror*. The main panel of Fig. 3.5 b) shows the first mode of the field for different values of the detuning between the cavity frequency ω_c and the high impedance qubit resonance frequency ω_J. We see a Rabi splitting in all first modes indicating avoided crossing with the coupling strength

$$\Omega_n = \frac{2\omega_J}{\sqrt{2\pi n C_J Z_0 \omega_J}} = \frac{2\omega_J}{\sqrt{2\pi n \frac{Z_0}{Z_J}}}. \tag{3.54}$$

On resonance, $\omega_J = n\omega_c$, this expression can be further reduced to

$$\Omega_T = \frac{2}{\sqrt{T C_J Z_0}}. \tag{3.55}$$

The inset of Fig 3.5 b) shows higher modes $\omega \approx n\omega_c$ for $\omega_c/\omega_J = 1$.

3.5 Spontaneous emission

In Paper I and III, we investigate the spontaneous emission of a transmon coupled to an open and semi-infinite TL, both in the low- and high-impedance regime. In the following, we summarise the main results. We calculate the qubit energy, which corresponds to the average excited state occupation probability. The energy of the qubit is given by

$$E_q(t) = \frac{(p_J(t) + p_0(t))^2}{2C_J} + \frac{p_0(t)^2}{2C_c} + \frac{\phi_J(t)^2}{2L_J}. \tag{3.56}$$

For low impedance, we find that the position of the atom with respect to the wavelength of the emitted electromagnetic field plays a crucial role in the behaviour. Firstly, we see the Purcell effect if the atom is placed at an anti-node of the field (see Fig. 3.6 a) yellow line), meaning that the coupling to the TL doubles compared to the coupling to an open TL (see Fig. 3.6 a) red line) [139]. Secondly, we find that the system converges into a dark state with finite excitation probability if the atom is placed at a node (see Fig. 3.6 a) black line) [140]. Both the transient dynamics and the steady-state value of the dark state excitation E_{DS} depend on the ratio of the low-impedance coupling to the TL γ_0 (3.19) and the round-trip time time. The energy E_{DS} is given by

$$\frac{E_{\mathrm{DS}}}{E_0} = \frac{1}{\left(1 + \frac{\gamma_0 T}{2}\right)^2},\tag{3.57}$$

where E_0 is the initial excitation energy of the qubit. Fig. 3.6 b) shows the time evolution of the qubit energy for different values of $\gamma_0 T$. The grey lines indicate the dark state energy (3.57). We see that the transient behaviour also strongly depends on $\gamma_0 T$, but the dynamics are non-trivial. For small $\gamma_0 T$ (green), the energy converges into a dark state very quickly, almost immediately after the first round trip. For bigger $\gamma_0 T$ (purple), the qubit becomes re-excited several times, and we see revival effects before it converges to the dark state.

In Paper III, where we investigate the high-impedance regime more closely, we find that the spontaneous emission behaviour changes significantly in the high-impedance regime. For instance, the decay rate changes, leading to a slower decay in the high impedance regime. We also find vacuum Rabi oscillations if the resonance frequency of the uncoupled qubit is close to the resonance frequency of the cavity created by the atom and the mirror $\omega_c \approx \omega_J$, see Fig. 3.7. If the dark state condition $\omega_c \approx \omega_0$ is fulfilled, the system converges to the same dark state determined by the low-impedance coupling strength γ_0, see Eq. (3.57). However, the latter is only true if the coupling capacitance C_c is small, meaning that $\omega_0 \approx \omega_J$. Otherwise, the system decays strictly and acts as if coupled to an open TL with the open TL coupling strength for high impedance γ_J. Interestingly, the plain presence of the mirror, away from the qubit-cavity resonance $n\omega_c \approx \omega_J$, reduces the coupling strength by a factor of 2, which we define as $\gamma_J^m = \gamma_J/2$. If the qubit and the cavity are on resonance, $n\omega_c \approx \omega_J$, the coupling reduces by another factor of 2 and decays as seen in Fig. 3.7.
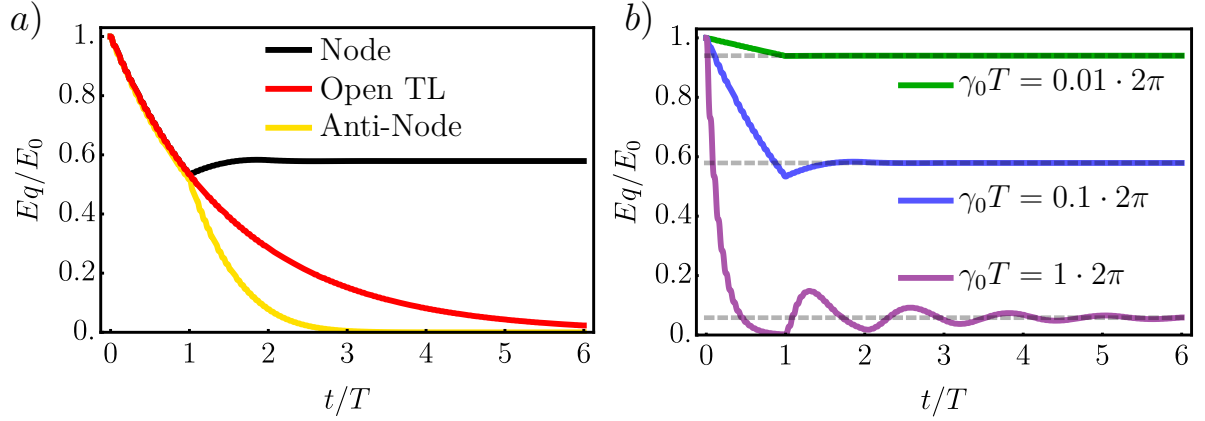
Figure 3.6: *a) Ratio between the energy E_q of an atom in front of a mirror and its initial excitation energy E_0 of an atom located at a node (black) and anti-node (yellow) of the electromagnetic field and an atom coupled to an open TL (red) as a function of time t normalised by the round-trip time T. If located at a node, the energy converges into a dark state with finite excitation probability, whereas we see the Purcell effect in the decay if the atom is located at a anti-node of the field.*
b) Ratio of the energy E_q of an atom in front of a mirror and its initial excitation energy E_0 as a function of time t normalised by the round-trip time T for different values of the ratio of the coupling γ_0 and round-trip time T, $\gamma_0 T = 0.01 \cdot 2\pi$ (green), $\gamma_0 T = 0.1 \cdot 2\pi$ (blue) and $\gamma_0 T = 1 \cdot 2\pi$ (purple) as a function of time t divided by the delay time T . In all cases, the atom is located at a node of the electromagnetic field. We see differences in both the transient behaviour and the steady state energy value. Whereas the dark state value is simply given by E_{DS} (3.57) (indicated by the grey dashed lines), the transient behaviour is not as trivial. If $\gamma_0 T$ is small (green), the energy converges almost immediately to the dark state after the first round trip. For higher $\gamma_0 T$ (purple), we see several revivals of the qubit energy after every round trip before the energy reaches its steady state value.
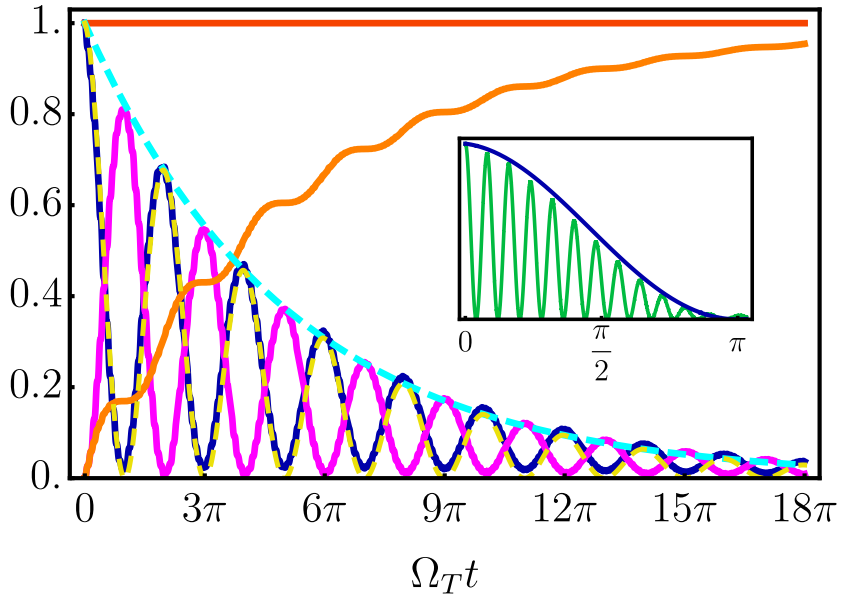
Figure 3.7: *Enery of the transmon (blue), trapped field between the atom and the mirror (pink), approximated decay with $\gamma_J^m/2$ (dashed cyan), outgoing field to the left (orange), total system energy (red) and $e^{-\gamma_J^m t/2}\cos^2(\Omega_T t/2)$ (dashed yellow) as a function of periods of the Rabi frequency Ω_T for $C_J/C_c = 0.5$, $Z_0/Z_J = 100$, $T = 2\pi/\omega_c$, $n\omega_c = \omega_J$, $n = 1$. The inset shows the qubit energy (blue) and flux ϕ_J^2 (green) during the first period. One can clearly see that the time scale of the transmon is different from the time scale of its variables.*

4 Light-matter interaction

In all articles, we deal with atoms coupled to an electromagnetic field. Even though most of our articles are within the framework of circuit QED, the methods often boil down to commonly used quantum optical methods. Quantum optics describes the interaction of atoms characterized by discrete energy levels with a quantized electromagnetic field, or photons. In the following, we introduce the essential parts of a quantum optical Hamiltonian by demonstrating the quantization of an electromagnetic field and deriving the coupling part between the atom and the field in the dipole approximation. We follow several sources throughout the derivations [141–143].

4.1 Atom Hamiltonian

We consider a multi-level system with $N+1$ energy eigenstates where the ground state is denoted by $|0\rangle$ and the excited states are denoted by $|i\rangle$, $i \in 1, \ldots, N$. The Hamiltonian of the multi-level system is given by

$$H_0 = \sum_{i=0}^{N} \hbar\omega_i |i\rangle\langle i|, \tag{4.1}$$

where $\hbar\omega_i$ is the energy of the i-th level. We define the operators of the multi-level system as follows

$$\sigma_{ji} = |i\rangle\langle j|, \tag{4.2}$$

where $i = j$ describe the occupation of the i-th level and the operators with $i \neq j$ describe the transition $j \to i$.

It is common to transform the Hamiltonian into a basis where the lowest energy level is moved to zero and the energy of the states is described by the transition frequencies from the first to the i-th level $\omega_{i0} = \omega_i - \omega_0$. To arrive at this basis, we perform a unitary transformation with the operator

$$T(t) = e^{-i\omega_0 t \sum_{j=0}^{N} \sigma_{jj}}, \tag{4.3}$$

with the property $T^\dagger T = TT^\dagger = \mathbb{1}$. The transformation of the Hamiltonian H_0 to the new Hamiltonian $\tilde{H}_0$ is given as follows.

We start with the Schrödinger equation which reads [144]

$$i\hbar \frac{\mathrm{d}}{\mathrm{d}t}|\Psi\rangle = H_0|\Psi\rangle. \tag{4.4}$$

We define a new state vector $|\Phi\rangle = T^\dagger|\Psi\rangle$ and calculate its time derivative

$$
\begin{aligned}
i\hbar \frac{\mathrm{d}}{\mathrm{d}t}|\Phi\rangle &= i\hbar \frac{\mathrm{d}T^\dagger}{\mathrm{d}t}|\Psi\rangle + i\hbar T^\dagger \frac{\mathrm{d}|\Psi\rangle}{\mathrm{d}t} \\
&= i\hbar \frac{\mathrm{d}T^\dagger}{\mathrm{d}t}|\Psi\rangle + T^\dagger H_0|\Psi\rangle \\
&= i\hbar \frac{\mathrm{d}T^\dagger}{\mathrm{d}t}|\Psi\rangle + T^\dagger H_0 TT^\dagger|\Psi\rangle \\
&= i\hbar \frac{\mathrm{d}T^\dagger}{\mathrm{d}t}T|\Phi\rangle + T^\dagger H_0 T|\Phi\rangle \\
&= \underbrace{\left(i\frac{\mathrm{d}T^\dagger}{\mathrm{d}t}T + T^\dagger H_0 T\right)}_{\tilde{H}_0}|\Phi\rangle, \tag{4.5}
\end{aligned}
$$

where we used the Schrödinger equation (4.4), the relation $TT^\dagger = \mathbb{1}$ and $T|\Phi\rangle = |\Psi\rangle$. We calculate the Hamiltonian $\tilde{H}_0$ for $T(t) = e^{-i\omega_0 t \sum_{j=0}^{N} \sigma_{jj}}$ and obtain

$$
\begin{aligned}
\tilde{H}_0 &= i\hbar \frac{\mathrm{d}T^\dagger}{\mathrm{d}t}T + T^\dagger H_0 T \\
&= -\hbar\omega_0 \sum_{j=0}^{N} \sigma_{jj} + H_0 \\
&= \hbar \sum_{j=0}^{N} (\omega_j - \omega_0)\, \sigma_{jj} \\
&= \hbar \sum_{j=1}^{N} \omega_{j0}\sigma_{jj} \tag{4.6}
\end{aligned}
$$

Thus we have arrived at a new Hamiltonian, where the energies are described by the transition frequencies from the ground state to higher energy levels. Further, we will from now on refer to $\tilde{H}_0$ as the atom Hamiltonian H_a.

4.2 Field Hamiltonian

In the following, we will quantize the electromagnetic field, which can be done in different ways. Here we choose the (non-Lorentz-invariant) Coulomb gauge, which is commonly used in non-relativistic quantum optics [141–143]. We start with the source-free Maxwell equations in free space,

$$\nabla \cdot \mathbf{E} = 0, \quad \nabla \cdot \mathbf{B} = 0, \tag{4.7}$$

$$\nabla \times \mathbf{E} = -\frac{\mathrm{d}}{\mathrm{d}t}\mathbf{B}, \quad \nabla \times \mathbf{B} = \frac{1}{c^2}\frac{\mathrm{d}}{\mathrm{d}t}\mathbf{E}, \tag{4.8}$$

where $\mathbf{E}$ and $\mathbf{B}$ are the electric and magnetic field, respectively, and $c = 1/\sqrt{\mu_0\epsilon_0}$ is the vacuum velocity of light. We introduce the vector potential $\mathbf{A}$ and the scalar potential ϕ, that fulfil

$$\mathbf{B} = \nabla \times \mathbf{A}, \tag{4.9}$$

$$\mathbf{E} = -\nabla\phi - \frac{\mathrm{d}}{\mathrm{d}t}\mathbf{A}. \tag{4.10}$$

Note that the Maxwell equations are gauge invariant under the following transformation

$$\mathbf{A} \to \tilde{\mathbf{A}} = \mathbf{A} + \nabla\chi, \quad \phi \to \tilde{\phi} = \phi - \frac{\mathrm{d}}{\mathrm{d}t}\chi, \tag{4.11}$$

where χ is an arbitrary scalar potential. We use this to our advantage and introduce the Coulomb gauge

$$\nabla \cdot \mathbf{A} = 0. \tag{4.12}$$

In the Coulomb gauge, we find the following equations of motion for the potentials

$$\Delta\phi = 0, \quad -\Delta\mathbf{A} + \frac{1}{c^2}\frac{\partial^2}{\partial t^2}\mathbf{A} = 0. \tag{4.13}$$

We now rewrite the vector potential $\mathbf{A}(\mathbf{r}, t)$ in terms of orthogonal and transverse eigenmode functions $\mathbf{u}(\mathbf{r}, t)$,

$$\mathbf{A}(\mathbf{r}, t) = \sum_k \sqrt{\frac{\hbar}{2\omega_k\epsilon_0}}\left(\alpha_k\mathbf{u}_k(\mathbf{r})e^{-i\omega_k t} + \alpha_k^*\mathbf{u}_k^*(\mathbf{r})e^{i\omega_k t}\right), \tag{4.14}$$

that fulfil

$$\nabla \cdot \mathbf{u}_k(\mathbf{r}) = 0, \quad \int_G d^3\mathbf{r}\, \mathbf{u}_k^*(\mathbf{r})\mathbf{u}_{k'}(\mathbf{r}) = \delta_{k,k'}. \tag{4.15}$$

Here we assumed a finite area G and a discrete spectrum of eigenfrequencies ω_k. If we put the ansatz for the vector potential Eq. (4.14) into the equation of motion Eq. (4.13), we find the following equation for the eigenmode functions

$$\left(\Delta + \frac{\omega_k^2}{c^2}\right)\mathbf{u}_k(\mathbf{r}) = 0, \tag{4.16}$$

which we identify with the Helmholtz-equation. Now that we expressed the vector potential in terms of eigenmode functions, it is straightforward to write down the Hamiltonian function of the field. It can be calculated by Legendre transformation of the Lagrangian, which can be derived through the calculus of variation [134]. The Hamilton function is given by the total energy of the electromagnetic field and reads,

$$H_f = \frac{1}{2}\int d^3\mathbf{r}\left(\epsilon_0\mathbf{E}^2 + \frac{1}{\mu_0}\mathbf{B}^2\right). \tag{4.17}$$

By using Maxwell's equation for the vector potential in Coulomb gauge,

$$\mathbf{E} = -\frac{d}{dt}\mathbf{A}, \quad \mathbf{B} = \nabla \times \mathbf{A}, \tag{4.18}$$

the electric and magnetic field can also be expressed with the eigenmode functions $\mathbf{u}_k(\mathbf{r})$. If we then use the properties of the eigenmode functions and Gauss' theorem, the Hamilton function can be written as

$$H_f = \sum_k \frac{\hbar\omega_k}{2}\left(\alpha_k\alpha_k^* + \alpha_k^*\alpha_k\right). \tag{4.19}$$

This has the form of a classical harmonic oscillator. Now we promote the classical parameters α_k to operators

$$\alpha_k \to \hat{a}_k, \quad \alpha_k^* \to \hat{a}_k^\dagger, \tag{4.20}$$

that fulfil the bosonic commutation relations

$$\left[\hat{a}_k, \hat{a}_{k'}^\dagger\right] = \delta_{k,k'}, \quad \left[\hat{a}_k^{(\dagger)}, \hat{a}_{k'}^{(\dagger)}\right] = 0. \tag{4.21}$$

Now we rewrite the classical Hamiltonian (4.19) with the operators $\hat{a}_k, \hat{a}_k^\dagger$ and arrive at the quantum mechanical harmonic oscillator

$$\hat{H} = \sum_k \hbar\omega_k \left(\hat{a}_k^\dagger \hat{a}_k + \frac{1}{2} \right). \tag{4.22}$$

We also rewrite the expressions for the vector potential, electric- and magnetic field with operators and find

$$\mathbf{A}(\mathbf{r}) = \sum_k \sqrt{\frac{\hbar}{2\omega_k\epsilon_0}} \left(\hat{a}_k \mathbf{u}_k(\mathbf{r}) + \hat{a}_k^\dagger \mathbf{u}_k^*(\mathbf{r}) \right), \tag{4.23}$$

$$\mathbf{E}(\mathbf{r}) = i \sum_k \sqrt{\frac{\hbar\omega_k}{2\epsilon_0}} \left(\hat{a}_k \mathbf{u}_k(\mathbf{r}) - \hat{a}_k^\dagger \mathbf{u}_k^*(\mathbf{r}) \right), \tag{4.24}$$

$$\mathbf{B}(\mathbf{r}) = \sum_k \sqrt{\frac{\hbar}{2\omega_k\epsilon_0}} \left[\hat{a}_k \left(\nabla \times \mathbf{u}_k(\mathbf{r}) \right) + \hat{a}_k^\dagger \left(\nabla \times \mathbf{u}_k^*(\mathbf{r}) \right) \right]. \tag{4.25}$$

4.3 Interaction Hamiltonian

The Hamiltonian of a system with a number of N charges q_i and mass m_i in an electromagnetic field is given by

$$H = \sum_i \frac{\left[\mathbf{p}_i - q_i \mathbf{A}\left(\mathbf{r}_i \right) \right]^2}{2m_i} + \frac{\epsilon_0}{2} \int \mathrm{d}^3\mathbf{r} \left(\mathbf{E}^2 + c^2\mathbf{B}^2 \right) \tag{4.26}$$

The kinetic term of the charges

$$m_i \dot{\mathbf{r}}_i = \frac{\partial H}{\partial \mathbf{p}_i} = \mathbf{p}_i - q_i \mathbf{A}(\mathbf{r}_i) \tag{4.27}$$

includes the vector potential $\mathbf{A}(\mathbf{r}_i)$. It couples the kinetic energy of the charges to the electromagnetic field and is called the *minimal coupling*. In the Hamiltonian (4.27), the electric and magnetic fields consist of both longitudinal and transverse parts,

$$\mathbf{E} = \mathbf{E}_\perp + \mathbf{E}_\parallel, \quad \mathbf{B} = \mathbf{B}_\perp + \mathbf{B}_\parallel. \tag{4.28}$$

We will now analyze the contribution of each part to the Hamiltonian. First, we decompose the electric field and use the following conditions

$$\nabla \cdot \mathbf{E}_\perp = 0 \quad \text{and} \quad \nabla \times \mathbf{E}_\parallel = 0, \quad \mathbf{E}_\perp = -\nabla\phi. \tag{4.29}$$

Using these relations, the contribution of the electric field to the Hamiltonian can be written as follows:

$$\frac{\epsilon_0}{2}\int d^3r\mathbf{E}^2 = \frac{\epsilon_0}{2}\int d^3\mathbf{r}\left(\mathbf{E}_\perp^2 + \mathbf{E}_\parallel^2\right)$$

$$= \frac{\epsilon_0}{2}\int d^3\mathbf{r}\,\mathbf{E}_\perp^2 - \frac{\epsilon_0}{2}\int d^3\mathbf{r}\,(\nabla\phi)^2$$

$$= \frac{\epsilon_0}{2}\int d^3\mathbf{r}\,\mathbf{E}_\perp^2 - \frac{\epsilon_0}{2}\int d^3\mathbf{r}\,(\phi\Delta\phi)$$

$$= \frac{\epsilon_0}{2}\int d^3\mathbf{r}\,\mathbf{E}_\perp^2 - \frac{1}{2}\int d^3\mathbf{r}\,(\phi\rho)\,. \tag{4.30}$$

Now we use the expression for the charge density $\rho(\mathbf{r}, t)$ of localized point-like charges

$$\rho(\mathbf{r}, t) = \sum_i^N q_i\delta^2\left(\mathbf{r} - \mathbf{r}_i\right), \tag{4.31}$$

and hence the scalar potential

$$\phi(\mathbf{r}, t) = \int d^3\mathbf{r}'\,\frac{\rho\left(\mathbf{r}', t\right)}{4\pi\epsilon_0\left|\mathbf{r} - \mathbf{r}'\right|}. \tag{4.32}$$

With this, the second term of (4.30) can be written as

$$\frac{1}{2}\int d^3\mathbf{r}\,\mathbf{E}_\parallel^2 = -\frac{1}{2}\int d^3\mathbf{r}\,\rho\phi = \int d^3\mathbf{r}\int d^3\mathbf{r}'\,\frac{\rho(\mathbf{r}, t)\rho\left(\mathbf{r}', t\right)}{8\pi\epsilon_0\left|\mathbf{r} - \mathbf{r}'\right|} \tag{4.33}$$

$$= \sum_{i,j}\frac{q_iq_j}{8\pi\epsilon_0\left|\mathbf{r}_i - \mathbf{r}_j\right|} = V_{\text{Coul}}. \tag{4.34}$$

So we see that the longitudinal parts of the electric field $\mathbf{E}_\parallel$ can be associated with the field that results from charged particles. For the magnetic field, we find that it only consists of transverse parts since there are no magnetic monopoles; hence the divergence of the magnetic field is zero

$$\nabla \cdot \mathbf{B} = 0 \rightarrow \mathbf{B}_\parallel = 0. \tag{4.35}$$

The same follows from the Coulomb gauge for the vector potential

$$\nabla \cdot \mathbf{A} = 0 \rightarrow \mathbf{A} = \mathbf{A}_\perp, \tag{4.36}$$

which means that the Hamiltonian only contains transverse parts of the corresponding field

$$H = \sum_{i=1}^N\frac{\left(\mathbf{p}_i - q_i\mathbf{A}_\perp\left(\mathbf{r}_i\right)\right)^2}{2m_i} + \frac{1}{8\pi\epsilon_0}\sum_{i,j}\frac{q_iq_j}{\left|\mathbf{r}_i - \mathbf{r}_j\right|} + \frac{\epsilon_0}{2}\int d^3\mathbf{r}\left(\mathbf{E}_\perp^2 + c^2\mathbf{B}_\perp^2\right). \tag{4.37}$$

Now we can quantize the Hamiltonian by rewriting the fields with operators according to Eq.s (4.23)-(4.25) and divide it into matter, field and interaction parts

$$H = H_{\text{matter}} + H_{\text{field}} + H_{\text{int}}, \tag{4.38}$$

$$H_{\text{matter}} = \sum_{i=1}^{N} \frac{\hat{\mathbf{p}}_i^2}{2m_i} + V_{\text{Coul}}, \tag{4.39}$$

$$H_{\text{field}} = \frac{\epsilon_0}{2} \int d^3\mathbf{r} \left(\mathbf{E}_\perp^2 + c^2 \mathbf{B}_\perp^2 \right), \tag{4.40}$$

$$H_{\text{int}} = -\sum_{i=1}^{N} \frac{q_i \hat{\mathbf{p}}_i \hat{\mathbf{A}}_\perp (\mathbf{r}_i)}{m_i} + \sum_{i=1}^{N} \frac{q_i^2 \hat{\mathbf{A}}_\perp^2 (\mathbf{r}_i)}{2m_i} - \sum_{i=1}^{N} \frac{g_i q_i \hbar \mathbf{S}_i \hat{\mathbf{B}} (\mathbf{r}_i)}{2m_i}. \tag{4.41}$$

Here, we included a term representing the interaction of the spin magnetic moments of the particles with the magnetic field. $\mathbf{S}_i$ is the spin of particle i and g_i is the Landé factor. This term is often neglected, which is a valid approximation if the momentum of the photons is small compared to the momentum of the charged particles, which is true in the optical and microwave regime. Furthermore, we expanded the minimal coupling term. Note that $\hat{\mathbf{p}} = -i\hbar\nabla$ and $\hat{\mathbf{A}}$ only commute since we are in the Coloumb gauge. The $\mathbf{A}^2$-term is often neglected for weak electromagnetic fields. However, there is an ongoing discussion of whether the $\mathbf{A}^2$-term can be neglected in circuit QED for all purposes [145, 146]. One example is a superradiant phase transition, which occurs if many emitters are strongly coupled to one mode of an electromagnetic field [65–67, 147]. In cavity QED, the no-go theorem that states the prohibition of a superradiant phase transition is well established [145, 148–150], whereas there are claims that a superradiant phase transition in circuit QED is possible [61, 64, 151, 152].

The Hamiltonian (4.38) is of a general form and describes the interaction of charged particles with an electromagnetic field in a non-relativistic regime. It is common to further simplify the atom-field interaction by introducing the dipole approximation, as we will show in the following.

4.3.1 Dipole approximation

In the dipole approximation, also called long-wavelength approximation, one assumes that the wavelength of the electromagnetic field $\sim 1/k$ is much longer than the interaction range of the particles, typically in the order of the Bohr radius a_0, hence $ka_0 \ll 1$. Meaning, the vector potential

can be assumed to be spatially independent. We evaluate the vector potential at the nuclear position $\mathbf{A}(\mathbf{r}_{\text{nuc}})$, which we choose to be located at $\mathbf{r}_{\text{nuc}} = 0$ [141]. The Hamiltonian (4.38) can then be written as

$$H_{\mathbf{pA}} = \sum_{i=1}^{N} \frac{\left(\hat{\mathbf{p}}_i - q_i \hat{\mathbf{A}}_\perp (0)\right)^2}{2m_i} + V_{\text{Coul}} + H_{\text{field}}, \tag{4.42}$$

where we now write the field part with creation and annihilation operators as in the previous section

$$H_{\text{field}} = \sum_k \hbar\omega_k \left(\hat{a}_k^\dagger \hat{a}_k + \frac{1}{2}\right). \tag{4.43}$$

Here, the interaction between light and matter is given by the product $\mathbf{p} \cdot \mathbf{A}$. It is possible to transform the Hamiltonian hence the form of the light-matter interaction, to a Hamiltonian with dipole interaction with the following unitary transformation

$$H_{\mathbf{dE}} = T H_{\mathbf{pA}} T^\dagger, \quad T = e^{-\frac{i}{\hbar}\mathbf{d}\cdot\mathbf{A}}, \tag{4.44}$$

where $\mathbf{d}$ is the total dielectric dipole moment

$$\hat{\mathbf{d}} = \sum_i q_i \hat{\mathbf{r}}_i \tag{4.45}$$

and $\mathbf{A}$ the now spatially independent vector potential

$$\hat{\mathbf{A}} = \sum_k \sqrt{\frac{\hbar}{2\omega_k\epsilon_0}} \left(\hat{a}_k \mathbf{u}_k(0) + \hat{a}_k^\dagger \mathbf{u}_k^*(0)\right) \tag{4.46}$$

The operators in the Hamiltonian (4.42) are transformed as follows

$$T\hat{\mathbf{r}}_i T^\dagger = \hat{\mathbf{r}}_i, \quad T\hat{\mathbf{A}}T^\dagger = \hat{\mathbf{A}}, \quad T\hat{\mathbf{p}}_i T^\dagger = \hat{\mathbf{p}}_i + q_i\hat{\mathbf{A}}, \tag{4.47}$$

$$T\hat{a}_k T^\dagger = \hat{a}_k + \lambda_k, \quad T\hat{a}_k^\dagger T^\dagger = \hat{a}_k^\dagger + \lambda_k^*, \quad \lambda_k = i\sqrt{\frac{1}{2\hbar\omega_k\epsilon_0}}\hat{\mathbf{d}}\cdot\mathbf{u}_k^*(0). \tag{4.48}$$

The unitary transformation from $H_{\mathbf{pA}}$ to $H_{\mathbf{dE}}$ removes the minimal coupling term from the momentum $\hat{\mathbf{p}}_i - q_i\hat{\mathbf{A}} \to \hat{\mathbf{p}}_i$. The coupling between light and matter anyway enters by transforming the field term of the Hamiltonian

$$T\hat{a}_k^\dagger \hat{a}_k T^\dagger = \hat{a}_k^\dagger \hat{a}_k + \lambda_k \hat{a}_k^\dagger + \lambda_k^* \hat{a}_k + |\lambda_k|^2. \tag{4.49}$$

The full dipole interaction Hamiltonian reads

$$H_{\mathbf{dE}} = H_{\mathrm{matter}} + H_{\mathrm{field}} + H_{\mathrm{dipole}} + \sum_k \frac{|\hat{\mathbf{d}} \cdot \hat{\mathbf{u}}_k(0)|^2}{2\epsilon_0}, \tag{4.50}$$

$$H_{\mathrm{dipole}} = -\hat{\mathbf{d}} \cdot \hat{\mathbf{E}} = -i \sum_k \sqrt{\frac{2\omega_k}{2\epsilon_0}} \hat{\mathbf{d}} \left(\mathbf{u}_k(0)\hat{a}_k - \mathbf{u}_k^*(0)\hat{a}_k^\dagger \right). \tag{4.51}$$

The last part of the Hamiltonian $\sum_k \frac{|\hat{\mathbf{d}} \cdot \hat{\mathbf{u}}_k(0)|^2}{2\epsilon_0}$ describes an energy correction and can be neglected if the considered dipole moments are rather small. Note that not only the Hamiltonian but also the states have to be transformed for the matrix elements to stay invariant,

$$|\Psi\rangle \to T|\Psi\rangle \Rightarrow \langle\Phi|\hat{O}|\Psi\rangle = \langle\Phi|T^\dagger T\hat{O}T^\dagger T|\Psi\rangle, \tag{4.52}$$

for any quantum mechanical operator $\hat{O}$. Interestingly, if we apply the unitary transformation to the electric field, we find that it will contain a polarisation part

$$T\mathbf{E}_\perp T^\dagger = i \sum_k \sqrt{\frac{2\omega_k}{2\epsilon_0}} \left(\mathbf{u}_k(\mathbf{r}) \left(\hat{a}_k + \lambda_k \right) - \mathbf{u}_k^*(\mathbf{r}) \left(\hat{a}_k^\dagger + \lambda_k^* \right) \right) \tag{4.53}$$

$$= \mathbf{E}_\perp(\mathbf{r}) - \frac{1}{\epsilon_0} \mathbf{P}_\perp(\mathbf{r}), \tag{4.54}$$

where $\mathbf{P}_\perp(\mathbf{r})$ is the transverse part of the polarisation density $\mathbf{P}(\mathbf{r}) = \mathbf{d}\delta(\mathbf{r})$ and therefore gives a connection to the dielectric displacement field $\mathbf{D} = \epsilon_0 \mathbf{E} + \mathbf{P}$.

4.4 The two-level system

The atom part of the Hamiltonian of a two-level system is given by

$$H_0 = \sum_{i=0}^1 \hbar\omega_i |i\rangle\langle i| = \hbar\omega_0 \sigma_{00} + \hbar\omega_1 \sigma_{11}, \tag{4.55}$$

where $|0\rangle$ is the ground state and $|1\rangle$ is the first excited state. The two-level system is commonly written with σ_z, one of the Pauli matrices,

$$\sigma_x = |0\rangle\langle 1| + |1\rangle\langle 0|, \quad \sigma_y = i\left(|1\rangle\langle 0| - |0\rangle\langle 1|\right), \quad \sigma_z = |0\rangle\langle 0| - |1\rangle\langle 1|. \tag{4.56}$$

To arrive at the corresponding expression for the Hamiltonian written with σ_z, we define the transition energy $\tilde{\omega}_0 = \omega_1 - \omega_0$ between the two levels and perform a unitary transformation as in section 4.1 with the operator $T(t) = e^{-i\left(-\omega_0 - \frac{\tilde{\omega}_0}{2}\right)\sigma_{00}t - i\left(-\omega_1 + \frac{\tilde{\omega}_0}{2}\right)\sigma_{11}t}$, which basically means that we shift the zero into the middle of the two energy levels. The Hamiltonian then takes its usual form

$$H_a = \frac{\tilde{\omega}_0}{2}\sigma_z. \tag{4.57}$$

In the following, we drop the tilde from the frequency and refer to ω_0 as the transition frequency between the two levels. The field part is given by

$$\hat{H}_{\text{field}} = \sum_k \hbar\omega_k \left(\hat{a}_k^\dagger \hat{a}_k + \frac{1}{2}\right). \tag{4.58}$$

In some cases, only one mode is considered, and the field part reduces to

$$\hat{H} = \hbar\omega \left(\hat{a}^\dagger \hat{a} + \frac{1}{2}\right). \tag{4.59}$$

The constant term is often neglected since it does not contribute to the dynamics of the system. Now, we want to derive the coupling part of the two-level system using the dipole interaction Hamiltonian that we derived before,

$$H_{\text{dipole}} = -\hat{\mathbf{d}} \cdot \hat{\mathbf{E}}. \tag{4.60}$$

For the two-level system, the dipole transition operator is given by

$$\hat{\mathbf{d}} = \langle 0|\mathbf{d}|1\rangle \left(|0\rangle\langle 1| + |1\rangle\langle 0|\right) = \langle 0|\mathbf{d}|1\rangle \left(\sigma_- + \sigma_+\right), \tag{4.61}$$

where we defined the transition operators

$$\sigma_- = |0\rangle\langle 1|, \quad \sigma_+ = |1\rangle\langle 0|. \tag{4.62}$$

With the expression for the electric field for one mode

$$\mathbf{E} = i\sqrt{\frac{\hbar\omega}{2\epsilon_0}} \left(\hat{a}\mathbf{u} - \hat{a}^\dagger\mathbf{u}^*\right), \tag{4.63}$$

the dipole interaction Hamiltonian becomes

$$H_{\text{dipole}} = -i\sqrt{\frac{\hbar\omega}{2\epsilon_0}} \langle 0|\mathbf{d}|1\rangle \left(\sigma_- + \sigma_+\right)\left(\hat{a}\mathbf{u} - \hat{a}^\dagger\mathbf{u}^*\right) \tag{4.64}$$

$$= \hbar \left(\sigma_+ + \sigma_-\right)\left(ga + g^*a^\dagger\right), \tag{4.65}$$

where the coupling g is defined as

$$\hbar g = -i\sqrt{\frac{\hbar\omega}{2\epsilon_0}}\langle 0|\mathbf{d}\cdot\mathbf{u}|1\rangle. \tag{4.66}$$

Without loss of generality, we can assume the coupling constant to be real and positive. Doing so, the total Hamiltonian of the two-level system becomes

$$H_{\text{two-level}} = \frac{\hbar\omega_0}{2}\sigma_z + g\left(\sigma_- + \sigma_+\right)\left(\hat{a} + \hat{a}^\dagger\right). \tag{4.67}$$

This Hamiltonian is not analytically diagonalizable. Therefore it is widespread to use the *rotating-wave approximation* (RWA). In the rotating-wave approximation, the excitation number is conserved which means that the part $\hat{a}\sigma_- + \hat{a}^\dagger\sigma_+$ is neglected and the Hamiltonian becomes

$$H_{\text{two-level}}^{\text{RWA}} = \frac{\hbar\omega_0}{2}\sigma_z + g\left(\sigma_-\hat{a}^\dagger + \sigma_+\hat{a}\right). \tag{4.68}$$

As we mentioned before, in the rotating-wave approximation the number of excitations is conserved and the corresponding operator $\mathcal{N} = \hat{a}^\dagger\hat{a} + \sigma_z$ commutes with the Hamiltonian, $[\mathcal{N}, H] = 0$. The rotating-wave approximation is only valid in the limit $g \ll \omega_0$.

4.5 Rabi oscillations

Now we study the dynamics of a driven two-level system. The system Hamiltonian is given by

$$H_S = \frac{\omega_0}{2}\sigma_z, \tag{4.69}$$

where ω_0 is the transition frequency of the qubit, and it interacts with an electromagnetic field,

$$\mathbf{E}(t) = \mathbf{E}_0^{(+)}e^{-i\omega_p t} + \mathbf{E}_0^{(-)}e^{i\omega_p t} = \mathbf{E}^{(+)} + \mathbf{E}^{(-)}, \tag{4.70}$$

where ω_p is the drive frequency, and $\mathbf{E}_0^\pm$ is the amplitude and polarisation vector of the electromagnetic field. We neglected the spatial dependence of the electromagnetic field, which is justified for a point-like coupling.

The interaction Hamiltonian within the dipole and RWA approximations is given by

$$H_{\text{int}} = -\mathbf{d}^{(+)}\mathbf{E}^{(-)} - \mathbf{d}^{(-)}\mathbf{E}^{(+)}, \tag{4.71}$$

where $\mathbf{d}^{(\pm)}$ are the positive- and negative-rotating components of the dipole operator $\mathbf{d}$,

$$\mathbf{d} = \mathbf{d}^{(+)} + \mathbf{d}^{(-)}. \tag{4.72}$$

For the two-level system, they read

$$\mathbf{d}^{(+)} = \langle 0|\mathbf{d}|1\rangle\sigma_+, \quad \mathbf{d}^{(-)} = \langle 1|\mathbf{d}|0\rangle\sigma_-, \tag{4.73}$$

where $|0\rangle$ and $|1\rangle$ are the ground and excited state of the two-level system, respectively. The interaction Hamiltonian then becomes

$$H_{\text{int}} = -\langle 0|\mathbf{d}|1\rangle\mathbf{E}_0^{(-)}\sigma_+ e^{i\omega_p t} - \langle 1|\mathbf{d}|0\rangle\mathbf{E}_0^{(+)}\sigma_- e^{-i\omega_p t} \tag{4.74}$$

$$= \frac{\Omega}{2}\sigma_+ e^{i\omega_p t} + \frac{\Omega^*}{2}\sigma_- e^{-i\omega_p t}, \tag{4.75}$$

where we defined the Rabi frequency $\Omega = (\Omega^*)^* = -2\langle 0|\mathbf{d}|1\rangle\mathbf{E}_0^{(-)}$. We now assume that $\Omega = \Omega^*$ and the Hamiltonian can be written as

$$H_{\text{Rabi}} = \frac{\omega_0}{2}\sigma_z + \frac{\Omega}{2}\left(\sigma_+ e^{i\omega_p t} + \sigma_- e^{-i\omega_p t}\right) \tag{4.76}$$

$$= \frac{\omega_0}{2}\sigma_z + \Omega\cos(\omega_p t)\sigma_x. \tag{4.77}$$

The dynamics of the Rabi Hamiltonian is governed by the Schrödinger equation,

$$H_{\text{Rabi}}|\Psi(t)\rangle = i\frac{\mathrm{d}}{\mathrm{d}t}|\Psi(t)\rangle. \tag{4.78}$$

With the following ansatz for the state vector

$$|\Psi(t)\rangle = c_0(t)e^{i\frac{\omega_0}{2}t}|0\rangle + c_1(t)e^{-i\frac{\omega_0}{2}t}|1\rangle, \tag{4.79}$$

and assuming an initially excited atom

$$|c_0(0)| = 1, \quad |c_1(0)| = 0, \tag{4.80}$$
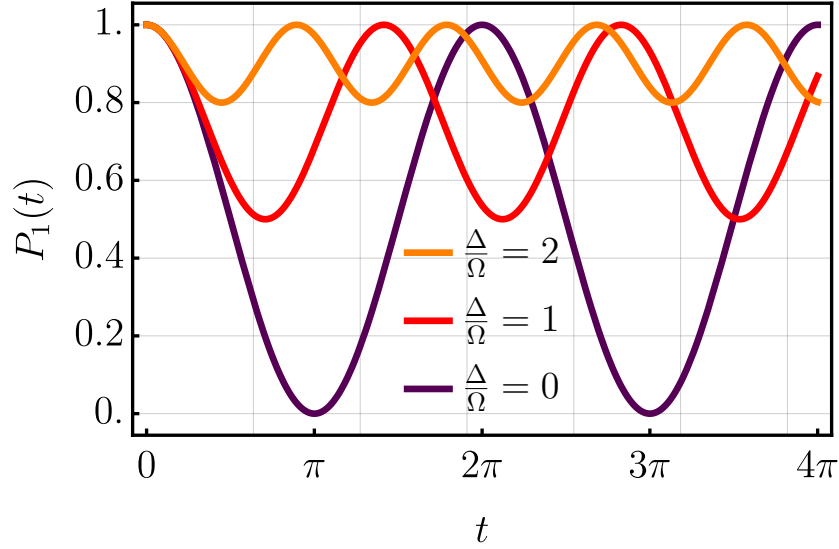
Figure 4.1: *Excited state occupation probability $P_1(t)$ of a coherently driven qubit as a function of time t with the following values of he detuning $\Delta = \omega_p - \omega_0$: $\Delta = 0$ (purple), $\Delta/\Omega = 1$ (red) and $\Delta/\Omega = 2$ (orange). The occupation probability decays and revives periodically with the Rabi frequency Ω_R. Only for $\Delta = 0$ it decays completely to zero.*

we find the following solution for the occupation probabilities $P_0(t)$ and $P_1(t)$ of the ground and excited state, respectively,

$$P_0(t) = |c_0(t)|^2 = \frac{\Omega^2}{\Omega_R^2} \sin^2\left(\frac{\Omega_R}{2}t\right) \tag{4.81}$$

$$P_1(t) = |c_1(t)|^2 = \cos^2\left(\frac{\Omega_R}{2}t\right) + \frac{\Delta^2}{\Omega_R^2} \sin^2\left(\frac{\Omega_R}{2}t\right), \tag{4.82}$$

where we introduced the Rabi frequency with detuning $\Delta = \omega_p - \omega_0$ between the probe and qubit frequency

$$\Omega_R = \sqrt{\Omega^2 + \Delta^2}. \tag{4.83}$$

In Fig. 4.1 we plot the occupation probability of the excited state $P_1(t)$ as a function of time for different detunings Δ. We find that only for resonant driving, the excitation probability $P_1(t)$ drops to zero before the qubit becomes re-excited again.

5 Open quantum systems

In many cases, the dynamics of a quantum system follows the Schrödinger equation and can be described by a unitary time evolution within a closed system with only a few degrees of freedom. However, for many systems, it is not easy to know the exact state at any given time because of, e.g., simply the lack of information. One reason could be that the system consists of many degrees of freedom and is, therefore, more difficult to describe. Many interesting cases that are studied consist of a smaller system coupled to a larger system with a vast number of degrees of freedom, usually referred to as a *reservoir* or *bath*. For these combined systems, one is often only interested in a specific part of the dynamics, e.g., how the small system evolves in the environment. The reduction to only a specific part of the entire system makes the system appear *open*, and we talk about *open quantum systems.* For open quantum systems, it can be of advantage to describe the dynamics in terms of the *density operator*, which describes the states in terms of statistical mixtures. The density operator for open quantum systems has a corresponding equation of motion called the *master equation.* The master equation is a handy tool to describe open quantum systems. Many systems that are studied in quantum optics are not truly closed but open. For example, if we investigate a number of emitters that are constantly driven by a laser, one is often more interested in the dynamics of the emitters and treats the electromagnetic field as a reservoir, which leaves the system of emitters *open.* The information that leaks from the system of emitters into the reservoir is lost, and the system decays into its ground state over time.

In the following, we will derive the master equation for a system coupled to a reservoir and give a specific example of a two-level system coupled to an electromagnetic field. In the derivation, we follow several references [135, 137, 143, 153–155].

5.1 The density matrix and the Liouville- von Neumann equation

In a closed quantum system, a state vector $|\Psi(t)\rangle$ evolves according to the Schrödinger equation [144],

$$i\hbar\frac{\mathrm{d}}{\mathrm{d}t}|\Psi(t)\rangle = H(t)|\Psi(t)\rangle, \tag{5.1}$$

where $H(t)$ is the system Hamiltonian. Planck's reduced constant $\hbar$ is set to one in the following. The expectation value of an observable $\hat{A}$ can be written as

$$\langle\hat{A}\rangle = \langle\Psi(t)|\hat{A}|\Psi(t)\rangle. \tag{5.2}$$

If we now define a projection operator onto the state $|\Psi(t)\rangle$,

$$\hat{P}_\Psi = |\Psi(t)\rangle\langle\Psi(t)|, \tag{5.3}$$

the expectation value of the observable $\hat{A}$ (5.2) can be rewritten as the *trace* of the projection operator and the observable

$$\langle\hat{A}\rangle = \mathrm{Tr}\left(\hat{P}_\Psi\hat{A}\right) = \mathrm{Tr}\left(|\Psi(t)\rangle\langle\Psi(t)|\hat{A}\right). \tag{5.4}$$

The trace of an operator X in a complete orthogonal system is given by

$$\mathrm{Tr}\left(X\right) = \sum_n\langle n|X|n\rangle, \tag{5.5}$$

and it is basis independent. In the description above, we knew how the state vector looks like at a given time, and we understand how it evolves. Therefore the projection operator only contains one state vector $|\Psi(t)\rangle$. However, this description becomes even more helpful if we miss information about the state vector at any given time and have to describe the expectation value of an observable with statistical mixtures. The projection operator now contains a set of possible states $|\Psi_n\rangle$ and weights p_n for the system to be in this state. From now on, we call the projection operator ρ the *density matrix* and define

$$\rho = \sum_n p_n|\Psi_n\rangle\langle\Psi_n|. \tag{5.6}$$

The density matrix has the following properties: It is normalised,

$$\mathrm{Tr}\left(\rho\right) = 1, \tag{5.7}$$

hermitian,

$$\rho = \rho^\dagger, \tag{5.8}$$

and positive definite,

$$\langle\alpha|\rho|\alpha\rangle \geq 0 \tag{5.9}$$

for any state $|\alpha\rangle$. Furthermore, we differentiate between *pure states* and *mixed states*. For pure states, all probabilities p_n are zero, except one which is one. This means the density matrix for a pure state is not a statistical mixture and reduces to $\rho = |\Psi(t)\rangle\langle\Psi(t)|$, as Eq. (5.3). Mixed states can have any probabilities (as long as they sum up to one). This leads to the following properties

$$\rho^2 = \rho, \quad \mathrm{Tr}\left(\rho^2\right) = 1, \quad \text{pure state}, \tag{5.10}$$
$$\rho^2 \neq \rho, \quad \mathrm{Tr}\left(\rho^2\right) < 1, \quad \text{mixed state}. \tag{5.11}$$

The expectation value of any observable $\hat{A}$ is then given by

$$\langle\hat{A}\rangle = \mathrm{Tr}\left(\rho\hat{A}\right). \tag{5.12}$$

Now we want to derive the Liouville-von Neumann equation, which is the equation of motion for the density matrix, which we derive from the Schrödinger equation (5.1). The solution of the Schrödinger equation can be written in terms of a unitary time-evolution operator $U(t, t_0)$ that transforms the systems state from an initial time t_0 to the time t,

$$|\Psi(t)\rangle = U(t, t_0)|\Psi(t_0)\rangle. \tag{5.13}$$

Inserting this into the Schrödinger equation, we find an equation of motion for the time-evolution operator

$$i\frac{\partial}{\partial t}U(t, t_0) = H(t)U(t, t_0). \tag{5.14}$$

Now we use this to rewrite the expression for the density matrix (5.6),

$$\rho(t) = \sum_n p_n U(t, t_0)|\Psi_n(t_0)\rangle\langle\Psi_n(t_0)|U^\dagger(t, t_0). \tag{5.15}$$

By assuming the density matrix at the initial time t_0 has the form

$$\rho(t_0) = \sum_n p_n |\Psi_n(t_0)\rangle\langle\Psi_n(t_0)|, \tag{5.16}$$

Eq. (5.15) can be rewritten as

$$\rho(t) = U(t, t_0)\rho(t_0)U^\dagger(t, t_0). \tag{5.17}$$

By taking the time derivative of this expression and comparing it to the equation of motion for the time-evolution operator (5.14), we find the equation of motion of the density matrix to be

$$\frac{\mathrm{d}}{\mathrm{d}t}\rho(t) = -i\left[H(t), \rho(t)\right]. \tag{5.18}$$

This equation is called the Liouville-von Neumann equation.

5.2 Master equation in the interaction picture

As we mentioned before, we consider a small system with a few degrees of freedom that is weakly coupled to an environment or reservoir with many degrees of freedom. Our primary interest lies in the evolution of the small system within the environment. For such an approach, it is of advantage to go to the interaction picture. The idea is that the interaction between the system and the reservoir is small, so the system evolves slowly within the reservoir and the time evolution of the system's state is governed by the interaction part of the Hamiltonian. With this assumption, we can derive the so-called master equation for the density matrix, as we will see in the following.

We consider the total Hamiltonian of a global system

$$H = H_S + H_R + V, \tag{5.19}$$

where H_S is the Hamiltonian of a system with few degrees of freedom, H_R is the reservoir Hamiltonian, and V is the interaction between the system and the reservoir. The density matrix of the system ρ fulfils the Liouville-von Neumann equation (5.18). By applying a unitary transformation with the operator $U(t) = \exp\left[i(H_S + H_R)(t)\right]$, the Liouville-von Neumann equation can be directly translated into the interaction picture, where it reads

$$\frac{\mathrm{d}}{\mathrm{d}t}\tilde{\rho}(t) = -i\left[\tilde{V}(t), \tilde{\rho}(t)\right], \tag{5.20}$$

where

$$\tilde{\rho}(t) = U(t)\rho(t)U^{\dagger}(t), \quad \tilde{V}(t) = U(t)VU^{\dagger}(t), \tag{5.21}$$

are the density matrix and interaction Hamiltonian in the interaction picture, respectively. By looking at the definition of $U(t)$, it is clear that the time evolution in the interaction picture is only governed by the interaction part of the Hamiltonian. This will be used to our advantage in the derivation of the master equation. The solution of Eq. (5.20) can be written as

$$\tilde{\rho}(t) = \tilde{\rho}(0) - i\int_0^t dt' \left[\tilde{V}(t'), \tilde{\rho}(t')\right], \tag{5.22}$$

where we set the initial time to zero. By inserting this solution into Eq. (5.20), we find the iterative equation

$$\frac{d}{dt}\tilde{\rho}(t) = -i\left[\tilde{V}(t), \tilde{\rho}(0)\right] - \int_0^t dt' \left[\tilde{V}(t), \left[\tilde{V}(t'), \tilde{\rho}(t')\right]\right]. \tag{5.23}$$

As mentioned before, the idea is to single out the small system's evolution from the global system. Therefore, we introduce the reduced density matrix of the small system by "tracing out" the reservoir degrees of freedom from the density matrix,

$$\tilde{\rho}_S(t) = \text{Tr}_R\tilde{\rho}(t), \tag{5.24}$$

which obeys the following equation of motion

$$\frac{d}{dt}\tilde{\rho}_S(t) = -i\text{Tr}_R\left\{\left[\tilde{V}(t), \tilde{\rho}(0)\right]\right\} - \text{Tr}_R\left\{\int_0^t dt' \left[\tilde{V}(t), \left[\tilde{V}(t'), \tilde{\rho}(t')\right]\right]\right\}. \tag{5.25}$$

Until now, the equations are exact. To continue, however, we need to make some approximations. First, we make the following assumptions about the reservoir. We assume that the reservoir is large compared to the system, in thermal equilibrium, and the coupling between the reservoir and the system is weak. This means that the states of the reservoir hardly vary due to the coupling to the system, and we can neglect the time dependence of the reservoirs' density matrix (that is defined by tracing out the system degrees of freedom),

$$\tilde{\rho}_R(t) = \text{Tr}_S\tilde{\rho}(t) \approx \tilde{\rho}_R(0) = \tilde{\rho}_R. \tag{5.26}$$

We now assume that the correlations between the system and the reservoir are small at the initial time $t = 0$ and contribute little to the system's evolution. With this assumption, we can write the total density matrix as

$$\tilde{\rho}(t) = \tilde{\rho}_S(t) \otimes \tilde{\rho}_R. \tag{5.27}$$

This approximation is called the *Born approximation*. Next, we assume that the interaction between the system and the reservoir is given by a product of the form $V = -SR$, where S and R are variables of the system and the reservoir, respectively. In the interaction picture, this can be written as

$$\tilde{V}(t) = -\tilde{S}(t)\tilde{R}(t), \tag{5.28}$$

where

$$\tilde{S}(t) = e^{iH_S t} S e^{-iH_S t}, \quad \tilde{R}(t) = e^{iH_R t} R e^{-iH_R t}, \tag{5.29}$$

since the variables of the system and the reservoir commute with each other. This type of coupling is for example given by the dipole approximation of an atom coupled to an electromagnetic field, see Sec. 4.3. With this assumption, Eq. (5.25) will contain terms of the form $\text{Tr}_R\left\{\tilde{\rho}_R \tilde{R}(t)\right\}$ and $\text{Tr}_R\left\{\tilde{\rho}_R \tilde{R}(t')\tilde{R}(t'')\right\}$. The first expression describes the average value of the observable in the reservoir, which we assume to be zero,

$$\text{Tr}_R\left\{\tilde{\rho}_R \tilde{R}(t)\right\} = 0. \tag{5.30}$$

From this it also follows that inside the reservoir, the average value of the interaction Hamiltonian itself vanishes for all times t,

$$\text{Tr}_R\left\{\tilde{\rho}_R \tilde{V}(t)\right\} = \tilde{S}(t)\text{Tr}_R\left\{\tilde{\rho}_R \tilde{R}(t)\right\} = 0. \tag{5.31}$$

Now we take a closer look at the terms of the form $\text{Tr}_R\left\{\tilde{\rho}_R \tilde{R}(t')\tilde{R}(t'')\right\}$, that describe correlations of the bath-observable at different times. Since we assume the reservoir to be in thermal equilibrium, it can be shown that this expression only depends on the time difference of the two times $\tau = t' - t''$,

$$g(t', t'') = g(\tau) = \text{Tr}_R\left\{\tilde{\rho}_R \tilde{R}(t')\tilde{R}(t'')\right\} = \text{Tr}_R\left\{\tilde{\rho}_R \tilde{R}(0)\tilde{R}(\tau)\right\} \tag{5.32}$$

where we defined the two-times correlation function $g(t', t'')$. We associate τ with the correlation time of the bath $\tau = \tau_R$. It can be shown that for an unstructured bath with a large number of degrees of freedom, the energy excitations average out, for large τ [135, 143]. Effectively, we can assume that the reservoir is in a stationary state with a short correlation time τ_R, compared to the time scale of the system's evolution in the interaction picture τ_S. In other words, the evolution of the system only depends on the present state of the bath and not on its past, and memory effects can be neglected. Such processes are called *Markov processes* and the corresponding approximation to neglect memory effects is called the *Markov approximation*. Using both the Born and the Markov approximation, the integral equation for $\tilde{\rho}_S(t)$ (5.25) can be simplified as follows: We remove the memory effects from the density matrix by replacing $\tilde{\rho}(t') \to \tilde{\rho}(t)$, we substitute $t' = t - s$, which lets us push the upper integral limit to ∞, since we assume that $\tau_R \ll \tau_S$, and we assume vanishing system-bath-correlations according to Eq. (5.27). The integral equation for $\tilde{\rho}_S(t)$ then reads

$$\frac{\mathrm{d}}{\mathrm{d}t}\tilde{\rho}_S(t) = -\int_0^\infty \mathrm{d}s \, \mathrm{Tr}_R \left\{ \left[\tilde{V}(t), \left[\tilde{V}(t-s), \tilde{\rho}_S(t) \otimes \tilde{\rho}_R \right] \right] \right\}. \tag{5.33}$$

5.2.1 The quantum-optical master equation

The Markovian master equation (5.33) derived in the previous section is valid for any Markovian process in the weak coupling regime. To proceed further, we now make more specific assumptions about the systems since we eventually want to derive the quantum-optical master equation. We assume an emitter coupled to a bath of many bosonic modes, where the coupling (in both the Schrödinger and the interaction picture) is of the form $\tilde{V}(t) = -\tilde{S}(t)\tilde{R}(t)$, as in Eq. (5.28), where S stands for *system* and R stands for *reservoir*. However, the derivation we do in the following is not specific for quantum optical systems, but we want to keep them in mind. We insert the ansatz (5.28) into the Markovian master equation (5.33) and obtain

$$\frac{\mathrm{d}}{\mathrm{d}t}\tilde{\rho}_S(t) = \int_0^\infty \left[\langle \tilde{R}(\tau)\tilde{R}(0)\rangle \left\{ \tilde{S}(t-\tau)\tilde{\rho}_S(t)\tilde{S}(t) - \tilde{S}(t)\tilde{S}(t-\tau)\tilde{\rho}_S(t) \right\} \right.$$
$$\left. + \left[\langle \tilde{R}(0)\tilde{R}(\tau)\rangle \left\{ \tilde{S}(t)\tilde{\rho}_S(t)\tilde{S}(t-\tau) - \tilde{\rho}_S(t)\tilde{S}(t-\tau)\tilde{S}(t) \right\} \right] \mathrm{d}\tau, \tag{5.34}$$

where we used that $\langle \tilde{R}(t)\tilde{R}(t-\tau)\rangle = \mathrm{Tr}_R\left\{ \tilde{R}(t)\tilde{R}(t-\tau) \right\} = \langle \tilde{R}(\tau)\tilde{R}(0)\rangle$ only depends on the time difference τ. Now we write $\tilde{S}$ in the eigenbasis

of the system Hamiltonian H_S, $H_S|n\rangle = \omega_n|n\rangle$,

$$\tilde{S}(t) = \sum_{m,n} e^{i\omega_m t}|m\rangle\langle m|S|n\rangle\langle n|e^{-i\omega_m t}$$

$$= \sum_{m,n} S_{mn}|m\rangle\langle n|e^{i\omega_{m,n}t} = \sum_{m,n} \tilde{S}_{mn}e^{i\omega_{mn}t}, \qquad (5.35)$$

where $\omega_{mn} = \omega_m - \omega_n$ and $\tilde{S}_{mn} = S_{mn}|m\rangle\langle n|$. Then with the definition

$$\Gamma_{mn} = \int_0^\infty \mathrm{d}\tau \langle \tilde{R}(\tau)\tilde{R}(0)\rangle e^{i\omega_{mn}\tau}, \qquad (5.36)$$

Eq. (5.34) becomes

$$\frac{\mathrm{d}}{\mathrm{d}t}\tilde{\rho}_S(t) = \sum_{m,n}\sum_{m',n'} \Gamma_{mn} e^{i(\omega_{m',n'}-\omega_{m,n})t}\left\{\tilde{S}_{mn}^\dagger\tilde{\rho}_S(t)\tilde{S}_{m'n'} - \tilde{S}_{m'n'}\tilde{S}_{mn}^\dagger\tilde{\rho}_S(t)\right\} + \text{h.c.}$$

$$(5.37)$$

To proceed from here, we perform the RWA, meaning that we neglect the fast rotating terms since we assume that they average out with respect to the time scale of the system correlation time. This means we only keep the terms that give $\omega_{m',n'} - \omega_{m,n} = 0$ and one of the sums can be resolved. This approximation is also called the *secular approximation*. However, this approximation can only be applied for non-equidistant energy spectra and not for, e.g., harmonic oscillators. This situation is called a *Liouvillian degeneracy* and it leads to a breakdown of the secular approximation [156, 157]. We divide Γ_{mn} into real and imaginary parts, $\Gamma_{mn} = \frac{1}{2}\gamma_{mn} + i\xi_{mn}$ and arrive at the following compact form of the master equation

$$\frac{\mathrm{d}}{\mathrm{d}t}\tilde{\rho}_S(t) = -i\left[H_{LS}, \tilde{\rho}_S(t)\right] + \mathcal{D}\tilde{\rho}_S(t), \qquad (5.38)$$

where we defined the *dissipator* that is, as the name says, responsible for the dissipation in the master equation

$$\mathcal{D}\tilde{\rho}_S(t) = \sum_{m,n} \gamma_{mn}\left(\tilde{S}_{mn}^\dagger\tilde{\rho}_S(t)\tilde{S}_{mn} - \frac{1}{2}\tilde{S}_{mn}\tilde{S}_{mn}^\dagger\tilde{\rho}_S(t) - \frac{1}{2}\tilde{\rho}_S(t)\tilde{S}_{mn}\tilde{S}_{mn}^\dagger\right)$$

$$+ \sum_{m,n} \gamma_{mm}\left(\tilde{S}_{mm}^\dagger\tilde{\rho}_S(t)\tilde{S}_{nn} - \frac{1}{2}\tilde{S}_{nn}\tilde{S}_{mm}^\dagger\tilde{\rho}_S(t) - \frac{1}{2}\tilde{\rho}_S(t)\tilde{S}_{nn}\tilde{S}_{mm}^\dagger\right) \qquad (5.39)$$

and the Lamb-shift Hamiltonian

$$H_{LS} = \sum_{m,n} \xi_{mn}\left|S_{mn}\right|^2|m\rangle\langle m| + \sum_m \xi_{mn}\left|S_{mm}\right|^2|m\rangle\langle m| \qquad (5.40)$$

that only renormalises the system's energies because it commutes with the system Hamiltonian and is therefore often neglected. We can transform Eq. (5.38) back from the interaction picture and find the master equation for the system to be

$$\frac{\mathrm{d}}{\mathrm{d}t}\rho_S(t) = -i\left[H_S, \rho_S(t)\right] + \mathcal{D}\rho_S(t). \tag{5.41}$$

The form of this master equation is very compact and a potent tool to calculate the evolution of any system that is weakly coupled to an environment with many degrees of freedom (although it has to fulfil all the criteria that we assumed while deriving the equation). As mentioned before, we are specifically interested in the master equation of one emitter coupled to the discrete modes of an electromagnetic field. The Hamiltonian of such a system reads

$$H = H_S + H_R + V, \tag{5.42}$$

$$H_S = \frac{\omega_0}{2}\sigma_z, \tag{5.43}$$

$$H_R = \sum_k \omega_k b_k^\dagger b_k, \tag{5.44}$$

$$V = S(t)R(t) = S(t)\sum_k g_k\left(b_k + b_k^\dagger\right), \tag{5.45}$$

where H_S describes a two-level system with transition frequency ω_0 and $b_k^\dagger$ and b_k create and annihilate an excitation in the electromagnetic field with frequency ω_k, respectively. We did not specify the system part in the coupling term $S(t)$ at this point since we want to discuss the effects of different coupling directions later on. With this Hamiltonian, we can write down a more specific expression for $\gamma_{mn} = \Gamma_{mn} + \Gamma_{mn}^*$,

$$\gamma_{mn} = \int_{-\infty}^{\infty} \mathrm{d}s\langle R^\dagger(\tau)R(0)\rangle e^{i\omega_{mn}\tau}, \quad \gamma_{mm} = \int_{-\infty}^{\infty} \mathrm{d}s\langle R^\dagger(\tau)R(0)\rangle, \tag{5.46}$$

$$\langle R^\dagger(\tau)R(0)\rangle = \sum_k g_k^2\left(N(\omega_k)e^{i\omega_k\tau} + \left[N(\omega_k) + 1\right]e^{-i\omega_k\tau}\right), \tag{5.47}$$

where $N(\omega_k)$ is the average number of photons in the mode k in thermal equilibrium, which is given by the Boltzmann distribution

$$N(\omega_k) = \frac{1}{e^{\beta\omega_k} + 1}, \tag{5.48}$$

where $\beta = 1/k_B T$ is the inverse of the product of the temperature T times the Boltzmann constant k_B. We see that for $T \to 0$, the average number of photons becomes zero. Since many experiments that work in the microwave regime are performed at close to 0 K, the number of photons is often set to zero. For optical frequencies, the number of photons is close to zero even at room temperature. However, we want to keep the photon number N finite. Now we replace the sum with an integral over all frequencies and the density of state, $\Sigma_k \to \int J(\omega)\,d\omega$, and find

$$\gamma_{mn} = \Gamma \begin{cases} 1 + N(\omega_{mn}), & \text{for} \quad \omega_{mn} > 0 \\ N(\omega_{mn}), & \text{for} \quad \omega_{mn} < 0 \end{cases}, \tag{5.49}$$

where $\Gamma = 2\pi J(|\omega_{mn}|)g(|\omega_{mn}|)^2$ is the spontaneous emission rate.

In the following, we are going to discuss different directions of the coupling with respect to the quantization of the qubit, σ_z. First, we assume *transverse coupling* along the x-direction. The coupling term of the system then reads $\tilde{S}(t) = \sigma_x(t) = \sigma_+ e^{i\omega_0 t} + \sigma_- e^{-i\omega_0 t}$, which means that $S(t)$ only contains off-diagonal elements. The dissipator for the transverse coupling then reads

$$\begin{aligned} \mathcal{D}\rho &= \Gamma(N+1)\left(\sigma_-\rho\sigma_+ - \frac{1}{2}\sigma_+\sigma_-\rho - \frac{1}{2}\rho\sigma_+\sigma_-\right) \\ &+ \Gamma N\left(\sigma_+\rho\sigma_- - \frac{1}{2}\sigma_-\sigma_+\rho - \frac{1}{2}\rho\sigma_-\sigma_+\right) \\ &\equiv \Gamma(N+1)\mathcal{D}\left[\sigma_-\right]\rho + \Gamma N\mathcal{D}\left[\sigma_+\right]\rho, \end{aligned} \tag{5.50}$$

where we define the *Linbladian super operator* $\mathcal{D}[X] = X\rho X^\dagger - \frac{1}{2}X^\dagger X\rho - \frac{1}{2}\rho X^\dagger X$ [158]. Next, we consider *longitudinal coupling* along the z-axis. The system coupling term then becomes $\tilde{S}(t) = \sigma_z = |0\rangle\langle 0| - |1\rangle\langle 1|$, which stays time independent even in the interaction picture, since the corresponding frequencies in the exponentials sum up to zero. The dissipator only contains diagonal terms for the coupling in the z-direction and reads

$$\mathcal{D}\rho = \frac{\Gamma_\phi}{2}\left(\sigma_z\rho\sigma_z - \rho\right) \equiv \Gamma_\phi \mathcal{D}\left[\sigma_z\right]\rho \tag{5.51}$$

where we defined the *pure dephasing rate* $\Gamma_\phi = \gamma_{00}/2 + \gamma_{11}/2$. With this, we can finally write down the full master equation for a qubit coupled to

a set of discrete modes at a finite temperature

$$\frac{\mathrm{d}}{\mathrm{d}t}\rho(t) = -i\left[-\frac{\omega_0}{2}, \rho\right] + \Gamma\left(N+1\right)\mathcal{D}\left[\sigma_-\right]\rho + \Gamma N \mathcal{D}\left[\sigma_+\right]\rho + \Gamma_\phi \mathcal{D}\left[\sigma_z\right]\rho.$$

(5.52)

The first term of Eq. (5.52) is simply the Liouville-von Neumann equation that governs the system's evolution under its own Hamiltonian. The second term leads to both a decay in the state population that is described by the diagonal elements (*relaxation*) and a decay of the off-diagonal elements (*dephasing*). The third term describes thermal excitation and vanishes for $N=0$ and is therefore often neglected. The forth term only leads to a decay of the off-diagonal terms, called *pure dephasing*. The name *dephasing* comes from the fact that the off-diagonal terms contain phase information of the states, leading to quantum mechanical interference. This information loss process is called *decoherence*.

5.3 Input-output relations

In the previous section, we derived the master equation for an emitter coupled to an electromagnetic field. There are many ways to investigate the interaction between light and matter. One way is to drive the qubit with a continuous field and measure its state by probing it with another weak field and measure the reflected or transmitted field [46, 83, 89]. Therefore it is helpful to derive *input-output* relations for the field that interacts with the qubit, which can be used to calculate the reflected and transmitted fields [154, 159]. Here we will demonstrate how to derive the input-output relations for a qubit coupled to an electromagnetic field in a way that was used in Paper II and Paper IV.

We start with a Hamiltonian of a qubit coupled to a field of continuous modes. Here, we add only one input/output channel to the system. Adding another channel does not significantly change the math but makes it slightly more tedious. We add another channel once we derived the input-output relations. The Hamiltonian we consider is similar to the one in the previous section (5.42) and reads

$$H = H_{\mathrm{sys}} + H_{\mathrm{field}} + H_{\mathrm{int}},$$

(5.53)

$$H_{\mathrm{sys}} = \frac{\omega_0}{2}\sigma_z,$$

(5.54)

$$H_{\text{field}} = \int_0^\infty d\omega\, \omega b_\omega^\dagger b_\omega, \tag{5.55}$$

$$H_{\text{int}} = \int_0^\infty d\omega g(\omega) \left[b_\omega^\dagger \sigma_- + b_\omega \sigma_+ \right], \tag{5.56}$$

where $b_\omega^\dagger$ and b_ω are bosonic ladder operators that create and annihilate a photonic excitation with frequency ω, respectively. The coupling is given by $g(\omega)$, which is generally frequency-dependent. Here, we assume a slowly varying coupling and approximate $g(\omega) = \sqrt{\Gamma/2\pi}$. Another simplification we do is extending the lower integral limits to $-\infty$, which is valid for $\Gamma \ll \omega_0$ since only the terms with frequencies close to ω_0 contribute [137]. With these assumptions the field and interaction parts of the Hamiltonian read

$$H_{\text{field}} = \int_{-\infty}^\infty d\omega\, \omega b_\omega^\dagger b_\omega, \tag{5.57}$$

$$H_{\text{int}} = \int_{-\infty}^\infty d\omega \sqrt{\frac{\Gamma}{2\pi}} \left(b_\omega^\dagger \sigma_- + b_\omega \sigma_+ \right). \tag{5.58}$$

We derive the input-output relations by calculating the Heisenberg equations of motion for b_ω and σ_-. The equation of motion for the bosonic operator b_ω reads

$$\frac{d}{dt} b_\omega(t) = i \int_{-\infty}^\infty d\omega\, \omega' \left[b_\omega^\dagger b_\omega, b_{\omega'} \right] + i \sqrt{\frac{\Gamma}{2\pi}} \int_{-\infty}^\infty d\omega \left[b_\omega^\dagger \sigma_-, b_{\omega'} \right]$$

$$= -i\omega b_\omega - i \sqrt{\frac{\Gamma}{2\pi}} \sigma_-. \tag{5.59}$$

The solution to this equation can be written as

$$b_\omega(t) = e^{-i\omega(t-t_0)} b_\omega(t_0) - i \sqrt{\frac{\Gamma}{2\pi}} \int_{t_0}^t dt' \sigma_-(t') e^{-i\omega(t-t')}, \tag{5.60}$$

where t_0 is the initial time $t_0 < t$. The equation of motion for σ_- is given by

$$\frac{d}{dt} \sigma_- = i \frac{\omega_0}{2} [\sigma_z, \sigma_-] + i \sqrt{\frac{\Gamma}{2\pi}} \int_{-\infty}^\infty d\omega [b_\omega \sigma_+, \sigma_-]$$

$$= -i\omega_0 \sigma_- + i\sigma_z \sqrt{\frac{\Gamma}{2\pi}} \int_{-\infty}^\infty d\omega\, b_\omega, \tag{5.61}$$

where we used the commutation relations $[\sigma_+, \sigma_-] = \sigma_z$, $[\sigma_-, \sigma_z] = 2\sigma_-$. We put the solution for b_ω (5.60) into Eq. (5.61) and find

$$
\begin{aligned}
\frac{\mathrm{d}}{\mathrm{d}t}\sigma_- = &- i\omega_0\sigma_- + i\sqrt{\frac{\Gamma}{2\pi}}\int_{-\infty}^{\infty} \mathrm{d}\omega\, e^{-i\omega(t-t_0)}b_\omega(t_0) \\
&+ \sigma_z\frac{\Gamma}{2\pi}\int_{-\infty}^{\infty} \mathrm{d}\omega \int_{t_0}^{t} \mathrm{d}t'\,\sigma_-(t')\,e^{-i\omega(t-t')} \\
= &- i\omega_0\sigma_- + i\sqrt{\Gamma}b_{\mathrm{in}}(t) + \frac{\Gamma}{2}\sigma_-,
\end{aligned}
\tag{5.62}
$$

where we used

$$
\frac{1}{2\pi}\int_{-\infty}^{\infty} \mathrm{d}\omega\, e^{-i\omega(t-t')} = \delta\left(t-t'\right),
\tag{5.63}
$$

and

$$
\int_{t_0}^{t} \mathrm{d}t'\,\sigma_-(t')\,\delta\left(t-t'\right) = \frac{1}{2}\sigma_-,
\tag{5.64}
$$

and defined the operator of the incoming field

$$
b_{\mathrm{in}}(t) = \frac{1}{\sqrt{2\pi}}\int_{-\infty}^{\infty} \mathrm{d}\omega\, e^{-i\omega(t-t_0)}b_\omega(t_0).
\tag{5.65}
$$

Instead of defining an incoming field at an earlier time $t_0 < t$, we can also write the solution for Eq. (5.59) at a later time $t_1 > t$ as,

$$
b_\omega(t) = e^{-i\omega(t-t_0)}b_\omega(t_1) + i\sqrt{\frac{\Gamma}{2\pi}}\int_{t}^{t_1} dt'\sigma_-(t')\,e^{-i\omega(t-t')},
\tag{5.66}
$$

and hence the equation of motion for σ_- becomes

$$
\frac{\mathrm{d}}{\mathrm{d}t}\sigma_- = -i\omega_0\sigma_- + i\sqrt{\Gamma}b_{\mathrm{out}}(t) - \frac{\Gamma}{2}\sigma_-,
\tag{5.67}
$$

where we defined the outgoing field at time $t_1 > t$

$$
b_{\mathrm{out}}(t) = \frac{1}{\sqrt{2\pi}}\int_{-\infty}^{\infty} \mathrm{d}\omega\, e^{-i\omega(t-t_1)}b_\omega(t_1).
\tag{5.68}
$$

Comparing both equations for σ_-, Eq.s (5.62) and (5.67), we find the *input-output relation* that connects the outgoing to the incoming field for a point-like coupling

$$
b_{\mathrm{out}}(t) = b_{\mathrm{in}}(t) + i\sqrt{\Gamma}\sigma_-.
\tag{5.69}
$$

This input-output relation corresponds to a qubit coupled to a semi-infinite waveguide. In the case of an open TL, we can easily expand this relation to another output channel. We do this by keeping the total decay rate constant and define

$$b_{\text{out}}^{L}(t) = b_{\text{in}}^{L}(t) + i\sqrt{\frac{\Gamma}{2}}\sigma_{-}, \qquad (5.70)$$

$$b_{\text{out}}^{R}(t) = b_{\text{in}}^{R}(t) + i\sqrt{\frac{\Gamma}{2}}\sigma_{-}, \qquad (5.71)$$

where $b_{\text{in/out}}^{L/R}(t)$ are the input/output fields on the left L and right R side if the qubit. It is common to assume a coherent probe field $\alpha_{\text{in/out}} = \langle b_{\text{in/out}} \rangle$ and, furthermore, one is most often interested in the steady-state output of the system. With these assumptions, and by assuming that we have only one probe field from the left side of the qubit, the input-output relations become

$$\alpha_{\text{out}}^{L}(t) = i\sqrt{\frac{\Gamma}{2}} \langle \sigma_{-} \rangle, \qquad (5.72)$$

$$\alpha_{\text{out}}^{R}(t) = \alpha_{\text{in}}^{L}(t) + i\sqrt{\frac{\Gamma}{2}} \langle \sigma_{-} \rangle, \qquad (5.73)$$

where $\alpha_{\text{out}}^{L}(t)$ is the reflected field and $\alpha_{\text{out}}^{R}(t)$ is the transmitted field. In the following, we calculate the reflection and transmission of a qubit coupled to an open waveguide.

5.4 Reflection of a qubit in a waveguide

Photon scattering on a qubit is a common way to characterise its properties, e.g., its transition frequency, decay rates or even its current state [46, 83, 89]. Scattering on a superconducting qubit in a one-dimensional waveguide has shown reflectance of up to 99% when probed by its exact transition frequency [138, 160–162]. In Paper II, we use coherent and incoherent scattering on a superconducting qubit to analyse the qubit's relaxation and decoherence times. In Paper III, we calculate the reflection of a transmon qubit in a high-impedance transmission line. In Paper IV, we calculate the reflection of various kinds of set-ups of an atom in front of a mirror where it is possible to achieve amplification of a probe signal.

In the following, we show how to calculate the reflection of a two-level system in a one-dimensional waveguide with two input-output channels probed by a coherent field using the master equation.

5.4.1 Two-level system in a rotating frame

We start with the Hamiltonian of a two-level system interacting with a coherent field

$$H = \frac{\omega_0}{2}\sigma_z + \frac{\Omega}{2}\left(\sigma_+ e^{i\omega_p t} + \sigma_- e^{-i\omega_p t}\right), \tag{5.74}$$

where ω_0 is the qubit frequency and ω_p is the frequency of the probe field. It is often convenient to transform the Hamiltonian into the rotating frame of the probe. The transformation is given by

$$H_{\mathrm{RF}} = R^\dagger(t) H R(t) + i\frac{\mathrm{d}R^\dagger(t)}{\mathrm{d}t}R(t), \tag{5.75}$$

with the unitary operator $R(t) = e^{-i\sigma_z \omega_p t}$. If we assume that the Rabi frequency is real $\Omega = \Omega^*$, the Hamiltonian in the rotating frame, which we for simplification denote by H, reads

$$H = \frac{\delta\omega}{2}\sigma_z + \frac{\Omega}{2}\left(\sigma_+ + \sigma_-\right), \tag{5.76}$$

where $\delta\omega = \omega_p - \omega_0$ is the detuning between the probe frequency and the transition frequency of the qubit.

5.4.2 Optical Bloch equations and reflection

Now starting with our simplified Hamiltonian in the rotating frame, we can easily calculate the optical Bloch equations of the two-level system with the help of the master equation. With the optical Bloch equations, we can solve for the steady-state solutions of the Pauli matrices. In order to calculate the reflection, we need the steady-state solution of the σ_- operator, which corresponds to one of the off-diagonal matrix elements of the 2×2 dimensional density matrix's steady-state solution ρ_S, according to $\langle\sigma_-\rangle = \mathrm{Tr}\left(\sigma_- \rho_S\right)$. The reflection coefficient is given by the ratio of the output- and input field,

$$r = \frac{\alpha_{\mathrm{out}}^L}{\alpha_{\mathrm{in}}^L}. \tag{5.77}$$

Using the input-output relations (5.72) and (5.73), this reflection coefficient reads

$$r = -i\frac{\Gamma}{\Omega}\langle\sigma_-\rangle. \tag{5.78}$$

Note that the input-output relation with only one input-output channel leads to an additional factor of two in front of the second term, which is the case in Paper II and IV since we deal with an atom in front of a mirror. However, here we chose to calculate the reflection and transmission of a qubit coupled to an open TL. The transmission is given by

$$t = 1 + r = 1 - i\frac{\Gamma}{\Omega}\langle\sigma_-\rangle. \tag{5.79}$$

The master equation for our system reads

$$\frac{\mathrm{d}}{\mathrm{d}t}\rho(t) = -i\left[\frac{\delta\omega}{2}\sigma_z + \frac{\Omega}{2}\left(\sigma_+ + \sigma_-\right), \rho\right] + \Gamma\mathcal{D}\left[\sigma_-\right]\rho, \tag{5.80}$$

where we neglected pure dephasing, $\Gamma_\phi = 0$, and assumed zero temperature without thermal excitations, $N = 0$. By using $\langle\sigma_i\rangle = \mathrm{Tr}\left(\sigma_i\rho\right)$, we find the following equations of motion which are called the *the optical Bloch equations* [163],

$$\langle\dot{\sigma}_z\rangle = \Gamma\left(1 - \langle\sigma_z\rangle\right) - i\Omega\left(\langle\sigma_+\rangle - \langle\sigma_-\rangle\right), \tag{5.81}$$

$$\langle\dot{\sigma}_+\rangle = \left(-i\delta\omega - \frac{\Gamma}{2}\right)\langle\sigma_+\rangle - i\frac{\Omega}{2}\langle\sigma_z\rangle \tag{5.82}$$

$$\langle\dot{\sigma}_-\rangle = \left(i\delta\omega - \frac{\Gamma}{2}\right)\langle\sigma_-\rangle + i\frac{\Omega}{2}\langle\sigma_z\rangle. \tag{5.83}$$

Now we solve for the steady state of these equations by setting $\left\langle\frac{\mathrm{d}}{\mathrm{d}t}\sigma_i\right\rangle = 0$. The solution for the steady-state value of $\langle\sigma_-\rangle$, which we need to calculate the reflection (5.78) and transmission (5.79), is given by

$$\langle\sigma_-\rangle = \frac{\Omega\left(i\frac{\Gamma}{2} + \delta\omega\right)}{\frac{\Gamma^2}{2} + 2\delta\omega^2 + \Omega^2}. \tag{5.84}$$

The reflection and the transmission then become

$$r = -\Gamma\frac{i\delta\omega - \frac{\Gamma}{2}}{\frac{\Gamma^2}{2} + 2\delta\omega^2 + \Omega^2}, \tag{5.85}$$

$$t = 1 - \Gamma\frac{i\delta\omega - \frac{\Gamma}{2}}{\frac{\Gamma^2}{2} + 2\delta\omega^2 + \Omega^2}. \tag{5.86}$$
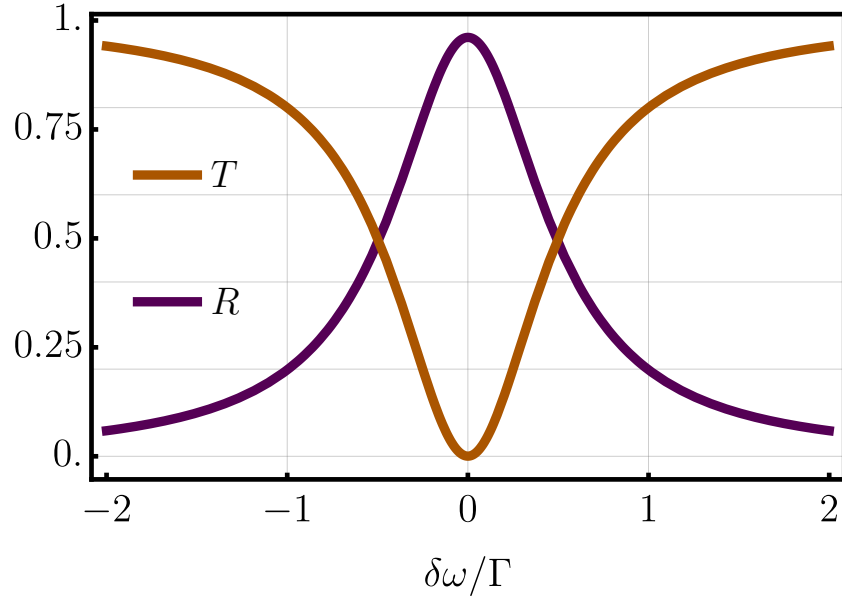
Figure 5.1: *Reflectance $R = |r|^2$ (purple) and transmittance $T = |t|^2$ (orange) as a function of the detuning between the probe frequency and the qubit frequency $\delta\omega/\Gamma = (\omega_p - \omega_0)/\Gamma$ for a weak probe $\Omega/\Gamma = 0.1$. The reflection is zero except around the resonance frequency of the qubit, where the reflection reaches unity. This happens because for a resonant probe, the qubit becomes excited and is able to reflect photons back into the incoming direction. The transmittance is unity except around the qubit frequency where the qubit acts as a mirror.*

The reflectance $R = |r|^2$ and transmittance $T = |t|^2$ are plotted as a function of the detuning $\delta\omega = \omega_p - \omega_0$ in Fig 5.1 for a weak probe field. The reflection is zero for all frequencies except around the resonance frequency of the qubit. Off-resonance, the qubit lets all the incoming photons pass, and the transmittance is one. On resonance, the qubit becomes excited and emits the photons back in the input direction, causing a reflectance of unity. The transmittance, on the other hand, becomes zero in this case due to destructive interference in the forward direction. The qubit probed by a weak resonant field acts like a short [138, 160–162].

6 The dressed state picture

In the previous chapter, we studied the interaction of light and matter in a semi-classical regime. This approach is sufficient for weak interactions, e.g., the reflection of a weak probe field on a qubit. However, when the atom is driven by a strong pump field, it is advantageous to treat the electromagnetic field in a different way. The strong pump field causes the energy structure of the atom to change. In fact, it merges the atom and the electromagnetic field into one inseparable system, and we speak of a so-called *dressed atom*. The atom's energy levels are effectively split into two levels separated by the Rabi frequency, which represents the strength of the pump field. Treating the system in the dressed state picture makes it possible to investigate an interesting property of the atom's spectral distribution, which shows a so-called *Mollow triplet*: a peak in the spectral density at the transition frequency of the bare atom accompanied by two smaller peaks between the "upper" and "lower" levels of the dressed states [164, 165]. In Paper II, we investigated the spectral density of a dressed atom both experimentally and theoretically. We used the fact that the Mollow triplet becomes asymmetric for off-resonant driving if pure dephasing is included to characterize the atom's different decay rates. Later in this chapter, we will explain the cause of the asymmetry. In Paper IV, we used the dressed state picture to investigate different set-ups to achieve a gain in the reflection of an atom in front of a mirror.

6.1 Energy spectrum of the dressed atom

In the following, we want to demonstrate how to derive the energy spectrum of the dressed atom [143]. We start by considering an atom that interacts with a laser field. The Hamiltonian of the uncoupled atom-laser system is given by

$$H = H_A + H_L, \tag{6.1}$$

$$H_A = \frac{\omega_0}{2}\sigma_z, \tag{6.2}$$
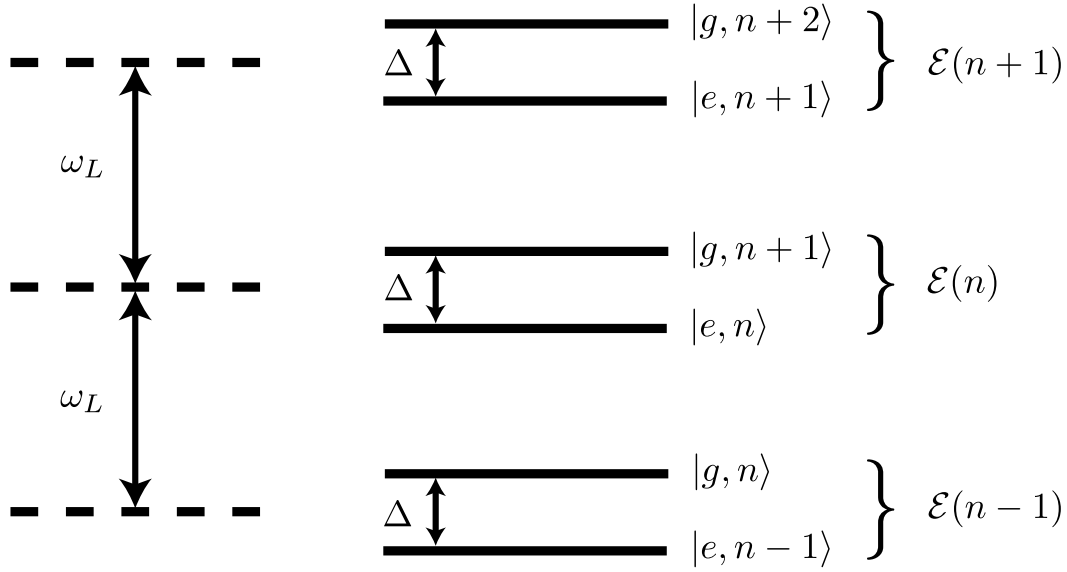
Figure 6.1: *Sketch of the energy structure of the combined atom-laser system. The dashed lines to the left show the energy levels of the laser excitations with equidistant levels separated by the frequency of one photon ω_L. The solid lines to the right show the energy levels of the combined system. For each laser excitation, there exists a manifold $\mathcal{E}(n)$ containing a pair of energy levels separated by the detuning $\Delta = \omega_L - \omega_0$.*

$$H_L = \omega_L \left(\hat{a}^\dagger a + \frac{1}{2} \right). \tag{6.3}$$

The eigenstates of the combined atom-laser system contain two quantum numbers, g or e, that indicate the ground and excited state of the qubit, respectively, and the number of laser photons n. The eigenstates can be divided in manifolds $\mathcal{E}(n)$ corresponding to the number of excitations that contain a pair of states each. These states are separated by the detuning between the atom's transition frequency and the laser frequency, $\Delta = \omega_L - \omega_0$. Each manifold contains the following set of states

$$\mathcal{E}(n) = \{ |g, n+1\rangle, |e, n\rangle \}. \tag{6.4}$$

A sketch of the energy structure is depicted in Fig. 6.1.

Now let us take a look at the coupling part of the Hamiltonian

$$V_{AL} = g \left(\sigma_+ + \sigma_- \right) \left(a^\dagger + a \right). \tag{6.5}$$

The coupling part couples the states of each manifold $\mathcal{E}(n)$ to each other. This means that the state $|g\rangle$ can absorb a laser photon and go to the

excited state $|e\rangle$. The matrix element of the coupling part within the manifold $\mathcal{E}(n)$ is given by

$$\langle e, n|V_{AL}|g, n+1\rangle = g\sqrt{n+1}. \tag{6.6}$$

In addition, the coupling part couples states from different manifolds to each other, e.g., the state $|g, n+1\rangle$ to $|e, n+2\rangle$, thus states separated by double the laser frequency $\pm 2\omega_L$. However, we neglect these kinds of transitions, which corresponds to applying the rotating wave approximation.

In most experiments, the driving is given by a coherent laser mode, and the coupling part of the Hamiltonian can be rewritten in terms of the Rabi frequency. The total coupled atom-laser Hamiltonian in the rotating wave approximation is then given by

$$H = \frac{\Delta}{2}\sigma_z + \frac{\Omega_R}{2}\left(\sigma_+ + \sigma_-\right) + \omega_L\left(\hat{a}^\dagger a + \frac{1}{2}\right), \tag{6.7}$$

with the two following eigenstates within the manifold $\mathcal{E}(n)$

$$|+, n\rangle = \sin\Theta|g, n+1\rangle + \cos\Theta|e, n\rangle \tag{6.8}$$
$$|-, n\rangle = \cos\Theta|g, n+1\rangle - \sin\Theta|e, n\rangle \tag{6.9}$$

with

$$\tan 2\Theta = -\frac{\Omega_R}{\Delta}, \quad \Theta \in [0, \pi/2). \tag{6.10}$$

The eigenvalues of the Hamiltonian are given by

$$\Omega_\pm = \pm\frac{1}{2}\sqrt{\Delta^2 + \Omega_R^2}, \tag{6.11}$$

and the two eigenstates are therefore separated by $\Omega = \sqrt{\Delta^2 + \Omega_R^2}$. For a resonant drive $\Delta = 0$, the splitting of the dressed states is given by the Rabi frequency Ω_R. A sketch of the dressed states can be seen in Fig. 6.2. It is interesting to look at the energy diagram of the dressed states, by plotting the eigenenergies as a function of the laser frequency. The most remarkable property of the dressed atom is the so-called *avoided crossing* of the eigenenergies. The uncoupled states $|g, n+1\rangle$ and $|e, n\rangle$ cross each other for zero detuning between the laser and the atom frequency $\Delta = 0$, whereas the dressed state energies do not cross but repel each other, see Fig. 6.3. The atom and the laser's energy structure can not be separated anymore in the regime of strong driving.
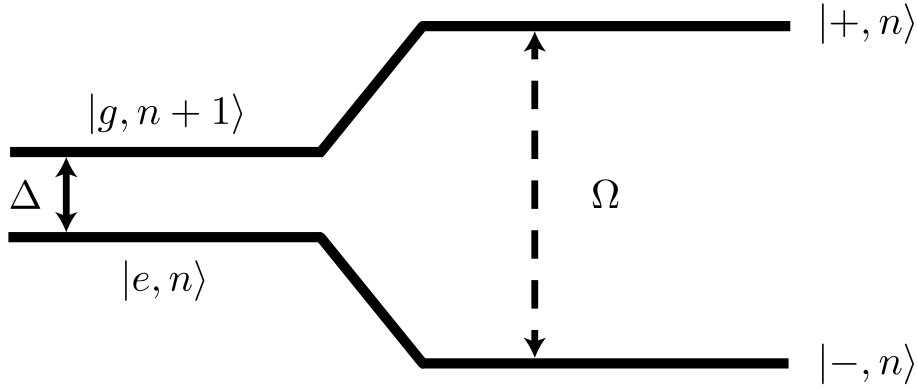
Figure 6.2: *Sketch of the dressed states of the manifold $\mathcal{E}(n)$. The coupling between the atom and the laser causes the uncoupled levels $|g, n+1\rangle$ and $|e, n\rangle$ to transform into the dressed states $|+, n\rangle$ and $|-, n\rangle$ that are separated by the frequency $\Omega = \sqrt{\Delta^2 + \Omega_R^2}$.*

6.2 Power spectrum and Mollow triplet

One consequence of the strong driving that leads to a dressed atom is a change of the atom's resonance fluorescence spectrum. As mentioned before, the spectrum contains one central peak and two additional side peaks with a distance of the Rabi frequency to the central peak. These peaks are known as the *Mollow triplet* [164]. Now we want to demonstrate how to calculate the power spectral density of a driven two-level system, where we closely follow Ref. [166].

As usual, we start by the Hamiltonian of a two-level system coupled to a coherent drive field

$$H = \frac{\Delta}{2}\sigma_z + \frac{\Omega}{2}\left(\sigma_+ + \sigma_-\right), \qquad (6.12)$$

where $\Delta = \omega_L - \omega_0$ is the detuning between the drive frequency ω_L and the qubit frequency ω_0 and Ω denotes the Rabi frequency that symbolizes the drive strength. To calculate the Bloch equations, we use the Master equation in Lindblad form,

$$\frac{\mathrm{d}}{\mathrm{d}t}\rho = -i[H, \rho] + \Gamma_1 \mathcal{D}\left[\sigma_-\right]\rho + \frac{\Gamma_\phi}{2}\mathcal{D}\left[\sigma_z\right]\rho, \qquad (6.13)$$

where $\mathcal{D}[X] = X\rho X^\dagger - 1/2X^\dagger X\rho - 1/2\rho X^\dagger X$ is the dissipator, Γ_1 is the relaxation rate of the qubit and Γ_ϕ is the pure dephasing rate. To write the Bloch equations in the rotating frame, we define the following new
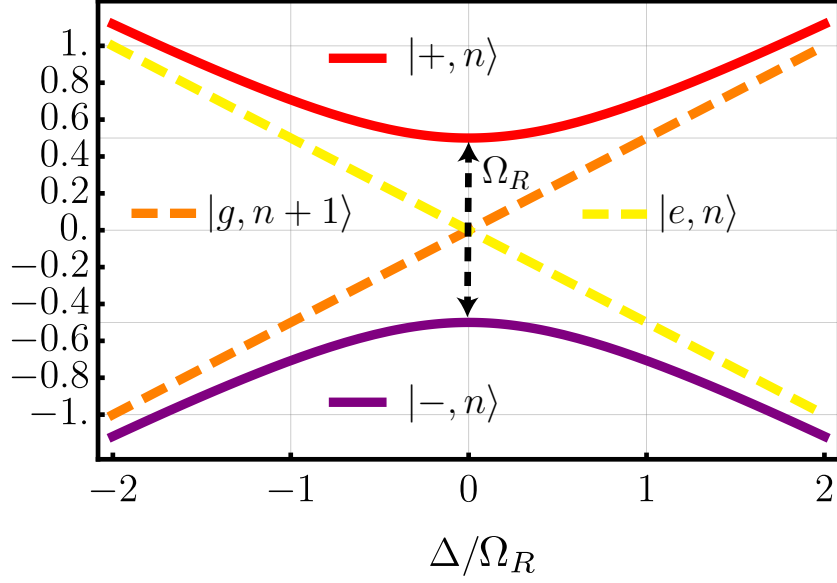
Figure 6.3: *Energy diagram (scaled with the Rabi frequency Ω_R) of the bare and dressed states corresponding to the manifold $\mathcal{E}(n)$ as a function of the detuning Δ. The bare states $|g, n+1\rangle$ (dashed orange) and $|e, n\rangle$ (dashed yellow) cross each other for zero detuning. The energy levels of the dressed states $|+, n\rangle$ (solid purple) and $|-, n\rangle$ (solid red) on the other hand repel each other at $\Delta = 0$. The splitting between the states at $\Delta = 0$ is given by the Rabi frequency Ω_R.*

variables:

$$s_1(t) = \rho_{10}(t) = \langle \sigma_-(t) \rangle \, e^{i\omega_L t}, \quad s_2(t) = \rho_{11}(t) = \langle \sigma_+(t)\sigma_-(t) \rangle. \quad (6.14)$$

With these definitions, the Bloch equations take the following form

$$\frac{\mathrm{d}}{\mathrm{d}t} \begin{pmatrix} s_1 \\ s_1^* \\ s_2 \end{pmatrix} = M \begin{pmatrix} s_1 \\ s_1^* \\ s_2 \end{pmatrix} + B, \quad (6.15)$$

where

$$M = \begin{pmatrix} i\Delta - \Gamma_2 & 0 & i\Omega \\ 0 & -i\Delta - \Gamma_2 & -i\Omega \\ i\Omega/2 & -i\Omega/2 & -\Gamma_1 \end{pmatrix}, \quad B = \begin{pmatrix} -i\Omega/2 \\ i\Omega/2 \\ 0 \end{pmatrix}, \quad (6.16)$$

where we introduced the total decoherence rate $\Gamma_2 = \Gamma_1/2 + \Gamma_\phi$. In the stationary state $t \gg \Gamma_{1,2}^{-1}$, the variables s_1 and s_2 read

$$\bar{s}_1 = \frac{\Omega\Gamma_1 (\Delta - i\Gamma_2)}{2 \left(\Omega^2\Gamma_2 + \Gamma_1 \left(\Delta^2 + \Gamma_2^2\right)\right)}, \quad (6.17)$$

$$\bar{s}_2 = \frac{\Omega^2\Gamma_2}{2 \left(\Omega^2\Gamma_2 + \Gamma_1 \left(\Delta^2 + \Gamma_2^2\right)\right)} \quad (6.18)$$

To determine the two-time correlation function of the atom, we define the following variables

$$s_3(\tau) = \langle \sigma_+(t)\sigma_-(t+\tau)\rangle \, e^{i\omega_L\tau} \tag{6.19}$$

$$s_4(\tau) = \langle \sigma_+(t)\sigma_+(t+\tau)\rangle \, e^{-i\omega_L(2t+\tau)} \tag{6.20}$$

$$s_5(\tau) = \langle \sigma_+\sigma_+(t+\tau)\sigma_-(t+\tau)\rangle \, e^{-i\omega_L\tau}. \tag{6.21}$$

With these new variables, the Bloch equations can be rewritten as

$$\frac{\mathrm{d}}{\mathrm{d}t}\begin{pmatrix} s_3 \\ s_4 \\ s_5 \end{pmatrix} = M \begin{pmatrix} s_3 \\ s_4 \\ s_5 \end{pmatrix} + B, \tag{6.22}$$

with the initial values $s_3(0) = \bar{s}_2$, and $s_4(0) = s_5(0) = 0$. The stationary values of these variables can be obtained by using the quantum regression theorem,

$$\tau \to \infty : \langle A(t)B(t+\tau)\rangle \to \langle A(t)\rangle\langle \bar{B}\rangle, \tag{6.23}$$

that applies for the two-time correlation of any observable A and B [163]. We find the stationary values of the new variables to be $\bar{s}_3 = |s_1|^2$, $\bar{s}_4 = (\bar{s}_1^*)^2$ and $\bar{s}_5 = \bar{s}_1^*\bar{s}_2$. To get rid of the constant part of Eq. (6.22), we once more define new variables $\delta s_j(\tau) = s_j(\tau) - \bar{s}_j$, for $j \in \{3, 4, 5\}$ and find

$$\frac{\mathrm{d}}{\mathrm{d}t}\begin{pmatrix} \delta s_3 \\ \delta s_4 \\ \delta s_5 \end{pmatrix} = M \begin{pmatrix} \delta s_3 \\ \delta s_4 \\ \delta s_5 \end{pmatrix} = M \cdot \delta S. \tag{6.24}$$

Now we take the Fourier transform $I_j(\omega) = \int_0^\infty \mathrm{d}\tau e^{i(\omega-\omega_L)}\delta s_j(\tau)$ which becomes

$$I(\omega) = [M + i(\omega - \omega_L)\mathbb{1}]^{-1}\left[\lim_{\tau\to\infty}\delta S(\tau)e^{i(\omega-\omega_L)\tau} - \delta S(0)\right]. \tag{6.25}$$

We use $\lim_{\tau\to\infty} e^{i(\omega-\omega_L)}\delta s_j(\tau) = 0$ and find

$$I(\omega) = -[M + i(\omega - \omega_L)\mathbb{1}]^{-1}\delta S(0). \tag{6.26}$$

The incoherent part of the power spectral density is given by

$$S_{\mathrm{i}}(\omega) = \frac{\Gamma_{\mathrm{r}}}{\pi}\,\mathrm{Re}\left[I_3(\omega)\right], \tag{6.27}$$

where Γ_r is the radiative decay rate and

$$I_3(\omega) = \frac{|\bar{s}_1|^2 - \bar{s}_2}{\mu_1} + \frac{\Omega^2 (\bar{s}_1^*)^2 - \Omega^2 \left(|\bar{s}_1|^2 - \bar{s}_2\right) \mu_2/\mu_1 - 2i\Omega\bar{s}_1^*\bar{s}_2\mu_2}{2\mu_1\mu_2\mu_3 + \Omega^2 (\mu_1 + \mu_2)}, \quad (6.28)$$

with $\mu_1 = -\Gamma_2 + i\delta\omega_0$, $\mu_2 = -\Gamma_2 + i\left(\omega + \omega_0 - 2\omega_L\right)$ and $\mu_3 = -\Gamma_1 + i\delta\omega_0$ where $\delta\omega_0 = \omega - \omega_0$. If the driving is strong $\Omega \gg \Gamma_{1,2}$ and on resonance with the qubit frequency the expression for $I_3(\omega)$ and hence $S_i(\omega)$ can be simplified to

$$I_3(\omega) \approx -\frac{1}{4\mu_1} - \frac{1}{4}\left\{\frac{1}{\Gamma_s + i\left(\delta\omega_0 + \Omega\right)} + \frac{1}{\Gamma_s + i\left(\delta\omega_0 - \Omega\right)}\right\} \quad (6.29)$$

and

$$S_i(\omega) \approx \frac{1}{\pi}\frac{\omega_0\Gamma_r}{4}\left\{\frac{\Gamma_s}{(\delta\omega_0 + \Omega)^2 + \Gamma_s^2} + \frac{2\Gamma_2}{(\delta\omega_0)^2 + \Gamma_2^2} + \frac{\Gamma_s}{(\delta\omega_0 - \Omega)^2 + \Gamma_s^2}\right\}, \quad (6.30)$$

where $\Gamma_r = \Gamma_1 - \Gamma_n$, $\Gamma_s = \Gamma_1/2 + \Gamma_2/2$, and Γ_n is the non-radiative decay rate.

In paper II, we measured and calculated the power spectral density to characterize the decay rates of an artificial superconducting qubit. Together with other measurements, we extracted the non-radiative decay rate and the pure dephasing rate from the power spectrum. Furthermore, we studied the off-resonant Mollow triplet, which shows an asymmetry caused by inequality of the transitions between the dressed states. Fig. 6.4 shows two plots from Paper II showing experimental data and a fit for the symmetric Mollow triplet (a) and the asymmetric Mollow triplet (b). To understand the asymmetry, we will take a closer look at the origin of the Mollow triplet and the corresponding transition matrix elements between the states.

6.2.1 Asymmetric Mollow triplet

Before we discuss the asymmetric Mollow triplet, let us look at the energy diagram and transition rates of a strongly driven two-level system. Fig. 6.5 depicts a sketch of the energy levels of two manifolds $\mathcal{E}(n + 1)$ and $\mathcal{E}(n)$. The transitions with the frequency of the qubit ω_0 from the $(+/-)$-subspace of $\mathcal{E}(n + 1)$ to the $(+/-)$-subspace of $\mathcal{E}(n)$ (depicted in
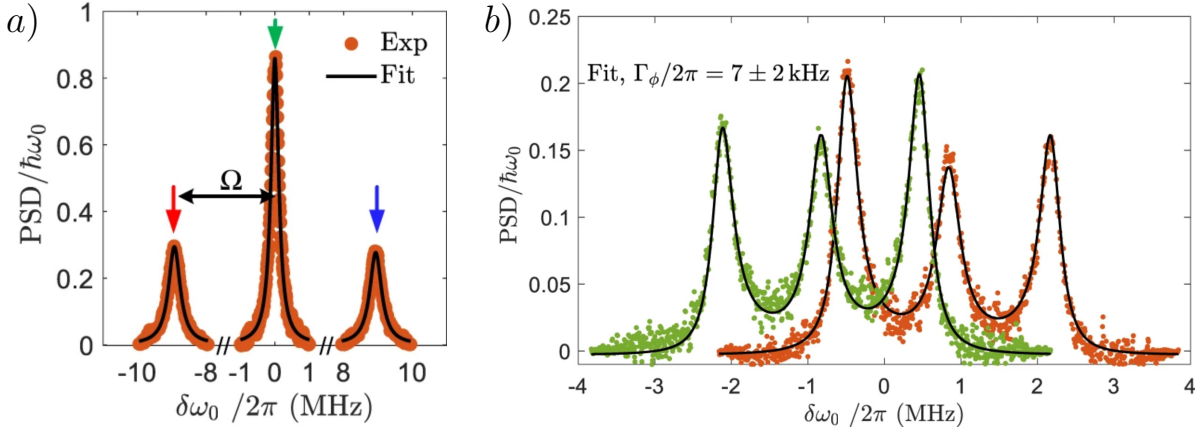
Figure 6.4: *Power spectral density (PSD) as a function of $\delta\omega_0$. a) shows the symmetric on-resonant Mollow triplet and b) shows the off-resonant Mollow triplet for negative (green dots) and positive (orange dots) detuning $\Delta = \omega_L - \omega_0$. For more details to the experimental set-up and data, see Paper II.*

green) give the middle peak of the Mollow triplet. The two outer peaks of the Mollow triplet are given by the transition from the $(-)$-subspace of $\mathcal{E}(n+1)$ to the $(+)$-subspace of $\mathcal{E}(n)$ with frequency $\omega_0 - \Omega$ (depicted in red) and the transition from the $(+)$-subspace of $\mathcal{E}(n+1)$ to the $(-)$-subspace of $\mathcal{E}(n)$ with frequency $\omega_0 + \Omega$ (depicted in blue).

To understand the symmetry (or asymmetry) of the Mollow triplet, we calculate the transition rates for the relaxation between the dressed states. They can be determined by calculating the matrix elements of the coupling term $\sigma_x = \sigma_+ + \sigma_-$ between the dressed states

$$\langle n, +|\sigma_x|n+1, +\rangle = \sin\Theta\cos\Theta, \tag{6.31}$$

$$\langle n, -|\sigma_x|n+1, +\rangle = \cos^2\Theta, \tag{6.32}$$

$$\langle n, +|\sigma_x|n+1, -\rangle = -\sin^2\Theta, \tag{6.33}$$

$$\langle n, -|\sigma_x|n+1, -\rangle = -\sin\Theta\cos\Theta. \tag{6.34}$$

with the definition of Θ given in (6.10). According to Fermi's golden rule, the transition rates are therefore given as follows

$$\Gamma_{++} \propto \sin^2\Theta\cos^2\Theta, \tag{6.35}$$

$$\Gamma_{+-} \propto \cos^4\Theta, \tag{6.36}$$

$$\Gamma_{-+} \propto \sin^4\Theta, \tag{6.37}$$

$$\Gamma_{--} \propto \sin^2\Theta\cos^2\Theta. \tag{6.38}$$

For a resonant drive $\Delta = 0$, the angle is given by $\Theta = \pi/4$ and all matrix elements, and therefore the transition rates have the same value.

Thus, the power spectrum is symmetric. In equilibrium and without pure dephasing, $\Gamma_\phi = 0$, the following equality holds for the probabilities

$$\Gamma_{+-}P_+ = \Gamma_{-+}P_-, \tag{6.39}$$

which means that the product of the transition rates from the $(+)$-subspace to the $(-)$-subspace Γ_{+-} and the occupation probability of the state to be in the $(+)$-subspace P_+ is equal the product of the transition from $(-)$-subspace to the $(+)$-subspace Γ_{-+} and the probability of being in the $(-)$-subspace P_-. For off-resonant driving, the transition rates change. If $\Delta < 0$ we find $\Gamma_{+-} > \Gamma_{-+}$ and if $\Delta > 0$, we find $\Gamma_{+-} < \Gamma_{-+}$, meaning that the transition corresponding to the dressed state that is closer to the bare qubit frequency has a higher transition rate. Despite the inequality of the transition rates, the spectrum remains symmetric since the occupation probability of the corresponding states changes so that the equality (6.39) still holds.

If we add pure dephasing, on the other hand, additional transitions between the states of the same manifold are possible according to

$$\langle n, +|\sigma_z|n, -\rangle = \langle n, -|\sigma_z|n, +\rangle = -2\sin\Theta\cos\Theta. \tag{6.40}$$

The equality (6.39) becomes modified with the pure dephasing

$$\left(\Gamma_{+-} + \Gamma_\phi\right)P_+ = \left(\Gamma_{-+} + \Gamma_\phi\right)P_-, \tag{6.41}$$

Since increasing pure dephasing causes the occupation probabilities to approach $P_+ = P_-$, the Mollow Triplet becomes asymmetric for off-resonant driving, since the transition rates Γ_{+-} and Γ_{-+} remain unchanged, leading to $\Gamma_{+-}P_+ \neq \Gamma_{-+}P_-$.
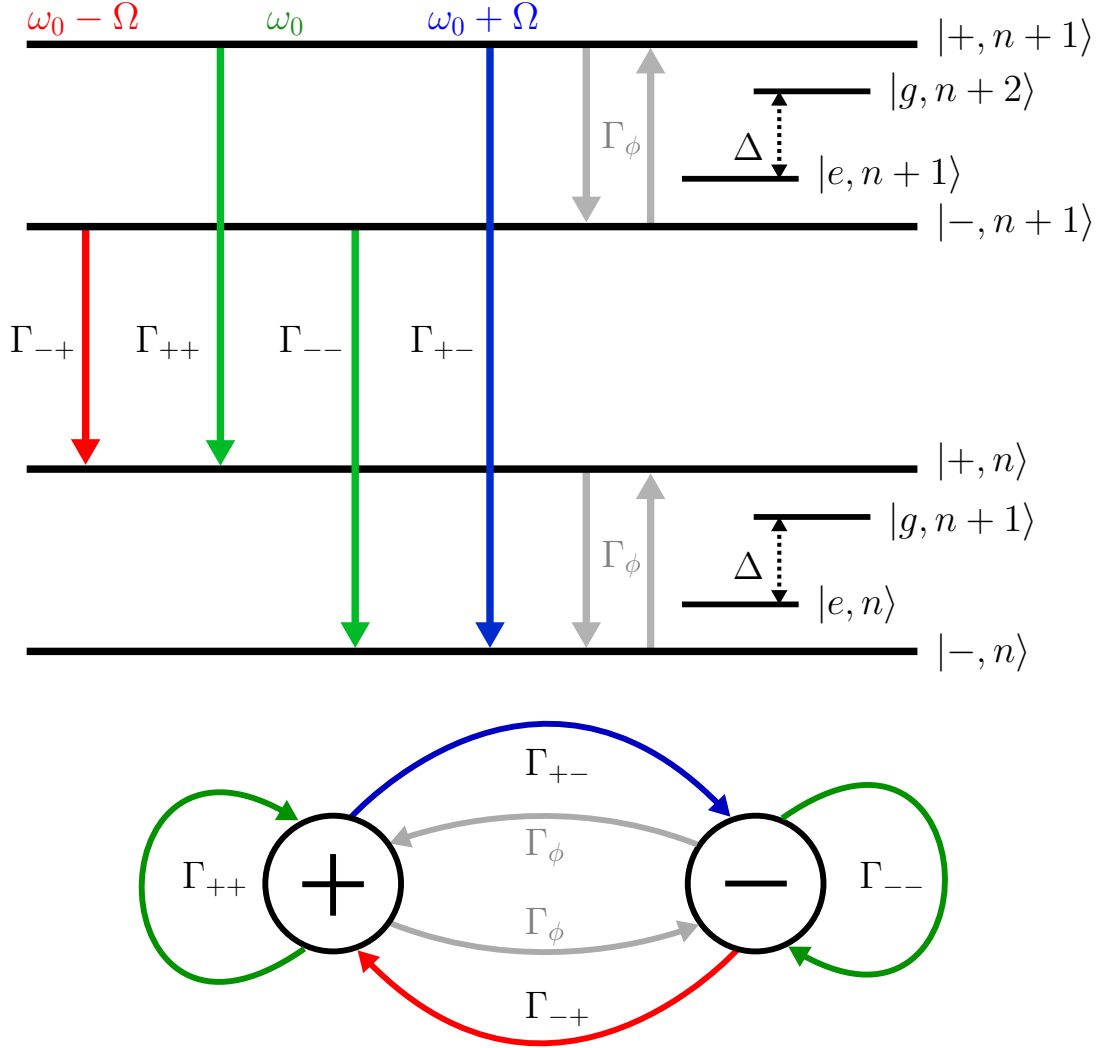
Figure 6.5: *a) Energy diagram of a strongly driven two-level system depicting the bare states and the dressed states of two different manifolds with the corresponding transition rates Γ between the dressed states. b) Sketch of the transition within and between the +- and −−-subspaces.*

7 Overview of the articles

7.1 Paper I: Semiclassical analysis of dark-state transient dynamics in waveguide circuit QED

In this article, we investigate the spontaneous emission dynamics of a transmon that is capacitively coupled to a 1D semi-infinite TL. We derive the Hamiltonian through circuit quantisation and calculate the Heisenberg equations of motion. Since we take time-delay effects that result from the finite travelling time of the electromagnetic waves to the mirror and back into account, the system's dynamics become non-trivial. To simplify the time-delay differential equations, we linearise the qubit by approximating the cosine potential of the transmon as a quadratic potential. After this step, we can solve for the systems average observables and are able to calculate the energy of the transmon. We find that the system dynamics strongly depend on the distance to the mirror and the coupling to the TL. The distance to the mirror with respect to the electromagnetic field mainly determines the decay after the first round-trip and the steady-state solution. If located at an anti-node of the field, the Purcell effect occurs and the decay rate compared to the initial decay rate given by the open TL decay rate is enhanced due to constructive interference. If located at a node of the electromagnetic field, on the other hand, the qubit converges into a dark state with a finite excitation probability of the excited state. This happens due to destructive interference. The value of the dark state excitation probability is determined only by the delay time and the (low-impedance) coupling strength. In addition, we derive an effective circuit model to investigate the influence of the TL impedance on the system's dynamics. We find that in a high-impedance regime, the dynamics and time scales of the system change. Interestingly, the dark state occupation even in the high-impedance regime is given by the low-impedance coupling strength. We investigate the dynamics of a transmon coupled to a TL in

more detail in paper III. Further, we rigorously derive a quantum optical system-reservoir model that resembles the transmon capacitively coupled to a semi-infinite TL and find agreeing results.

7.2 Paper II: Characterising decoherence rates of a superconducting qubit by direct microwave scattering

This article was an experimental collaboration. We characterise the decay rates of a superconducting qubit coupled to the end of a TL with different measurements: Coherent and incoherent scattering, on- and off-resonant fluorescence and time-resolved dynamics. By combining the results of all methods, we can characterise the decay and decoherence rates of the qubit and discriminate between pure dephasing and non-radiative decay. The article contains the results of all experiments and theoretical derivations and explanations to the origin of, for example, the off-resonant asymmetric Mollow triplet.

7.3 Paper III: Transmon in a semi-infinite high-impedance transmission line: Appearance of cavity modes and Rabi oscillations

Paper III is a continuation of Paper I. Here, we investigate the regime of a characteristic TL impedance bigger than the characteristic impedance of the transmon. First, we investigate the scattering at the transmon in an open TL. In the low-impedance regime, the reflectance at the transmon is close to zero except for at its (coupled) resonance frequency, where it becomes excited and reflects the incoming field. In the high-impedance regime, on the other hand, the transmon becomes highly reflective everywhere except near its (uncoupled) resonance frequency. We find that both the reflectance and the resonance frequency of the qubit change in the high-impedance regime. It acts as a mirror due to the strong capacitive coupling to the ground. Next, we investigate spontaneous emission of a transmon coupled to a semi-infinite TL, an atom in front of a

mirror. As mentioned before, the atom becomes highly reflective in the high-impedance regime, resembling a mirror. As a result, the atom creates its own cavity with the mirror. This results in the appearance of vacuum Rabi-oscillations in the spontaneous emission. By probing the atom in front of a mirror, we see Rabi splitting in the field trapped between the atom and the mirror and higher cavity modes. We derive the high-impedance coupling strength and Rabi frequency through functional analysis and find agreement with the numerical results.

7.4 Paper IV: Ultimate quantum limit for amplification: a single atom in front of a mirror

In this article, we theoretically demonstrate three different types of on-chip amplification methods of an atom coupled to a semi-infinite waveguide. The first type we investigate consists of a driven Λ-type three-level system where population inversion is created between the first excited state and the ground state. By probing the first transition, we find a gain in the reflection of up to 25% whereas only 12.5% was achieved in an open TL [92]. Also, we provide detailed calculations for a typical transmon qubit that can be used to fit experimental results. The second system we investigate is a driven two-level system. The driving is strong enough to induce an energy splitting (dressed states) in the two-level system. Due to higher-order processes between the transitions of the dressed states, we find an amplification gain of 6.9% of the atom in front of a mirror compared to the open TL, where the gain is given by 3.4%. The last system we investigate in this article is a strongly two-photon driven three-level system. Here we achieve a gain in the reflection due to population inversion between the dressed states by up to 6.2% for the atom in front of a mirror compared to the 3% of the open TL [93]. We also calculate the optimal drive strength to achieve the most favourable results.

8 Summary and outlook

In this thesis, we first introduced the quantization of electrical circuits, an essential part of circuit QED. We introduced basic components of electrical circuits and demonstrated how to quantize one-dimensional coplanar waveguides or transmission lines. We demonstrated different boundary conditions of the transmission line: either open, semi-infinite or shorted on both sides. Then we proceeded to introduce superconducting qubits: an SCPB and a charge-insensitive transmon. In the next section, where we investigated a transmon coupled to a transmission line, we demonstrated the methods used in Paper I and III and summarised their main results. In Paper I, we investigate spontaneous emission of a transmon coupled to a semi-infinite TL and take the time-delay effects into account resulting from the travelling time of the electromagnetic waves to the mirror and back. We find that both the transient dynamics and the steady state strongly depend on the atoms' position and coupling with respect to the electromagnetic field, resulting in the Purcell effect or the convergence into a dark state. Paper III is a continuation of Paper I, where we investigate the same set-up but focus on the high-impedance regime, meaning that the characteristic impedance of the transmission line exceeds the impedance of the transmon. We find that the system dynamics in the high-impedance regime change drastically. The qubit becomes highly reflective and creates its own cavity with the mirror, resulting in cavity modes and vacuum Rabi oscillations. The high-impedance regime has only recently become experimentally available, and it would be interesting to realize our theoretical results in an experiment. Another continuation of our work could be the inclusion of a non-linearity to the energy levels since we linearised the equations of motion of the transmon qubit. Even though we believe the linearisation is valid in the regimes that we investigate, it would be interesting to see possible variations to the system dynamics or even new purely quantum mechanical effects.

In the next part of the thesis, we focused on quantum optical methods and systems inspired by the circuit QED set-ups investigated in Paper II and IV. We first demonstrated how to quantize an electromagnetic field

and derived the light-matter coupling Hamiltonian within the dipole approximation. We then introduced open quantum systems and derived the quantum optical master equation, a powerful tool to investigate light-matter interaction, used in Paper II and IV. The next chapter introduced the dressed atom, meaning that the atom strongly interacts with an electromagnetic field, and the atom's energy levels can no longer be separated from the field's energy levels. In Paper II, where we performed several experiments in order to characterize the different decay rates of a superconducting qubit placed at the end of a transmission line, the dressed atom becomes essential in the characterization and discrimination of non-radiative decay from the pure dephasing rate. We could extract both mentioned rates by fitting theory to the measurement data of the on- and off-resonant driven dressed atom and the resulting power spectral density. When driven off-resonantly, pure dephasing leads to an asymmetry in the power spectral density, an effect that we explained in Paper II and this thesis. In this work, we demonstrated how to characterize decay rates, which can be helpful to improve circuit QED set-ups by engineering the decay channels of the qubit to reach higher efficiency or coherence times. The improvement of such a set-up can increase the fidelity of detecting single photons and superconducting quantum computers.

In Paper IV, we investigated three different amplification mechanisms with set-ups of an atom coupled to a semi-infinite waveguide. Signal amplification is crucial to achieve good signal-to-noise ratios [167–170]. The set-ups we propose are compact and engineerable on-chip. The considered systems all show amplification due to different mechanisms: population inversion between the bare states, the dressed states and multi-photon processes between the dressed states. We find that for all systems, the atom in front of a mirror can achieve higher amplification than its equivalent in an open waveguide due to the following reasons: The semi-infinite waveguide has only one output channel and, therefore, doubles the signal output. Another reason is the tunability of the transition rates between the states due to interference. When creating population inversion, it is crucial to create a meta-stable state. The tunability of the decay rates can make population inversion between both the pure states and the dressed states more efficient. However, in the systems we investigate, the reduction of output channels had a stronger effect in increasing the amplification than the tunability of the decay rates. A follow up to our work could be to find systems where the tunability has a higher impact and achieve even higher gains. Another idea is to add more qubits to the system. Inter-

ference effects between several qubits might lead to even higher gains. Furthermore, since experiments inspired this theoretical work, we hope that the proposed systems can be realized in future experiments.

References

[1] A. Einstein, "Zur Elektrodynamik bewegter Körper", Annalen der Physik **322**, 891–921 (1905) (cit. on p. 1).

[2] C. Monroe, D. M. Meekhof, B. E. King, and D. J. Wineland, "A "Schrödinger Cat" Superposition State of an Atom", Science **272**, 1131–1136 (1996) (cit. on p. 1).

[3] M. Brune, E. Hagley, J. Dreyer, X. Maître, A. Maali, C. Wunderlich, J. M. Raimond, and S. Haroche, "Observing the Progressive Decoherence of the "Meter" in a Quantum Measurement", Phys. Rev. Lett. **77**, 4887–4890 (1996) (cit. on p. 1).

[4] "Measuring and Manipulating individual Quantum Systems", The Royal Swedish Academy of Science (2012) (cit. on p. 1).

[5] R. P. Feynman, "Simulating physics with computers", International Journal of Theoretical Physics **21**, 467–488 (1982) (cit. on p. 1).

[6] M. A. Nielsen and I. L. Chuang, *Quantum Computation and Quantum Information* (Cambridge University Press, 2000) (cit. on p. 2).

[7] A. Montanaro, "Quantum algorithms: an overview", npj Quantum Information **2**, 15023 (2016) (cit. on p. 2).

[8] R. D. Somma, S. Boixo, H. Barnum, and E. Knill, "Quantum Simulations of Classical Annealing Processes", Phys. Rev. Lett. **101**, 130504 (2008) (cit. on p. 2).

[9] E. Farhi, J. Goldstone, and S. Gutmann, *A Quantum Approximate Optimization Algorithm*, 2014, arXiv:`1411.4028` (cit. on p. 2).

[10] E. Farhi and A. W. Harrow, *Quantum Supremacy through the Quantum Approximate Optimization Algorithm*, 2019, arXiv:`1602.07674` (cit. on p. 2).

[11] A. Aspuru-Guzik, A. D. Dutoi, P. J. Love, and M. Head-Gordon, "Simulated Quantum Computation of Molecular Energies", Science **309**, 1704–1707 (2005) (cit. on p. 2).

[12] A. Peruzzo, J. McClean, P. Shadbolt, M.-H. Yung, X.-Q. Zhou, P. J. Love, A. Aspuru-Guzik, and J. L. O'Brien, "A variational eigenvalue solver on a photonic quantum processor", Nature Communications **5**, 4213 (2014) (cit. on p. 2).

[13] C. Hempel, C. Maier, J. Romero, J. McClean, T. Monz, H. Shen, P. Jurcevic, B. P. Lanyon, P. Love, R. Babbush, A. Aspuru-Guzik, R. Blatt, and C. F. Roos, "Quantum Chemistry Calculations on a Trapped-Ion Quantum Simulator", Phys. Rev. X **8**, 031022 (2018) (cit. on p. 2).

[14] E. Farhi and H. Neven, *Classification with Quantum Neural Networks on Near Term Processors*, 2018, arXiv:1802.06002 (cit. on p. 2).

[15] J. R. McClean, S. Boixo, V. N. Smelyanskiy, R. Babbush, and H. Neven, "Barren plateaus in quantum neural network training landscapes", Nature Communications **9**, 4812 (2018) (cit. on p. 2).

[16] I. Cong, S. Choi, and M. D. Lukin, "Quantum convolutional neural networks", Nature Physics **15**, 1273–1278 (2019) (cit. on p. 2).

[17] A. Smith, M. S. Kim, F. Pollmann, and J. Knolle, "Simulating quantum many-body dynamics on a current digital quantum computer", npj Quantum Information **5**, 106 (2019) (cit. on p. 2).

[18] N. P. D. Sawaya, T. Menke, T. H. Kyaw, S. Johri, A. Aspuru-Guzik, and G. G. Guerreschi, "Resource-efficient digital quantum simulation of d-level systems for photonic, vibrational, and spins Hamiltonians", npj Quantum Information **6**, 49 (2020) (cit. on p. 2).

[19] M. J. Bremner, A. Montanaro, and D. J. Shepherd, "Average-Case Complexity Versus Approximate Simulation of Commuting Quantum Computations", Phys. Rev. Lett. **117**, 080501 (2016) (cit. on p. 2).

[20] S. Boixo, S. V. Isakov, V. N. Smelyanskiy, R. Babbush, N. Ding, Z. Jiang, M. J. Bremner, J. M. Martinis, and H. Neven, "Characterizing quantum supremacy in near-term devices", Nature Physics **14**, 595–600 (2018) (cit. on p. 2).

[21] A. Bouland, B. Fefferman, C. Nirkhe, and U. Vazirani, "On the complexity and verification of quantum random circuit sampling", Nature Physics **15**, 159–163 (2019) (cit. on p. 2).

[22] S. Aaronson and L. Chen, "Complexity-Theoretic Foundations of Quantum Supremacy Experiments", in 32nd Computational Complexity Conference (CCC 2017), Vol. 79, edited by R. O'Donnell, Leibniz International Proceedings in Informatics (LIPIcs) (2017), 22:1–22:67 (cit. on p. 2).

[23] C. Neill et al., "A blueprint for demonstrating quantum supremacy with superconducting qubits", Science **360**, 195–199 (2018) (cit. on p. 2).

[24] S. Bravyi, D. Gosset, and R. König, "Quantum advantage with shallow circuits", Science **362**, 308–311 (2018) (cit. on p. 2).

[25] M. Kjaergaard, M. E. Schwartz, J. Braumüller, P. Krantz, J. I.-J. Wang, S. Gustavsson, and W. D. Oliver, "Superconducting Qubits: Current State of Play", Annual Review of Condensed Matter Physics **11**, 369 (2020) (cit. on pp. 2, 4).

[26] B. M. Terhal, "Quantum error correction for quantum memories", Rev. Mod. Phys. **87**, 307–346 (2015) (cit. on p. 2).

[27] J. Preskill, "Quantum Computing in the NISQ era and beyond", Quantum **2**, 79 (2018) (cit. on p. 2).

[28] F. Arute et al., "Quantum supremacy using a programmable superconducting processor", Nature **574**, 505–510 (2019) (cit. on p. 2).

[29] G. J. Mooney, G. A. L. White, C. D. Hill, and L. C. L. Hollenberg, *Whole-device entanglement in a 65-qubit superconducting quantum computer*, 2021, arXiv:`2102.11521` (cit. on p. 2).

[30] M. Gong et al., *Quantum walks on a programmable two-dimensional 62-qubit superconducting processor*, 2021, arXiv:`2102.02573` (cit. on p. 2).

[31] E. Pednault, J Gunnels, D. Maslov, and J. Gambetta, "On "Quantum Supremacy"", IBM Research Blog (2019) (cit. on p. 2).

[32] J. Clarke and F. K. Wilhelm, "Superconducting quantum bits", **453**, 1031–1042 (2008) (cit. on pp. 2, 15).

[33] A. F. Kockum and F. Nori, "Quantum Bits with Josephson Junctions", in *Fundamentals and Frontiers of the Josephson Effect*, edited by F. Tafuri (Springer International Publishing, Cham, 2019), pp. 703–741 (cit. on p. 2).

[34] M. H. devoret and J. M. Martinis, "Implementing Qubits with Superconducting Integrated Circuits", Quantum Information Processing **3**, 163–203 (2004) (cit. on p. 2).

[35] G Wendin, "Quantum information processing with superconducting circuits: a review", Reports on Progress in Physics **80**, 106001 (2017) (cit. on pp. 2, 3, 15).

[36] J. M. Martinis, "Superconducting phase qubits", Quantum Information Processing **8**, 81–103 (2009) (cit. on p. 2).

[37] J. Q. You and F. Nori, "Superconducting Circuits and Quantum Information", Physics Today **58**, 42–47 (2005) (cit. on p. 2).

[38] M. H. Devoret and R. J. Schoelkopf, "Superconducting Circuits for Quantum Information: An Outlook", Science **339**, 1169–1174 (2013) (cit. on p. 2).

[39] B. Josephson, "Possible new effects in superconductive tunnelling", Physics Letters **1**, 251–253 (1962) (cit. on p. 2).

[40] Y. Makhlin, G. Schön, and A. Shnirman, "Quantum-state engineering with Josephson-junction devices", Rev. Mod. Phys. **73**, 357–400 (2001) (cit. on p. 2).

[41] M. H. Devoret, J. M. Martinis, and J. Clarke, "Measurements of Macroscopic Quantum Tunneling out of the Zero-Voltage State of a Current-Biased Josephson Junction", Phys. Rev. Lett. **55**, 1908–1911 (1985) (cit. on p. 2).

[42] Y. Makhlin, G. Schön, and A. Shnirman, "Josephson-junction qubits with controlled couplings", Nature **398**, 305–307 (1999) (cit. on pp. 3, 20).

[43] Y. Nakamura, Y. A. Pashkin, and J. S. Tsai, "Coherent control of macroscopic quantum states in a single-Cooper-pair box", Nature **398**, 786–788 (1999) (cit. on p. 3).

[44] V. Bouchiat, D. Vion, P. Joyez, D. Esteve, and M. H. Devoret, "Quantum Coherence with a Single Cooper Pair", Physica Scripta **T76**, 165 (1998) (cit. on pp. 3, 17, 19).

[45] J. Koch, T. M. Yu, J. Gambetta, A. A. Houck, D. I. Schuster, J. Majer, A. Blais, M. H. Devoret, S. M. Girvin, and R. J. Schoelkopf, "Charge-insensitive qubit design derived from the Cooper pair box", Phys. Rev. A **76**, 1–19 (2007) (cit. on pp. 3, 15, 19).

[46] J. J. Burnett, A. Bengtsson, M. Scigliuzzo, D. Niepce, M. Kudra, P. Delsing, and J. Bylander, "Decoherence benchmarking of superconducting qubits", npj Quantum Information **5**, 54 (2019) (cit. on pp. 3, 63, 66).

[47] J. M. Martinis, "Qubit metrology for building a fault-tolerant quantum computer", npj Quantum Information **1**, 15005 (2015) (cit. on p. 3).

[48] A. Wallraff, D. I. Schuster, A. Blais, L. Frunzio, R. S. Huang, J. Majer, S. Kumar, S. M. Girvin, and R. J. Schoelkopf, "Strong coupling of a single photon to a superconducting qubit using circuit quantum electrodynamics", Nature **431**, 162–167 (2004) (cit. on pp. 3, 4).

[49] A. Blais, R.-S. Huang, A. Wallraff, S. M. Girvin, and R. J. Schoelkopf, "Cavity quantum electrodynamics for superconducting electrical circuits: An architecture for quantum computation", Phys. Rev. A **69**, 062320 (2004) (cit. on pp. 3, 4).

[50] X. Gu, A. F. Kockum, A. Miranowicz, Y.-x. Liu, and F. Nori, "Microwave photonics with superconducting quantum circuits", Physics Reports **718-719**, 1–102 (2017) (cit. on pp. 3, 4).

[51] J. Q. You and F. Nori, "Atomic physics and quantum optics using superconducting circuits", Nature **474**, 589–597 (2011) (cit. on p. 3).

[52] M. Devoret, S. Girvin, and R. Schoelkopf, "Circuit-QED: How strong can the coupling between a Josephson junction atom and a transmission line resonator be?", Annalen der Physik **16**, 767–779 (2007) (cit. on p. 3).

[53] M. Bamba and T. Ogawa, "Recipe for the Hamiltonian of system-environment coupling applicable to the ultrastrong-light-matter-interaction regime", Phys. Rev. A **89**, 023817 (2014) (cit. on p. 3).

[54] A. Frisk Kockum, A. Miranowicz, S. De Liberato, S. Savasta, and F. Nori, "Ultrastrong coupling between light and matter", Nature Reviews Physics **1**, 19–40 (2019) (cit. on p. 3).

[55] D. Zueco and J. García-Ripoll, "Ultrastrongly dissipative quantum Rabi model", Phys. Rev. A **99**, 013807 (2019) (cit. on p. 3).

[56] J. A. Mlynek, A. A. Abdumalikov, C. Eichler, and A. Wallraff, "Observation of Dicke superradiance for two artificial atoms in a cavity with high decay rate", Nature Communications **5**, 5186 EP – (2014) (cit. on p. 3).

[57] L. Magazzù, P. Forn-Díaz, R. Belyansky, J. L. Orgiazzi, M. A. Yurtalan, M. R. Otto, A. Lupascu, C. M. Wilson, and M. Grifoni, "Probing the strongly driven spin-boson model in a superconducting quantum circuit", Nature Communications **9** (2018) (cit. on p. 3).

[58] L. Magazzù and M. Grifoni, "Transmission spectra of an ultra-strongly coupled qubit-dissipative resonator system", J. Stat. Mech (2019) (cit. on p. 3).

[59] P. Forn-Díaz, J. J. García-Ripoll, B. Peropadre, J.-L. Orgiazzi, M. A. Yurtalan, R. Belyansky, C. M. Wilson, and A. Lupascu, "Ultrastrong coupling of a single artificial atom to an electromagnetic continuum in the nonperturbative regime", Nature Physics **13**, 39 (2017) (cit. on p. 3).

[60] P. Forn-Díaz, L. Lamata, E. Rico, J. Kono, and E. Solano, "Ultrastrong coupling regimes of light-matter interaction", Reviews of Modern Physics **91**, 025005 (2019) (cit. on p. 3).

[61] P. Nataf and C. Ciuti, "No-go theorem for superradiant quantum phase transitions in cavity QED and counter-example in circuit QED", Nature Communications **1**, 72 EP – (2010) (cit. on pp. 3, 45).

[62] M. Bamba, K. Inomata, and Y. Nakamura, "Superradiant Phase Transition in a Superconducting Circuit in Thermal Equilibrium", Phys. Rev. Lett. **117**, 1–5 (2016) (cit. on p. 3).

[63] M. Bamba and N. Imoto, "Circuit configurations which may or may not show superradiant phase transitions", Phys. Rev. A **96**, 053857 (2017) (cit. on p. 3).

[64] D. De Bernardis, T. Jaako, and P. Rabl, "Cavity quantum electrodynamics in the nonperturbative regime", Phys. Rev. A **97**, 043820 (2018) (cit. on pp. 3, 45).

[65] K. Hepp and E. H. Lieb, "On the superradiant phase transition for molecules in a quantized radiation field: the dicke maser model", Annals of Physics **76**, 360–404 (1973) (cit. on pp. 3, 45).

[66] C. Emary and T. Brandes, "Chaos and the quantum phase transition in the Dicke model", Phys. Rev. E **67**, 066203 (2003) (cit. on pp. 3, 45).

[67] C. Emary and T. Brandes, "Quantum Chaos Triggered by Precursors of a Quantum Phase Transition: The Dicke Model", Phys. Rev. Lett. **90**, 044101 (2003) (cit. on pp. 3, 45).

[68] D. Roy, C. M. Wilson, and O. Firstenberg, "Colloquium: Strongly interacting photons in one-dimensional continuum", Rev. Mod. Phys. **89**, 021001 (2017) (cit. on p. 3).

[69] O. Astafiev, K. Inomata, A. O. Niskanen, T. Yamamoto, Y. A. Pashkin, Y. Nakamura, and J. S. Tsai, "Single artificial-atom lasing", Nature **449**, 588–590 (2007) (cit. on p. 3).

[70] S Ashhab, J. R. Johansson, A. M. Zagoskin, and F. Nori, "Single-artificial-atom lasing using a voltage-biased superconducting charge qubit", New Journal of Physics **11**, 023030 (2009) (cit. on p. 3).

[71] J. Q. You, Y.-x. Liu, C. P. Sun, and F. Nori, "Persistent single-photon production by tunable on-chip micromaser with a superconducting quantum circuit", Phys. Rev. B **75**, 104516 (2007) (cit. on p. 3).

[72] M. Marthaler, Y. Utsumi, D. S. Golubev, A. Shnirman, and G. Schön, "Lasing without Inversion in Circuit Quantum Electrodynamics", Phys. Rev. Lett. **107**, 093901 (2011) (cit. on p. 3).

[73] H. Zheng, D. J. Gauthier, and H. U. Baranger, "Waveguide QED: Many-body bound-state effects in coherent and Fock-state scattering from a two-level system", Phys. Rev. A **82**, 063816 (2010) (cit. on p. 3).

[74] T. Tufarelli, M. S. Kim, and F. Ciccarello, "Non-Markovianity of a quantum emitter in front of a mirror", Phys. Rev. A **90**, 012113 (2014) (cit. on pp. 3, 4).

[75] E. Sanchez-Burillo, D. Zueco, J. J. Garcia-Ripoll, and L. Martin-Moreno, "Scattering in the Ultrastrong Regime: Nonlinear Optics with One Photon", Phys. Rev. Lett. **113**, 263604 (2014) (cit. on p. 3).

[76] T. Tufarelli, F. Ciccarello, and M. S. Kim, "Dynamics of spontaneous emission in a single-end photonic waveguide", Phys. Rev. A **87**, 013820 (2013) (cit. on p. 3).

[77] E. Sánchez-Burillo, L. Martín-Moreno, J. J. García-Ripoll, and D. Zueco, "Full two-photon down-conversion of a single photon", Phys. Rev. A **94**, 053814 (2016) (cit. on p. 3).

[78] E. Sánchez-Burillo, D. Zueco, L. Martín-Moreno, and J. J. García-Ripoll, "Dynamical signatures of bound states in waveguide QED", Phys. Rev. A **96**, 023831 (2017) (cit. on p. 3).

[79] O. Astafiev, A. M. Zagoskin, A. A. Abdumalikov, Y. A. Pashkin, T. Yamamoto, K. Inomata, Y. Nakamura, and J. S. Tsai, "Resonance Fluorescence of a Single Artificial Atom", Science **327**, 840–843 (2010) (cit. on p. 4).

[80] A. González-Tudela, V. Paulisch, H. J. Kimble, and J. I. Cirac, "Efficient Multiphoton Generation in Waveguide Quantum Electrodynamics", Phys. Rev. Lett. **118**, 213601 (2017) (cit. on p. 4).

[81] V. Paulisch, H. J. Kimble, J. I. Cirac, and A. González-Tudela, "Generation of single- and two-mode multiphoton states in waveguide QED", Phys. Rev. A **97**, 053831 (2018) (cit. on p. 4).

[82] F. Quijandría, I. Strandberg, and G. Johansson, "Steady-State Generation of Wigner-Negative States in One-Dimensional Resonance Fluorescence", Phys. Rev. Lett. **121**, 263603 (2018) (cit. on p. 4).

[83] I. C. Hoi, A. F. Kockum, L. Tornberg, A. Pourkabirian, G. Johansson, P. Delsing, and C. M. Wilson, "Probing the quantum vacuum with an artificial atom in front of a mirror", Nature Physics **11**, 1045–1049 (2015) (cit. on pp. 4, 63, 66).

[84] P. Y. Wen, A. F. Kockum, H. Ian, J. C. Chen, F. Nori, and I.-C. Hoi, "Reflective Amplification without Population Inversion from a Strongly Driven Superconducting Qubit", Phys. Rev. Lett. **120**, 063603 (2018) (cit. on p. 4).

[85] P. Y. Wen, K.-T. Lin, A. F. Kockum, B. Suri, H. Ian, J. C. Chen, S. Y. Mao, C. C. Chiu, P. Delsing, F. Nori, G.-D. Lin, and I.-C. Hoi, "Large Collective Lamb Shift of Two Distant Superconducting Artificial Atoms", Phys. Rev. Lett. **123**, 233602 (2019) (cit. on p. 4).

[86] J. Eschner, C. Raab, F. Schmidt-Kaler, and R. Blatt, "Light interference from single atoms and their mirror images", Nature **413**, 495 (2001) (cit. on p. 4).

[87] M. A. Wilson, P. Bushev, J. Eschner, F. Schmidt-Kaler, C. Becher, R. Blatt, and U. Dorner, "Vacuum-Field Level Shifts in a Single Trapped Ion Mediated by a Single Distant Mirror", Phys. Rev. Lett. **91**, 213602 (2003) (cit. on p. 4).

[88] F. Dubin, D. Rotter, M. Mukherjee, C. Russo, J. Eschner, and R. Blatt, "Photon Correlation versus Interference of Single-Atom Fluorescence in a Half-Cavity", Phys. Rev. Lett. **98**, 183003 (2007) (cit. on p. 4).

[89] Y. Lu, A. Bengtsson, J. J. Burnett, E. Wiegand, B. Suri, P. Krantz, A. F. Roudsari, A. F. Kockum, S. Gasparinetti, G. Johansson, and P. Delsing, "Characterizing decoherence rates of a superconducting qubit by direct microwave scattering", npj Quantum Information **7**, 35 (2021) (cit. on pp. 4, 63, 66).

[90] M. Bradford and J.-T. Shen, "Spontaneous emission in cavity QED with a terminated waveguide", Phys. Rev. A **87**, 063830 (2013) (cit. on p. 4).

[91] E. Wiegand, P. Y. Wen, P. Delsing, I. Hoi, and A. F. Kockum, "Ultimate quantum limit for amplification: a single atom in front of a mirror", New Journal of Physics (2021) (cit. on p. 4).

[92] O. V. Astafiev, A. A. Abdumalikov, A. M. Zagoskin, Y. A. Pashkin, Y. Nakamura, and J. S. Tsai, "Ultimate On-Chip Quantum Amplifier", Phys. Rev. Lett. **104**, 183603 (2010) (cit. on pp. 4, 83).

[93] K. Koshino, H. Terai, K. Inomata, T. Yamamoto, W. Qiu, Z. Wang, and Y. Nakamura, "Observation of the Three-State Dressed States in Circuit Quantum Electrodynamics", Phys. Rev. Lett. **110**, 263601 (2013) (cit. on pp. 4, 83).

[94] E. Wiegand, B. Rousseaux, and G. Johansson, "Semiclassical analysis of dark-state transient dynamics in waveguide circuit QED", Phys. Rev. A **101**, 033801 (2020) (cit. on p. 4).

[95] E. Wiegand, B. Rousseaux, and G. Johansson, "Transmon in a semi-infinite high-impedance transmission line: Appearance of cavity modes and Rabi oscillations", Phys. Rev. Research **3**, 023003 (2021) (cit. on p. 4).

[96] A. Ask and G. Johansson, *Non-Markovian steady states of a driven two-level system*, 2021, arXiv:2102.11140 (cit. on p. 4).

[97] A. L. Grimsmo, "Time-Delayed Quantum Feedback Control", Phys. Rev. Lett. **115**, 060402 (2015) (cit. on p. 4).

[98] H. Pichler and P. Zoller, "Photonic Circuits with Time Delays and Quantum Feedback", Phys. Rev. Lett. **116**, 093601 (2016) (cit. on p. 4).

[99] H. Pichler, S. Choi, P. Zoller, and M. D. Lukin, "Universal photonic quantum computation via time-delayed feedback", Proceedings of the National Academy of Sciences **114**, 11362–11367 (2017) (cit. on p. 4).

[100] P.-O. Guimond, M Pletyukhov, H Pichler, and P Zoller, "Delayed coherent quantum feedback from a scattering theory and a matrix product state perspective", Quantum Science and Technology **2**, 044012 (2017) (cit. on p. 4).

[101] L. Guo, A. F. Kockum, F. Marquardt, and G. Johansson, "Oscillating bound states for a giant atom", Phys. Rev. Research **2**, 043014 (2020) (cit. on pp. 4, 5).

[102] S. Guo, Y. Wang, T. Purdy, and J. Taylor, "Beyond spontaneous emission: Giant atom bounded in the continuum", Phys. Rev. A **102**, 033706 (2020) (cit. on p. 4).

[103] B. Kannan, M. J. Ruckriegel, D. L. Campbell, A. F. Kockum, J. Braumüller, D. K. Kim, M. Kjaergaard, P. Krantz, A. Melville, B. M. Niedzielski, A. Vepsäläinen, R. Winik, J. L. Yoder, F. Nori, T. P. Orlando, S. Gustavsson, and W. D. Oliver, "Waveguide quantum electrodynamics with superconducting artificial giant atoms", Nature **583**, 775 (2020) (cit. on p. 4).

[104] A. F. Kockum, "Quantum Optics with Giant Atoms - the First Five Years", in *International Symposium on Mathematics, Quantum Theory, and Cryptography (Mathematics for Industry, vol 33)* (Springer, 2021), pp. 125–146 (cit. on p. 4).

[105] I. V. Pechenezhskiy, R. A. Mencia, L. B. Nguyen, Y.-H. Lin, and V. E. Manucharyan, "The superconducting quasicharge qubit", Nature **585**, 368–371 (2020) (cit. on pp. 4, 28).

[106] D. Niepce, J. Burnett, and J. Bylander, "High Kinetic Inductance NbN Nanowire Superinductors", Phys. Rev. Applied **11**, 044014 (2019) (cit. on p. 4).

[107] N. A. Masluk, I. M. Pop, A. Kamal, Z. K. Minev, and M. H. Devoret, "Microwave Characterization of Josephson Junction Arrays: Implementing a Low Loss Superinductance", Phys. Rev. Lett. **109**, 137002 (2012) (cit. on p. 4).

[108] T. Weißl, B. Küng, E. Dumur, A. K. Feofanov, I. Matei, C. Naud, O. Buisson, F. W. J. Hekking, and W. Guichard, "Kerr coefficients of plasma resonances in Josephson junction chains", Phys. Rev. B **92**, 104508 (2015) (cit. on p. 4).

[109] N. Samkharadze, A. Bruno, P. Scarlino, G. Zheng, D. P. DiVincenzo, L. DiCarlo, and L. M. K. Vandersypen, "High-Kinetic-Inductance Superconducting Nanowire Resonators for Circuit QED in a Magnetic Field", Phys. Rev. Applied **5**, 044004 (2016) (cit. on p. 4).

[110] R. Kuzmin, R. Mencia, N. Grabon, N. Mehta, Y. H. Lin, and V. E. Manucharyan, "Quantum electrodynamics of a superconductor–insulator phase transition", Nature Physics **15**, 930–934 (2019) (cit. on p. 4).

[111] J. Puertas Martínez, S. Léger, N. Gheeraert, R. Dassonneville, L. Planat, F. Foroughi, Y. Krupko, O. Buisson, C. Naud, W. Hasch-Guichard, S. Florens, I. Snyman, and N. Roch, "A tunable Josephson platform to explore many-body quantum optics in circuit-QED", npj Quantum Information **5**, 19 (2019) (cit. on p. 4).

[112] M. T. Bell, I. A. Sadovskyy, L. B. Ioffe, A. Y. Kitaev, and M. E. Gershenson, "Quantum Superinductor with Tunable Nonlinearity", Phys. Rev. Lett. **109**, 137003 (2012) (cit. on p. 4).

[113] P. Winkel, I. Takmakov, D. Rieger, L. Planat, W. Hasch-Guichard, L. Grünhaupt, N. Maleeva, F. Foroughi, F. Henriques, K. Borisov, J. Ferrero, A. V. Ustinov, W. Wernsdorfer, N. Roch, and I. M. Pop, "Nondegenerate Parametric Amplifiers Based on Dispersion-Engineered Josephson-Junction Arrays", Phys. Rev. Applied **13**, 024015 (2020) (cit. on p. 4).

[114] Y. Krupko, V. D. Nguyen, T. Weißl, E. Dumur, J. Puertas, R. Dassonneville, C. Naud, F. W. J. Hekking, D. M. Basko, O. Buisson, N. Roch, and W. Hasch-Guichard, "Kerr nonlinearity in a superconducting Josephson metamaterial", Phys. Rev. B **98**, 094516 (2018) (cit. on p. 4).

[115] J. T. Peltonen, P. C. J. J. Coumou, Z. H. Peng, T. M. Klapwijk, J. S. Tsai, and O. V. Astafiev, "Hybrid rf SQUID qubit based on high kinetic inductance", Scientific Reports **8**, 10033 (2018) (cit. on p. 4).

[116] L. Grünhaupt, N. Maleeva, S. T. Skacel, F. Calvo M.and Levy-Bertrand, A. V. Ustinov, H. Rotzinger, A. Monfardini, G. Catelani, and I. M. Pop, "Loss Mechanisms and Quasiparticle Dynamics in Superconducting Microwave Resonators Made of Thin-Film Granular Aluminum", Phys. Rev. Lett. **121**, 117001 (2018) (cit. on p. 4).

[117] D. Niepce, J. J. Burnett, M. G. Latorre, and J. Bylander, "Geometric scaling of two-level-system loss in superconducting resonators", Superconductor Science and Technology **33**, 025013 (2020) (cit. on p. 4).

[118] I. V. Pechenezhskiy, R. A. Mencia, L. H. B. Nguyen, Y.-H. Lin, and V. E. Manucharyan, "Quantum dynamics of quasicharge in an ultrahigh-impedance superconducting circuit", arXiv: Superconductivity (2019) (cit. on p. 4).

[119] V. E. Manucharyan, J. Koch, L. I. Glazman, and M. H. Devoret, "Fluxonium: Single Cooper-Pair Circuit Free of Charge Offsets", Science **326**, 113–116 (2009) (cit. on p. 4).

[120] L. Grünhaupt, M. Spiecker, D. Gusenkova, N. Maleeva, S. T. Skacel, I. Takmakov, F. Valenti, P. Winkel, H. Rotzinger, W. Wernsdorfer, A. V. Ustinov, and I. M. Pop, "Granular aluminium as a superconducting material for high-impedance quantum circuits", Nature Materials **18**, 816–819 (2019) (cit. on p. 4).

[121] L. B. Nguyen, Y.-H. Lin, A. Somoroff, R. Mencia, N. Grabon, and V. E. Manucharyan, "High-Coherence Fluxonium Qubit", Phys. Rev. X **9**, 041041 (2019) (cit. on p. 4).

[122] J. Koch, V. Manucharyan, M. H. Devoret, and L. I. Glazman, "Charging Effects in the Inductively Shunted Josephson Junction", Phys. Rev. Lett. **103**, 217004 (2009) (cit. on p. 4).

[123] I. M. Pop, K. Geerlings, G. Catelani, R. J. Schoelkopf, L. I. Glazman, and M. H. Devoret, "Coherent suppression of electromagnetic dissipation due to superconducting quasiparticles", Nature **508**, 369–372 (2014) (cit. on p. 4).

[124] W. Guichard and F. W. J. Hekking, "Phase-charge duality in Josephson junction circuits: Role of inertia and effect of microwave irradiation", Phys. Rev. B **81**, 064508 (2010) (cit. on p. 4).

[125] A. Stockklauser, P. Scarlino, J. V. Koski, S. Gasparinetti, C. K. Andersen, C. Reichl, W. Wegscheider, T. Ihn, K. Ensslin, and A. Wallraff, "Strong Coupling Cavity QED with Gate-Defined Double Quantum Dots Enabled by a High Impedance Resonator", Phys. Rev. X **7**, 011030 (2017) (cit. on p. 4).

[126] A. Ask, M. Ekström, P. Delsing, and G. Johansson, "Cavity-free vacuum-Rabi splitting in circuit quantum acoustodynamics", Phys. Rev. A **99**, 013840 (2019) (cit. on p. 5).

[127] G. Hétetka, L. Slodička, M. Hennrich, and R. Blatt, "Single Atom as a Mirror of an Optical Cavity", Phys. Rev. Lett. **107**, 133002 (2011) (cit. on p. 5).

[128] M. Mirhosseini, E. Kim, X. Zhang, A. Sipahigil, P. B. Dieterle, A. J. Keller, A. Asenjo-Garcia, D. E. Chang, and O. Painter, "Cavity quantum electrodynamics with atom-like mirrors", Nature **569**, 692–697 (2019) (cit. on p. 5).

[129] M. H. Devoret, "Quantum Fluctuations", Les Houches Session LXIII, p. 351–386 (1995) (cit. on p. 7).

[130] S. M. Girvin, *Circuit QED : Superconducting Qubits Coupled to Microwave Photons* (cit. on pp. 7, 16, 20).

[131] W. Nolting, *Grundkurs Theoretische Physik 2 - Analytische Mechanik* (Springer, 2010) (cit. on p. 9).

[132] D. M. Pozar, *Microwave Engineering* (Wiley, 2005) (cit. on p. 10).

[133] B. Yurke and J. S. Denker, "Quantum network theory", Phys. Rev. A **29**, 1419–1437 (1984) (cit. on p. 10).

[134] M. E. Peskin and D. V. Schroeder, *An Introduction to Quantum Field Theory* (Westview Press, 1995) (cit. on pp. 13, 42).

[135] S. R. Sathyamoorthy, "Quantum Optics in Superconducting Circuits", PhD thesis (Department of Microtechnology and Nanoscience, 2017) (cit. on pp. 13, 19, 53, 59).

[136] Y. Makhlin, G. Schön, and A. Shnirman, "Quantum-state engineering with Josephson-junction devices", Rev. Mod. Phys. **73**, 357–400 (2001) (cit. on pp. 16, 17, 19).

[137] A. Frisk-Kockum, "Quantum Optics with Artificial Atoms", PhD thesis (Department of Microtechnology and Nanoscience, 2014) (cit. on pp. 19, 53, 64).

[138] B Peropadre, J Lindkvist, I.-C. Hoi, C. M. Wilson, J. J. Garcia-Ripoll, P Delsing, and G Johansson, "Scattering of coherent states on a single artificial atom", New Journal of Physics **15**, 035009 (2013) (cit. on pp. 34, 66, 69).

[139] E. M. Purcell, "Spontaneous emission probabilities at radio frequencies", Phys. Rev. **69**, 681 (1946) (cit. on p. 36).

[140] U. Dorner and P. Zoller, "Laser-driven atoms in half-cavities", Phys. Rev. A **66**, 023816 (2002) (cit. on p. 36).

[141] D. A. Steck, "Quantum and Atom Optics", 2011 (cit. on pp. 39, 41, 46).

[142] T. Brandes, "Quantenmechanik II", Lecture Notes, 2012 (cit. on pp. 39, 41).

[143] C. Cohen-Tannoudji, G. Grynberg, and J. Dupont-Roc, *Atom-Photon Interactions: Basic Processes and Applications* (Wiley, New York, 1992) (cit. on pp. 39, 41, 53, 59, 71).

[144] E. Schrödinger, "An Undulatory Theory of the Mechanics of Atoms and Molecules", Phys. Rev. **28**, 1049–1070 (1926) (cit. on pp. 40, 54).

[145] O. Viehmann, J. Von Delft, and F. Marquardt, "Superradiant phase transitions and the standard description of circuit QED", Physical Review Letters **107**, 1–5 (2011) (cit. on p. 45).

[146] T. Jaako, Z.-L. Xiang, J. J. Garcia-Ripoll, and P. Rabl, "Ultrastrong-coupling phenomena beyond the Dicke model", Phys. Rev. A **94**, 033850 (2016) (cit. on p. 45).

[147] R. H. Dicke, "Coherence in Spontaneous Radiation Processes", Phys. Rev. **93**, 99–110 (1954) (cit. on p. 45).

[148] K. Rzążewski, K. Wódkiewicz, and W. Żakowicz, "Phase Transitions, Two-Level Atoms, and the A^2 Term", Phys. Rev. Lett. **35**, 432–434 (1975) (cit. on p. 45).

[149] K. Rzążewski and K. Wódkiewicz, "Comment on "Instability and Entanglement of the Ground State of the Dicke Model"", Phys. Rev. Lett. **96**, 089301 (2006) (cit. on p. 45).

[150] J. M. Knight, Y. Aharonov, and G. T. C. Hsieh, "Are super-radiant phase transitions possible?", Phys. Rev. A **17**, 1454–1462 (1978) (cit. on p. 45).

[151] G. Chen, Z. Chen, and J. Liang, "Simulation of the superradiant quantum phase transition in the superconducting charge qubits inside a cavity", Phys. Rev. A **76**, 055803 (2007) (cit. on p. 45).

[152] N. Lambert, Y.-n. Chen, R. Johansson, and F. Nori, "Quantum chaos and critical behavior on a chip", Phys. Rev. B **80**, 165308 (2009) (cit. on p. 45).

[153] H. P. Breuer and F. Petruccione, *The theory of open quantum systems* (Oxford University Press, Great Clarendon Street, 2002) (cit. on p. 53).

[154] C. W. Gardiner and P. Zoller, *Quantum Noise*, edited by H. Haken, second (Springer, 2000) (cit. on pp. 53, 63).

[155] J. Lindkvist, "Quantum Optics and Relativistic Motion with Superconducting Circuits", PhD thesis (Department of Microtechnology and Nanoscience, 2015) (cit. on p. 53).

[156] I. Rau, G. Johansson, and A. Shnirman, "Cavity quantum electrodynamics in superconducting circuits: Susceptibility at elevated temperatures", Phys. Rev. B **70**, 054521 (2004) (cit. on p. 60).

[157] A. Maassen van den Brink and A. M. Zagoskin, "Liouville Invariance in Quantum and Classical Mechanics", Quantum Information Processing **1**, 55–72 (2002) (cit. on p. 60).

[158] G. Lindblad, "On the generators of quantum dynamical semigroups", Communications in Mathematical Physics **48**, 119–130 (1976) (cit. on p. 62).

[159] C. W. Gardiner and M. J. Collett, "Input and output in damped quantum systems: Quantum stochastic differential equations and the master equation", Phys. Rev. A **31**, 3761–3774 (1985) (cit. on p. 63).

[160] J.-T. Shen and S. Fan, "Coherent Single Photon Transport in a One-Dimensional Waveguide Coupled with Superconducting Quantum Bits", Phys. Rev. Lett. **95**, 213001 (2005) (cit. on pp. 66, 69).

[161] J. T. Shen and S. Fan, "Coherent photon transport from spontaneous emission in one-dimensional waveguides", Opt. Lett. **30**, 2001–2003 (2005) (cit. on pp. 66, 69).

[162] G. Romero, J. J. García-Ripoll, and E. Solano, "Microwave Photon Detector in Circuit QED", Phys. Rev. Lett. **102**, 173602 (2009) (cit. on pp. 66, 69).

[163] H. J. Carmichael, *Statistical Methods in Quantum Optics 1 - Master Equations and Fokker-Planck Equations* (Springer, 2002) (cit. on pp. 68, 76).

[164] B. R. Mollow, "Power Spectrum of Light Scattered by Two-Level Systems", Physical Review **188**, 1969–1975 (1969) (cit. on pp. 71, 74).

[165] B. R. Mollow, "Stimulated Emission and Absorption near Resonance for Driven Systems", Phys. Rev. A **5**, 2217–2222 (1972) (cit. on p. 71).

[166] K. Koshino and Y. Nakamura, "Control of the radiative level shift and linewidth of a superconducting artificial atom through a variable boundary condition", New Journal of Physics **14**, 043005 (2012) (cit. on p. 74).

[167] A. A. Clerk, M. H. Devoret, S. M. Girvin, F. Marquardt, and R. J. Schoelkopf, "Introduction to quantum noise, measurement, and amplification", Reviews of Modern Physics **82**, 1155 (2010), arXiv:0810.4729 (cit. on p. 86).

[168] J. Aumentado, "Superconducting Parametric Amplifiers: The State of the Art in Josephson Parametric Amplifiers", IEEE Microwave Magazine **21**, 45–59 (2020) (cit. on p. 86).

[169] H. A. Haus and J. A. Mullen, "Quantum Noise in Linear Amplifiers", Phys. Rev. **128**, 2407–2413 (1962) (cit. on p. 86).

[170] C. M. Caves, "Quantum limits on noise in linear amplifiers", Phys. Rev. D **26**, 1817–1839 (1982) (cit. on p. 86).